



# Adaptive MAC layer for interference limited WSN

Viktor Toldov

## ► To cite this version:

| Viktor Toldov. Adaptive MAC layer for interference limited WSN. Networking and Internet Architecture [cs.NI]. Université Lille 1 Sciences et technologies, 2017. English. tel-01493094

HAL Id: tel-01493094

<https://hal.inria.fr/tel-01493094>

Submitted on 20 Mar 2017

**HAL** is a multi-disciplinary open access archive for the deposit and dissemination of scientific research documents, whether they are published or not. The documents may come from teaching and research institutions in France or abroad, or from public or private research centers.

L'archive ouverte pluridisciplinaire **HAL**, est destinée au dépôt et à la diffusion de documents scientifiques de niveau recherche, publiés ou non, émanant des établissements d'enseignement et de recherche français ou étrangers, des laboratoires publics ou privés.

UNIVERSITÉ LILLE 1 - SCIENCES ET TECHNOLOGIES

ÉCOLE DOCTORALE ED RÉGIONALE SPI 72

IEMN - UMR CNRS 8520

---

## Adaptive MAC layer for interference limited WSN

---

*Author :* Viktor TOLDOV

*Présentée et soutenue publiquement le 24/01/2017  
pour l'obtention du titre de Docteur  
de l'Université Lille 1 - Sciences et Technologies  
Spécialité Micro et nano technologies, acoustique et  
télécommunications  
Numéro d'ordre : 42262*

### **Composition du jury :**

*Rapporteurs :*

**Yannis POUSSET**

Prof. Univ. of Poitiers, France

**Hervé RIVANO**

CR Inria, France

*Examinateurs :*

**Chiara BURATTI**

Research Associate Univ. of Bologna, Italy

**Antoine GALLAIS**

MCF Univ. of Strasbourg, France

**Gilles GRIMAUD**

Prof. Univ. Lille 1, France

**Martine LIENARD**

Prof. Univ. Lille 1, France

*Directeur de thèse :*

**Laurent CLAVIER**

Prof. IMT, Télécom Lille, France

*Co-directeur de thèse :*

**Nathalie MITTON**

DR Inria, France



*À la mémoire de mon grand-père.*



“О сколько нам открытий чудных  
Готовит просвещенья дух  
И опыт, сын ошибок трудных,  
И гений, парадоксов друг,  
И случай, бог изобретатель.”

А.С. Пушкин

*“Oh so many wonderful discoveries  
the Enlightenment Spirit brings to us,  
together with the Experience — the child of hard mistakes,  
and the Genius — the friend of paradoxes,  
and the Chance — the Lord of inventions”*

A.S. Pushkin



## *Remerciements*

Tout d'abord, je voudrais remercier mes directeurs de thèse : Mme Nathalie MITTON et M. Laurent CLAVIER, pour leur encadrement durant ma thèse et mon stage de fin d'études. Merci pour votre expérience que vous avez partagée avec moi, vos conseils et vos encouragements. Merci pour le temps que vous m'avez consacré.

J'ai eu la chance de travailler dans un environnement pluridisciplinaire des laboratoires IRCICA, Inria et IEMN. Je tiens à remercier tous les membres du groupe CSAM de l'IEMN et de l'équipe-projet FUN d'Inria qui étaient toujours prêts à m'aider, pour leur soutien et l'ambiance agréable de travail. Plus particulièrement je voudrais remercier Román IGUAL PEREZ pour son apport technique et théorique et pour une collaboration enrichissante qui a donné lieu à de très bons résultats. Je remercie également Arash MASKOOKI, Mohamed El Amine SEDDIK et Rahul VYAS pour leur contribution importante.

Je remercie vivement Roudy DAGHER, Abdoul Aziz MBACKE, Simon DUQUENNOY, Tahiry RAZAFINDRALAMBO, Cristina CANO et Valeria LOSCRI pour les échanges intéressants et leurs conseils.

J'adresse également mes remerciements à Rédha KASSI, Bernard VERBEKE, Julien VANDAELE et Lamine KONE pour leurs conseils techniques et la mise à disposition de matériel.

Je remercie aussi Anne REJL, Peggy STANKOWSKI, Nora BEN-BAHLOULI, Malika HABBAS, Ahmed BEN ABDESELAM et Michel SOULAGE qui m'ont aidé à résoudre des problèmes administratifs et logistiques.

Je voudrais également remercier mes collègues de l'Université de Stellenbosch en Afrique du Sud avec qui j'ai eu l'opportunité de travailler, notamment Dr. Riaan WOLHUTER, JP MEIJERS, SP LE ROUX, Sajid SHEIKH et Willie PRETORIUS.

Finalement, je voudrais exprimer ma gratitude à tous mes proches, ma famille et mes amis. Merci à Albina pour le support aux moments difficiles. Merci à ma mère, ma grand-mère, mon oncle, ma tante et mes cousins pour leur aide et les encouragements. Un grand merci à mon père et mon grand-père qui ont été des exemples pour moi et m'ont motivé à me lancer dans cette aventure scientifique particulièrement enrichissante.



# Abstract

**Title:** *Adaptive MAC layer for interference limited WSN*

In the era of the Internet of Things (IoT), the number of connected devices is growing dramatically. Often, connected objects use Industrial, Scientific and Medical (ISM) radio bands for communication. These kind of bands are available without license, which facilitates development and implementation of new connected objects. However, it also leads to an increased level of interference in these bands. Interference not only negatively affect the Quality of Service, but also causes energy losses, which is especially unfavorable for the energy constrained Wireless Sensor Networks (WSN). In the present thesis the impact of the interference on the energy consumption of the WSN nodes is studied experimentally. The experimental results were used to estimate the lifetime of WSN nodes under conditions of different levels of interference. Then, a Thompson sampling based Cognitive Radio adaptive solution is proposed and evaluated via both, simulation and hardware implementation. Results show that this approach finds the best channel quicker than other state of the art solutions. An extension for multihop WSN was proposed for this Cognitive Radio solution and evaluated by hardware implementation in the framework of EWSN Dependability Competition. Finally, an adaptive WildMAC MAC layer protocol is proposed for the usecase of the LIRIMA PREDNET wildlife animal tracking project. Obtained field range test data were used to theoretically estimate cell densities and deployment zone coverage in this Low Power Wide Area Network (LPWAN). Then performance of the protocol was evaluated in WSNet simulation. The results show performance that allows to respect PREDNET project requirements with the given coverage.



# Résumé

**Titre:** *Couche MAC adaptative pour réseaux de capteurs limités par l'interférence*

A l'époque de l'Internet des Objets, le nombre de dispositifs communicants ne cesse d'augmenter. Souvent, les objets connectés utilisent des bandes de fréquences « industriel, scientifique et médical (ISM) » pour effectuer les communications. Ces bandes sont disponibles sans licence, ce qui facilite le développement et le déploiement de nouveaux objets connectés. Cependant, cela mène aussi au fait que le niveau d'interférences augmente dans les bandes ISM. Les interférences ont non seulement un impact négatif sur la qualité de service, mais aussi elles causent des pertes de messages couteuses en énergie, ce qui est particulièrement nocif pour les nœuds capteurs souvent limités en énergie. Dans cette thèse, l'impact des interférences sur la consommation énergétique des nœuds capteurs est étudié expérimentalement. Les résultats de ces expérimentations sont utilisés pour estimer la durée de vie des nœuds capteurs en fonction de différents niveaux d'interférence subis. Puis, un algorithme de Radio Cognitive basé sur la technique d'échantillonnage de Thompson est proposé et évalué par la simulation et implémentation. Les résultats montrent que l'approche proposée trouve le meilleur canal plus vite que les autres techniques de l'état de l'art. De plus, une extension multi sauts est proposée pour cette technique de la Radio Cognitive. Cette extension est évaluée par expérimentation lors d'une compétition EWSN Dependability Competition. Finalement, le protocole adaptatif WildMAC est proposé pour le cas d'usage du projet LIRIMA PREDNET qui consiste à surveiller des animaux sauvages. Les résultats de tests de portée sur le terrain sont utilisés pour estimer théoriquement les densités des cellules du réseau ainsi que la couverture de ce réseau de type LPWAN. Puis, les performances sont évaluées par simulation avec le simulateur WSNet. Les résultats montrent que la solution proposée respecte les contraintes imposées par le projet PREDNET dans la zone ciblée.



# Contents

<b>Remerciements</b>	vii
<b>Abstract</b>	ix
<b>Résumé</b>	xi
<b>Contents</b>	xiii
<b>List of Figures</b>	xvii
<b>List of Tables</b>	xxi
<b>List of Abbreviations</b>	xxiii
<b>1 Global introduction</b>	1
1.1 Context . . . . .	2
1.1.1 Internet of Things (IoT) . . . . .	2
1.1.2 Wireless Sensor Networks (WSN) . . . . .	4
1.1.3 Wireless Sensor Node structure . . . . .	6
1.1.4 Particularities of RF communications which can impact the energy consumption . . . . .	8
Interference . . . . .	8
Collisions . . . . .	8
Fading . . . . .	8
Other factors . . . . .	9
1.2 WSN communication stack . . . . .	9
1.2.1 Physical layer . . . . .	10
1.2.2 Data Link Layer . . . . .	11
1.2.3 Network Layer . . . . .	11
1.2.4 Transport Layer . . . . .	12
1.2.5 Application Layer . . . . .	12
1.3 Particular WSN application usecase: LIRIMA PREDNET project . . . . .	13
1.3.1 Functional requirements . . . . .	13
1.3.2 Other wildlife tracking projects . . . . .	14
1.4 LPWAN networks . . . . .	15
1.4.1 Sigfox . . . . .	16
1.4.2 Ingenu (ex. RPMA) . . . . .	16
1.4.3 LoRa . . . . .	17

1.5	Contributions of this thesis . . . . .	18
1.6	Structure of the thesis . . . . .	19
<b>2</b>	<b>Experimental study of interference impact on the energy consumption in WSN</b>	<b>21</b>
2.1	Chapter introduction . . . . .	21
2.2	Motivation and Related works . . . . .	22
2.3	Description of the platform . . . . .	24
2.4	Experimental setup . . . . .	25
2.4.1	Ideal case scenario . . . . .	27
2.4.2	Real case scenario . . . . .	28
2.5	Measurement results . . . . .	28
2.5.1	Measurement approach . . . . .	28
2.5.2	Ideal case . . . . .	30
2.5.3	Real case . . . . .	32
2.5.4	Measurement analysis . . . . .	32
TX side . . . . .	32	
RX side . . . . .	34	
2.5.5	Lifetime evaluation depending on RSSI . . . . .	35
Ideal case . . . . .	35	
Real case . . . . .	37	
2.5.6	Using Wi-Fi as a interfering network . . . . .	39
2.6	Long term distributed interference measurements . . . . .	41
Description of the platform . . . . .	41	
Experimental setup . . . . .	42	
Results . . . . .	43	
2.6.1	Discussion . . . . .	45
2.7	Chapter conclusion . . . . .	47
<b>3</b>	<b>Thompson Sampling based Cognitive ratio solution for Multihop WSN</b>	<b>49</b>
3.1	Chapter introduction . . . . .	49
3.2	Related works . . . . .	54
3.3	Optimal Algorithms for Multi-Armed Bandit . . . . .	56
3.3.1	Channel selection modeling . . . . .	56
3.3.2	Adaptation of UCB approach . . . . .	57
3.3.3	Adaptation of $\epsilon$ -greedy . . . . .	59
3.4	Thompson Sampling Based Learning Algorithm . . . . .	61
3.5	Performance evaluation . . . . .	64
3.5.1	Simulation based on generated channel samples . . .	64
3.5.2	Simulation over the real channel measurements . . .	65
3.5.3	Experimentation via real WSN hardware implementation . . . . .	66
3.5.4	Evaluation results . . . . .	68

3.6 Multihop extension . . . . .	70
3.6.1 Test application scenario: EWSN 2016 dependability competition . . . . .	70
3.6.2 Proposed multihop solution based on Thompson sampling approach . . . . .	73
3.6.3 Performance evaluation results and discussion . . . . .	75
3.7 Chapter conclusion . . . . .	75
<b>4 Distributed adaptive MAC protocol for WSN-based wildlife protection</b>	<b>77</b>
4.1 Chapter introduction . . . . .	77
4.1.1 Existing MAC protocols . . . . .	79
4.2 Our contribution : the WildMAC protocol . . . . .	80
4.2.1 General Time division structure . . . . .	81
4.2.2 Timeslot structure . . . . .	82
Control part . . . . .	82
First and Second TX/RX parts . . . . .	86
4.2.3 Multichannel operation structure . . . . .	86
4.2.4 Timeslot reservation and channel access . . . . .	88
4.2.5 Communication example . . . . .	92
4.3 Performance evaluation . . . . .	93
4.3.1 Chosen LoRa communication parameters . . . . .	93
4.3.2 Range test and coverage simulation . . . . .	93
Range test . . . . .	93
Coverage simulation . . . . .	95
Obtained results . . . . .	95
4.3.3 Cell capacity estimation . . . . .	96
4.3.4 Kruger park coverage estimation . . . . .	98
4.3.5 WSNet implementation and simulation results . . . . .	98
One hop scenario . . . . .	99
Multihop scenario . . . . .	100
4.4 Chapter conclusion . . . . .	105
<b>5 Conclusions and perspectives</b>	<b>107</b>
5.1 Conclusions . . . . .	107
5.2 Impact of the thesis . . . . .	109
5.3 Perspectives . . . . .	109
<b>Bibliography</b>	<b>111</b>
<b>List of Publications</b>	<b>123</b>



# List of Figures

1.1 Examples of the licence-free bands in the world . . . . .	2
1.2 WSN architecture. . . . .	4
1.3 WSN node structure. . . . .	6
1.4 WSN communication stack. . . . .	10
2.1 Example of currents of CC2420 radio module (red curve) and MSP430 micro controller (blue curve) measured by Synergie platform. . . . .	22
2.2 Elements of the measurement platform. . . . .	24
2.3 Connection between the WSN430 node and Synergie platform	25
2.4 Scenarios of the experiment: a) in anechoic chamber, b) in office-type lab environment. . . . .	26
2.5 Example of a successful X-MAC transmission. . . . .	27
2.6 Examples of combinations of type packets TX-RX. . . . .	30
2.7 Energy consumption vs RSSI per packet type in ideal case. . . . .	31
2.8 Energy consumption vs RSSI per packet type in real case. . . . .	33
2.9 Avg. energy, total number of packets and total energy per packet type on TX side. . . . .	34
2.10 Energy statistics per type of packet on RX side: average energy, number of packets and total energy consumption. Ideal case. . . . .	35
2.11 Packet distribution per RSSI window on TX - Ideal case. . . . .	36
2.12 Packet distribution per RSSI window on TX - Real case. . . . .	38
2.13 Energy consumption vs RSSI per packet type (Wi-Fi scenario). . . . .	40
2.14 End node . . . . .	42
2.15 IEEE 802.15.4 and IEEE 802.11 channels allocation in 2.4 GHz ISM band. Credits: NI . . . . .	42
2.16 Node placement map . . . . .	43
2.17 One week interference measurement. . . . .	43
2.18 Evolution of the perceived level of interference depending the used channel (IRCICA TELECOM Lab) . . . . .	45
2.19 Evolution of the perceived level of interference depending the used channel (FIT IoT-LAB) . . . . .	46
3.1 Dynamic spectrum access . . . . .	50
3.2 A sample from one week interference measurements. The node is situated in the middle of the lab. . . . .	54

3.3	Relative throughput comparison of different algorithms on 10 accessible channels ( $\mu = 0.80$ ). Oracle (The user that knows the best channel from the beginning) has relative throughput 1. . . . .	65
3.4	Schematic of experiment setup. . . . .	66
3.5	Spectrum measurements: a) No user activity. b) One user browsing the web. c) One user downloading a large file. . . . .	67
3.6	Experimental setup: 3 pairs of laptops occupy 3 orthogonal channels of Wi-Fi (1, 6, 11) . . . . .	68
3.7	Relative throughput on three accessible channels using a) Synthetically generated channel observations. b) Real-time measurements c) Empirical real-time test-bed. . . . .	69
3.8	Dependability competition scenario description. Credits: Carlo Alberto Boano . . . . .	71
3.9	TelosB node connected to the control platform. Credits: Carlo Alberto Boano . . . . .	72
3.10	Experimental area map at the Institute for Technical Informatics of the Graz University of Technology. The source and the sink nodes are represented by dark blue stars, whereas the intermediate nodes are represented as blue spots. Credits: Carlo Alberto Boano . . . . .	72
3.11	Proposed Multihop solution . . . . .	74
4.1	Slotted Aloha based algorithm with reservation. Global flowchart . . . . .	82
4.2	General Timeslot structure . . . . .	83
4.3	An example of rank discovery process . . . . .	84
4.4	Inter-layer interference. . . . .	86
4.5	Inter-rank frequency division structure . . . . .	87
4.6	Combination of Time/frequency division techniques . . . . .	88
4.7	Opposite time-division structure . . . . .	89
4.8	Inter-rank frequency division structure with hopping . . . . .	90
4.9	Long term timeslot reservation for Rank 1 nodes . . . . .	90
4.10	One-time on-demand timeslot reservation for Rank 1 nodes	91
4.11	Inter-rank frequency division structure with hopping . . . . .	92
4.12	Fixed receiver side node . . . . .	94
4.13	Coverage map . . . . .	96
4.14	Example of rhinoceros distribution in a 13 km cell . . . . .	97
4.15	Estimated coverage in the Kruger Park . . . . .	98
4.16	Number of reservation successes versus number of occupied timeslots . . . . .	99
4.17	PER versus number of occupied timeslots . . . . .	100
4.18	Example of rhinoceros distribution with reduced densities for higher ranks . . . . .	101

4.19 Probability of the reception of a message before the expiration of a given number of superframes. Initial rank: a) 1 b) 2 c) 3 d) 4 e) 5. . . . .	103
---	-----



# List of Tables

1.1	Examples of ISM bands . . . . .	1
2.1	Number of transmissions per packet sent by TX and of received duplicated packets on RX. . . . .	28
2.2	Avg. energy, maximum number of transmitted packets and lifetime of the node per RSSI window - Ideal case. . . . .	37
2.3	Avg. energy, maximum number of transmitted packets and lifetime of the node per RSSI window - Real case. . . . .	39
2.4	Results of energy, number of packets and total energy per type of packet on TX side. Real case. . . . .	41
3.1	Evaluation results in multihop scenario . . . . .	75
4.1	PER per rank . . . . .	102
4.2	Average number of physical transmissions per rank . . . . .	104
4.3	Percentage of nodes estimated their rank as R per per zone of minimal transmissions. The used format is mean(SD); The values are given in % . . . . .	104



# List of Abbreviations

<b>ACK</b>	Acknowledgment
<b>ADC</b>	Analog-to-Digital Converter
<b>AP</b>	Access Point
<b>BTS</b>	Base Transceiver Station
<b>BW</b>	Bandwidth
<b>CAD</b>	Channel Activity Detection
<b>CCA</b>	Clear Channel Assessment
<b>CR</b>	Cognitive Radio
<b>CRC</b>	Cyclic Redundancy Check
<b>CRSN</b>	Cognitive Radio Sensor Networks
<b>CR-WSN</b>	Cognitive Radio Wireless Sensor Networks
<b>CSMA</b>	Carrier Sence Multiple Access
<b>CSS</b>	Chirp Spread Spectrum
<b>CTF</b>	Clear To Forward
<b>CTS</b>	Clear To Send
<b>DBPSK</b>	Differential Binary Phase Shift Keying
<b>DSSS</b>	Direct Sequence Spread Spectrum
<b>FEC</b>	Forward Error Correction
<b>FFT</b>	Fast Fourier Transform
<b>FHSS</b>	Frequency Hopping Spread Spectrum
<b>GNSS</b>	General Purpose Input/Output
<b>GPIO</b>	General Purpose Input/Output
<b>GPS</b>	Global Positioning System
<b>GSM</b>	Global System for Mobile Communications
<b>IEEE</b>	Institute of Electrical and Electronics Engineers
<b>IoT</b>	Internet of Things
<b>ISM</b>	Industrial, Scientific and Medical
<b>ITM</b>	Irregular Terrain Model
<b>LLC</b>	Logical Link Control
<b>LPWAN</b>	Low-Power Wide-Area Network
<b>LQI</b>	Link Quality Indicator
<b>LTE</b>	Long Term Evolution
<b>MAC</b>	Medium Access Control
<b>MCU</b>	Microcontroller Unit
<b>NACK</b>	Negative Acknowledgment
<b>NB-IoT</b>	Narrowband IoT
<b>NIC</b>	Network Interface Cards

<b>OFDM</b>	Orthogonal Frequency-Division Multiplexing
<b>OS</b>	Operating System
<b>PER</b>	Packet Error Rate
<b>PN</b>	Pseudo-Noise
<b>PPP</b>	Poisson Point Process
<b>PV</b>	Photovoltaic
<b>QoS</b>	Quality of Service
<b>RDC</b>	Radio Duty Cycle
<b>RF</b>	Radio Frequency
<b>RSSI</b>	Received Signal Strength Indicator
<b>RTF</b>	Request To Forward
<b>RTS</b>	Request To Send
<b>RX</b>	Receiver
<b>SF</b>	Spreading Factor
<b>SFD</b>	Start Frame Delimiter
<b>SFr</b>	Superframe
<b>SN</b>	Sensor Network
<b>SOC</b>	State Of Charge
<b>SSID</b>	Service Set IDentifier
<b>TS</b>	Timeslot
<b>TSCH</b>	Timeslotted Channel Hopping
<b>TTL</b>	Time To Live
<b>TX</b>	Transmitter
<b>UCB</b>	Upper Confidence Bound
<b>UNB</b>	Ultra Narrow Band
<b>UWB</b>	Ultra Wide Band
<b>Wi-Fi</b>	Wireless Fidelity
<b>WSN</b>	Wireless Sensor Network

# Chapter 1

## Global introduction

Today, in the era of the Internet of Things (IoT), the number of connected objects increases dramatically [44, 43]. Wireless Sensor Networks (WSN) constitute a significant part of the IoT. In general, this kind of networks uses the Industrial, Scientific and Medical (ISM) radio bands to transmit data. These bands are license-free, but, on the other hand, a lot of devices and different technologies share the same frequency band. Moreover, some license based spectrum technologies could also be interested to use ISM bands (*e.g.*, LTE-U [20]). This makes the electromagnetic interference an important issue. Some ISM bands defined by ITU-R [67] are presented in Table 1.1. As we can notice from the table, the large part of the spectrum is available in the millimeter-wave bands (especially starting from 24 GHz). These bands represent an important interest for both, academia and industry [94],[62]. However, these bands are more suitable for high-speed, short-range point to point communications, which is different form the context of the WSN. On the other part of the ISM spectrum, some low frequency bands are available. However, the bandwidth of this bands is about a few kHz, which makes questionable the possibility to use them to accommodate billions of connected devices.

It is important to note that not all the license-free bands are available worldwide. Some examples of license-free bands available indifferent countries are presented in Figure 1.1.

TABLE 1.1: Examples of ISM bands

Frequency range	Center frequency	Bandwidth
6,765 - 6,795 MHz	6.78 MHz	30 kHz
13,553 - 13,567 MHz	13.56 MHz	14 kHz
26.957 - 27.283 MHz	27.12 MHz	326 kHz
40.66 - 40.7 MHz	40.68 MHz	40 kHz
433.05 - 434.79 MHz	433.92 MHz	1.84 MHz
902 - 928 MHz	915 MHz	26 MHz
2.4 - 2.5 GHz	2.45 GHz	100 MHz
5.725 - 5.875 GHz	5.8 GHz	150 MHz
24 - 24.25 GHz	24.125 GHz	250 MHz
61 - 61.5 GHz	61.25 GHz	500 MHz
122 - 123 GHz	122.5 GHz	1 GHz
244 - 246 GHz	245 GHz	2 GHz

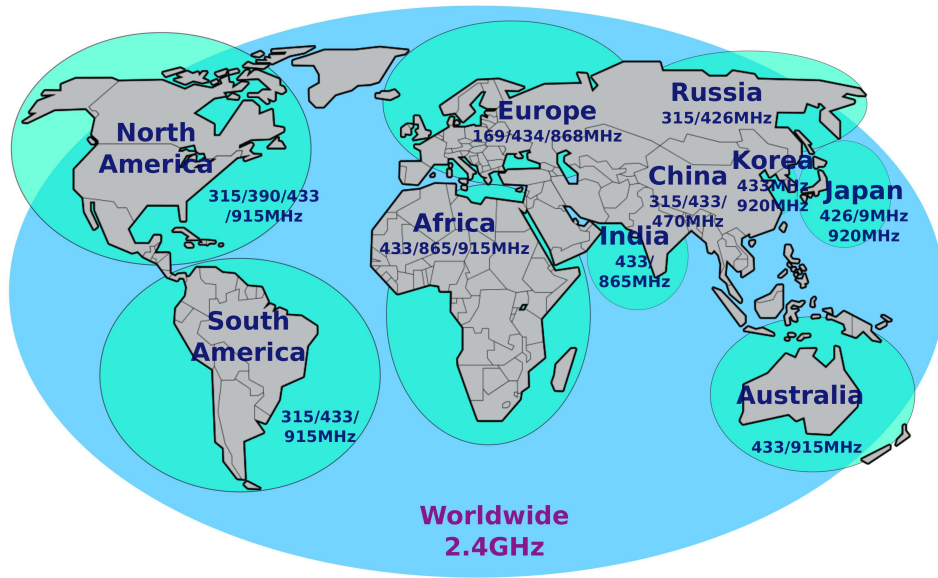


FIGURE 1.1: Examples of the licence-free bands in the world

The worldwide available 2.4 GHz band is one of the license-free bands used in WSNs. However, this band became crowded [112]. Sub-GHz bands also represent an interest for IoT, especially with the arrival of Low Power Wide Range networks (LPWAN). However, these bands have a bandwidth of a few MHz, thus they can be overfilled soon.

The growing number of connected devices on one hand and the lack of available license-free spectrum on the other hand make the electromagnetic interference an important issue for IoT. The access to the medium in the license-free spectrum and successful data transmissions will be hard to achieve, which will decrease the performance of final applications and even block the further development of IoT. The development of an adaptable communication solution is, thus, required in order to optimize the performance of IoT solutions under growing interference conditions.

In this thesis we develop a Medium Access Control (MAC) protocol for a specific usecase of Wireless Sensor Networks (WSN) - wildlife animal tracking. More in details the context of this thesis and our particular usecase are described in the following sections.

## 1.1 Context

### 1.1.1 Internet of Things (IoT)

With the constantly growing number of connected devices [44], the Internet of Things (IoT), an actively developing telecommunication paradigm, has gained an important interest in both, academia and industry. This term was used for the first time by K. Ashton in the title of its presentation in 1999

[10]. Since then, multiple definitions could be found in the literature. In [10] the following definition is proposed: "The Internet of Things allows people and things to be connected Anytime, Anyplace with Anything and Anyone, ideally using Any path/network and Any service" which emphasizes the widespread character of this paradigm.

The IoT covers different fields of applications[81], [50], among others:

- healthcare,
- home automation,
- smart city,
- smart agriculture,
- smart environment,
- industrial control,
- emergency management.

IoT incorporates different technologies, *e.g.* sensor hardware and firmware, communication technologies, cloud, data processing [81] in order to collect and consume data from billions of sensors all over the world. IoT could be considered as a next step of the evolution of Sensor Networks (SN) along with the fusion with other fields of study, especially related to data analysis. According to the forecast of HP, the number of sensors can reach one trillion by 2030 and then, the data generated by IoT will represent the most important part of Big Data [25]. Indeed, in this case the IoT data will possess the three main characteristics of Big Data (the "3V"):

- Volume, due to huge number of sensor nodes;
- Velocity, because of increasing sampling rates and improvement of other characteristics of sensing devices;
- Variety, due to a large spectrum of possible parameters to measure.

In its report, Intel confirms that Big Data in IoT has three features conforming to the Big Data paradigm (see [25] for details):

- abundant terminals generating masses of data;
- data generated by IoT is usually semi-structured or unstructured;
- data of IoT are useful only when they are analyzed.

The authors of [25] define the following three layers in a process of data acquisition in IoT:

- sensing layer, responsible for measurements of different values,

- network layer, which aims to ensure the delivery of measured values from sensors to the data consumption unit (storage and treatment unit),
- application layer, where the data are finally used.

The first two layers rely on SNs, which represent an essential component of IoT [81]. Indeed, SNs provide majority of hardware infrastructure for IoT and ensure data collection. As most of the sensors deployed today are wireless, this work is focused on Wireless Sensor Networks (WSN). This concept is described in the next section.

### 1.1.2 Wireless Sensor Networks (WSN)

WSNs consist of a large amount of tiny sensor nodes, which act as both data generators and network relays [5]. WSNs are mostly developed for specific application purposes in contrary to IoT which can be explained as a general purpose sensor network [81]. The architecture of a WSN is presented in the Figure 1.2.

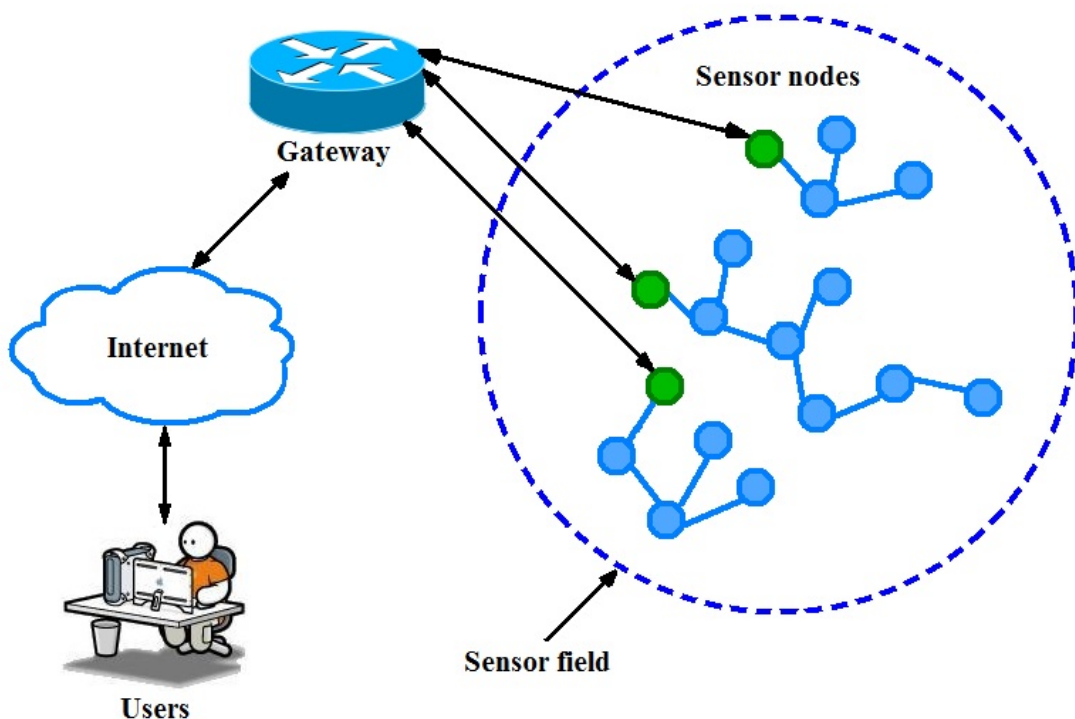


FIGURE 1.2: WSN architecture.

Sensor nodes are distributed in random or planned way over the target area called a *sensor field*. Depending on the application, *sensor field* could be presented as a geographic zone, a structure (e.g. building), a human or animal body *etc*. Then, specific parameters in the *sensor field* are monitored by the WSN. Data could be generated by sensor nodes regularly, on demand or triggered by an event [22], as, for example, a detected fire. Measured values

are forwarded towards a collecting unit called *sink* which can also perform a function of gateway between WSN and another network, *e.g.* the Internet. The role of the *sink* node is to transmit the collected data from a WSN to the user or processing unit (*e.g.* cloud). A *sink* node is also in charge of sending commands from user to nodes. For example, in some cases, WSN can contain nodes with actuators, which can be controlled by commands from the *sink*. Depending on the WSN topology, data from sensor nodes are sent either directly (one-hop networks) or by passing through other sensor nodes (multihop networks). Based on the communication technology used in a WSN, different network topologies are possible. The most frequently used network topologies are:

- Mesh topology (*e.g.*, ZigBee [46])
- Tree topology (*e.g.*, RPL [18])
- Star topology (*e.g.*, Sigfox[92])

In the two former cases, each node can perform the functions of a router and is able to forward messages from other nodes. In this situation, short range Radio Frequency (RF) technologies are often used (*e.g.* IEEE 802.15.4). To maintain this kind of topologies, self-organizing capabilities of the sensor nodes are required. Indeed, in case of failure of an intermediate node, the routing path must be modified in order to guarantee the continuity of WSN service. To do so, complex routing algorithms are used. With the arrival of Low Power Wide Area Networks (LPWAN) (*e.g.*, Sigfox[92], LoRa[76]) providing long range communications, a new trend in modern WSN is to shift to the star topology. In this case, it is supposed that the entire *sensor field* is in range of a sink node, which could be called base station. Sensor nodes can, thus, transmit the data directly to the base station and save energy since the nodes do not have to receive and forward packets from other nodes. However, a full coverage of the *sensor field* is not always possible.

Depending on the application, sensor nodes can be mobile or static [86]. The sink node is often considered as static, however, in some applications, the sink node can be also mobile [70].

From hardware and software point of view, WSNs can be homogeneous or heterogeneous. In the first case, sensor nodes are based on an identical hardware/software platform and, thus, have identical resources. In the second case, some nodes have extended resources (*e.g.* multiple radios, extended storage capacity). In most of the cases, sensor nodes have identical resources whereas a sink node is based on more advanced platforms.

In many cases, Wireless Sensor nodes have very constrained resources in terms of memory, processing capacity and energy. On one hand, this is because of the need to keep the production cost as minimal as possible in order to be able to deploy billions of nodes. On the other hand, it can be due to

the specific application restrictions. Available energy represents one of the most important resource limitations for WSN nodes. Indeed, the majority of sensor nodes are battery-powered. At the same time, some applications as, for example, wildlife animal tracking, impose strict limitations on size and weight of wearable nodes, which means limited battery capacity. Besides, access to the nodes can be restrained after installation (*e.g.* the sensor nodes are embedded in the wall of building, installed on the body of a bird or randomly distributed by being dropped off a plane over a woodland). Moreover, as mentioned before, a WSN can be composed of a large number of nodes. So, battery replacement represents a hard if not impossible task. Thus, the lifetime of the WSN node is often defined by the lifetime of one battery charge. That is why it is crucial to avoid the energy waste and optimize the energy consumption within each sensor node in order to extend its lifetime and, thus, the lifetime of the whole WSN. For some applications, the required lifetime of WSN must exceed 10 years, which emphasizes the importance of the research aiming to find the main reasons of energy losses and develop techniques to outcome them and extend the lifetime.

### 1.1.3 Wireless Sensor Node structure

The simplified structure of a wireless sensor node is presented on Figure 1.3

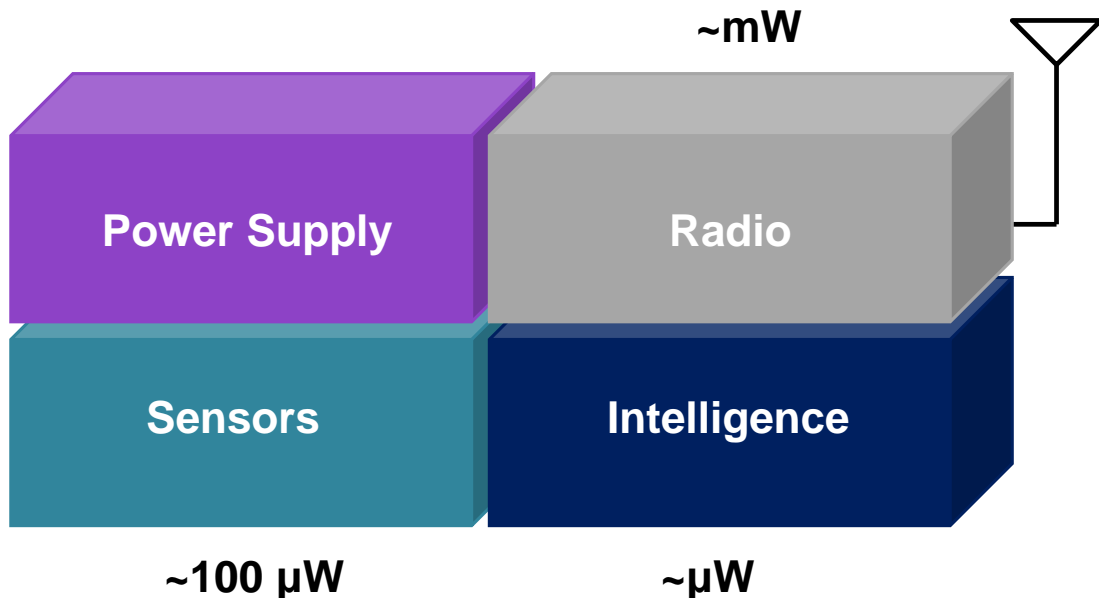


FIGURE 1.3: WSN node structure.

A sensor node contains 4 main blocks:

- Sensors: this block comprises different sensors required to perform measurements in the *sensor field*. The type of sensors depends on the application of the WSN. This part of the sensor node is in charge of

generating data. Depending on the type of the sensor, the energy consumption of this part is about hundreds of microwatts. Some examples of sensors are: temperature sensor, humidity sensor, accelerometer.

- Radio module: this block is required in order to send measured values and receive control messages. The energy consumption of this component depends on the used RF module and is about a few milliwatts.
- Computational part of the node (intelligence): usually represented by a microcontroller (MCU) and a memory. This component is required to control all other parts of the node. The MCU ensures that measurements are carried out and transmitted at the right moments. It also executes Medium Access Control (MAC) and routing algorithms by using the internal service information as, for example, the feedback from RF module (*e.g.* Received Signal Strength Indicator (RSSI), number of unsuccessful transmissions) or a current State Of Charge (SOC). In some cases this part of the node comprises also a flash memory to store the measured values to be sent later. The energy consumption of a MCU could be about few microwatts<sup>1</sup>.
- Power Supply: this part is in charge of providing the electric energy required to power all other components of the node. It is composed by two kinds of elements: energy storage devices (microbattery, supercapacitor) and energy harvesting devices (Photovoltaic (PV) cells [106], vibration energy harvesting devices [98] *etc.*). The energy harvesting devices are optional since they increase the cost of production of the sensor nodes and often cannot provide enough energy to let the node function without battery. So, the battery is still the most used energy supply unit.

In some cases, nodes can be connected directly to the power line. However, even though it removes the energy constraint, in this case the list of possible applications is significantly reduced.

As we can notice, among all the parts of a WSN node, RF module represents the greatest energy consumption. Since the nodes are often battery-powered, it is important to develop an efficient control strategy, which will adjust the behavior of the RF module in order to avoid possible important energy waists. Many factors related to RF communications which can have a pernicious effect on the nodes lifetime have to be taken into account. These factors are described in Section 1.1.4.

---

<sup>1</sup>The values of the energy consumption can vary depending on the hardware components used.

### 1.1.4 Particularities of RF communications which can impact the energy consumption

In this subsection we present different factors of radio communication which can impact the energy consumption of the nodes. These factors must be considered to design low power WSNs.

#### Interference

As it was mentioned before, WSN often use ISM bands. These bands are shared between different radio technologies and the number of devices which use these bands is increasing. The signals of different technologies are incompatible, but have a pernicious impact on each other. Interfering signals can lead to the reception of corrupted packets. In many cases, corrupted packets have to be retransmitted, and each retransmission is a waste of energy.

#### Collisions

Wireless nodes share the same medium - radio channel. That means the possibility of collisions - simultaneous transmissions carried out by multiple nodes. When a collision happens, there is a big chance that all the messages involved in the collision are lost and, thus, transmitted again<sup>2</sup>. Each retransmission causes energy losses.

#### Fading

In real environments different objects and structures surrounding deployed WSN nodes (*e.g.*, trees, walls, mountains), lead to signal reflections. Fading is caused by interference between multiple versions of the transmitted signal (*i.e.*, main signal path and its reflections) arrived at the receiver at slightly different times. These signals (called multipath waves) are combined at the receiver antenna which can lead to the important variations of the detected resulting signal both in amplitude and phase. These variations can cause packet corruption.

In this thesis we focus on these three described above factors. All of them are the examples of the interference in general but with different sources (other RF technologies, other WSN nodes using the same RF technology and reflected signals respectively).

We studied experimentally the impact of the interference on the energy consumption of the WSN nodes and we proposed adaptable MAC layer techniques allowing the decrease of the impact of the interference on the WSN communications.

---

<sup>2</sup>Depending on the application functional requirements.

There are also other factors of the RF communications which can lead to the energy waste. These factors will not be studied in this thesis.

### Other factors

**Idle Listening.** Usually, Wireless Sensor nodes spend most of the time in sleep mode in order to save energy [22]. In this mode the radio module is turned off and, thus is unable to receive any messages. In case of a multi-hop network, sensor nodes are in general unaware of the Radio Duty Cycle (RDC) schedules of surrounding nodes. If the transmitter node switches its radio on for a long time in order to determine whether desirable receiver node is active, an important amount of energy will be wasted. The same situation is valid for the receiver node, when it switches its radio on to check whether there is a possible transmission for this node.

**Overhearing.** A wireless sensor node has to receive a packet first in order to determine, whether it is a destination node for the packet or not. To receive the packet, the node has to demodulate and decode packet data, then it performs a Cyclic Redundancy Check (CRC) in order to check the integrity of the message. If the packet is not corrupted, the node compares the value of the destination address field of the packet with its own address. In case of a match, the node accepts the packet for the following processing. Otherwise, the packet is dropped. In case of a multihop network, nodes are likely to receive packets destined to other nodes, which means that many packets will be dropped after decoding, and, thus, energy will be wasted.

**Protocol overhead.** The energy is consumed during the transmission of each bit of data, including control and management packets and headers. This type of data is not useful for the final user of the WSN. However, these data are important to ensure the communication in the WSN. It is important, then, to reduce as much as possible the amount of control and management data transmitted within the WSN, but without performance degradation of the communication process.

## 1.2 WSN communication stack

A simplified version of the communication stack used in WSN, proposed in [5] is depicted in Figure 1.4

The behavior of the sensor node could be adjusted in each layer in order to reduce the impact of the interference. As in case of a ISO/OSI model[114], each layer of the WSN communication stack is responsible of specific limited missions. Moreover, each layer has some parameters which can be adjusted and can provide some feedback values that can be used by

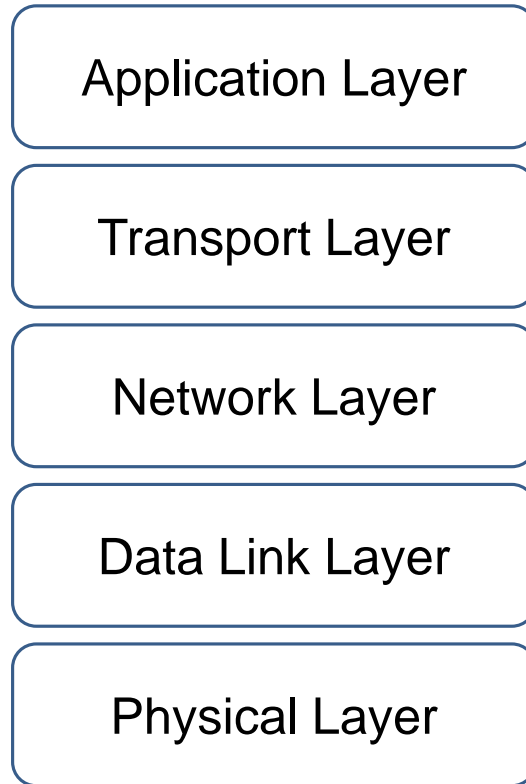


FIGURE 1.4: WSN communication stack.

other layers. These missions, adjustable parameters and possible feedback values will be described below for each layer.

### 1.2.1 Physical layer

The Physical layer defines how the message will be transmitted over the wireless medium, which includes, for example, modulation techniques, frequency selection and signal detection. Some examples of possible adjustable parameters are:

- Channel number (center frequency),
- Modulation,
- Transmission bitrate,
- Transmission power.

Some examples of feedback values which can be provided by the Physical layer are:

- RSSI,
- Result of the CRC check,
- Link Quality Indicator (LQI)[63].

As the Physical Layer activity is carried out by the radio chip, available adjustable options and feedback values depend on the hardware used.

### 1.2.2 Data Link Layer

Data Link layer is responsible for transmission control between neighboring nodes. This layer contains two sublayers: Logical Link Control (LLC) layer and Medium Access Control (MAC) layer. The LLC layer is in charge of the multiplexing of datastreams and providing an interface to upper layers. The MAC layer is responsible for the communication link establishment between two neighboring nodes and medium sharing rules. Another important task for MAC layer is Radio Duty Cycle (RDC) control. MAC protocol decides, when to switch the transceiver off in order to save the energy, and on to ensure communications.

Examples of adjustable parameters in the Data Link Layer are:

- Maximum number of retransmissions,
- Energy detection threshold to determine whether the channel is busy,
- RDC parameters (active/sleep duration).

Some examples of feedback values available at the Data Link layer are:

- Number of performed transmissions before success/failure,
- Success/failure of connection establishment,
- Failure caused by upper layer (NACK message)[63]

The functionality of the Data Link layer can be performed fully or partially by the RF module, or totally by the MCU.

### 1.2.3 Network Layer

The network layer is in charge of the construction of a route for a packet which has to pass through a multihop network. Routing algorithms on the Network Layer choose a next hop node by using a specific metric. Some examples of the parameters available in the Network Layer are:

- Maximum number of hops authorized,
- Period of sending for control messages.

Examples of feedback values available at the Network layer are:

- Distance to the Sink node in number of hops,
- Number of active neighbors.

In one-hop LPWAN networks, the routing functionalities are in general not used since all nodes are supposed to be able to communicate directly with a Sink. It can help to facilitate the development of node's firmware and save energy since RDC management is simplified. However, disabling of multihop capabilities negatively affects robustness of the system. Indeed, if for some reason a LPWAN sensor node is out of range (*e.g.*, a metallic obstacle is placed close to the node), all the messages from this node will be lost.

In multihop networks, Network Layer protocols can help to avoid interfered zones by choosing a proper next hop node. It is possible also to minimize the number of hops in order to decrease the probability of losing packets in intermediate transmissions.

#### 1.2.4 Transport Layer

Two main functionalities of the Transport Layer in WSN are reliability and congestion control. However, in contrary to computer networks, the nodes of a WSN are very constrained in terms of resources and energy consumption. Thus, the functionalities of this layer are often shifted to lower layers.

An example of an adjustable parameter of the Transport Layer is the maximum buffer size and as a feedback value - the current buffer length.

Congestion control is important in multihop networks. Indeed, for some applications, packets lost because of the overflowed node's buffer will be retransmitted, which will increase the medium load and interference level in the WSN.

#### 1.2.5 Application Layer

The Application Layer ensures the functionalities of the application of the WSN. Application layer solutions provide data for the final user. The application layer data is a payload to be sent through the network to the Sink.

Possible adjustable parameters in the Application Layer are related to the specific application and its functional requirements and can include:

- Data generation period,
- Data sampling rate,
- Data resolution for each sample,
- Data compression strategy.

Possible feedback values at the Application Layer can be related to the Quality of Service (QoS) (*e.g* delay, data losses).

The described adjustable parameters from all the layers can be controlled together in a coordinated way. In this case, the controlling algorithm

will use the feedback values from all the layers as an input, and then tweak the adjustable parameters of each layer. It is the basis of Cross-layer solutions[90].

This thesis is mostly focused on lower layers of communication stack (Physical and MAC). However, in Chapter 4, a communication protocol which implements some cross-layer functionalities for a real application of WSN will be proposed.

## 1.3 Particular WSN application usecase: LIRIMA PREDNET project

The Inria FUN<sup>3</sup> team of Inria Lille is collaborating with Stellenbosch University in South Africa in the framework of the project LIRIMA PREDNET<sup>4</sup>. The aim of the project is to develop a Wireless Sensor Network (WSN) that is able to operate in sparsely populated outlying rural and wilderness areas, for efficient monitoring and protection of resources and ecosystems. One case of application of the PREDNET WSN is related to the rhinoceros tracking and protection. These animals become more and more often victims of poaching because of their horns [27, 95]. In the present moment about 9000 rhinoceros live in the southern part of the Kruger Park (the habitat area is about 5000 square km ) - the potential zone of implementation of the system. Thus, the current average density of rhinoceros in Kruger Park is about 1.7 animals per square kilometer.

The WSN should help final user (biologists, zoologists) to regularly gather information about every animal of targeted specie (e.g. position, heart rate, acceleration data...) within the zone of monitoring (normal mode). Moreover, the WSN has to deliver the urgent alarm messages from animals in danger (alarm mode).

### 1.3.1 Functional requirements

South African specialists have established the following key requirements for the animal tracking system in order to fit the application needs and make it efficient:

- The data provided by different sensors (GPS, pulse oximeter, accelerometer ...) must be sent at least every 15 minutes. Data are gathered at different rates (depending on the sensor type) between transmissions.
- The WSN must be operational in the entire southern part of the Kruger Park where most of the rhino population lives.

---

<sup>3</sup>Self-Organizing Future Ubiquitous Networks, <https://team.inria.fr/fun/fr/>

<sup>4</sup>PREDator adhoc NETwork, <https://iww.inria.fr/prednet/en/>

- Weight of wearable device should not exceed 500 grams.
- Battery life must be guaranteed during several years.
- The robustness of communications must be guaranteed (especially for the alarm mode).
- While latency for the normal mode is not critical, the delivery time for an urgent alarm message must not exceed 1 minute.

### 1.3.2 Other wildlife tracking projects

Other wildlife tracking projects are described in literature. Even though the final aim of these projects is similar to the PREDNET project, there are several differences in the concept.

For example, ZebraNet project[70] aims to track wild animals in central Kenya. Nevertheless the project focuses mainly on zebras, the developed network could be applied for different kind of animals. The authors emphasize the fully mobile nature of the sensor network developed within the project. Not only end nodes (devices, carrying by zebras), but also base stations (the data sinks) are considered mobile. The challenge of this solution is the unknown time of the BTS availability. It is supposed that the base station can arrive close to the animals between noon and midnight. The nodes, thus have to search for a BTS during long time which is energy consuming. Moreover, that introduces huge delays in data collection (at least 12 hours). These factors make this solution unsuitable to meet the requirements of the PREDNET project (see the Section 1.3.1). This fact also makes ZebraNet solution unsuitable for urgent mode operation. Moreover, the weight of the equipment, carried by zebras was about 1.1 kg, which is also too high in PREDNET project.

In [30] an ultra low power WSN for tracking bats in the wild is proposed. Small size of the bats strictly limits acceptable maximum weight of the carried nodes to 2 grams including battery. Small battery size limits the amount of available energy in the node. To meet the energy limitations and lower the energy consumption of the nodes, a low power wake-up receiver is integrated in the carried by the bats devices. The collected data are sent to the ground base station when a bat carrying the node flies close enough to this latter. When it happens, the wake-up signal (which is sent periodically by the base station) is received by the low power receiver in order to activate the main transmitter and send the data. Small communication range with ground stations (about 50 m) leads to spontaneous communications in the system. Relatively high mobility of the bats along with small monitoring area (comparatively to the Kruger park) make the communication opportunity happen often. However, as it will be shown in Section 4.3.4, impossibility to cover all the habitat area in the Kruger park and relatively

low mobility of rhinoceros will cause high delays for message transmissions, which is unacceptable for the alarm messages in the framework of the PREDNET project.

Similar application for flying foxes (fruit bats) is described in [96]. The authors propose a 3-tier system containing mobile nodes installed on the animals, gateways and cloud service. In this case, the multihop communications are not provided which, as we will show in Chapter 4, makes impossible rapid delivery of alarm messages from uncovered by gateway zones. However, authors propose to adapt the behavior of the nodes depending on the current state of charge which can evolve due to both, energy consumption and energy harvesting. This option can be useful in the framework of PREDNET project.

In [103] an inverse-GPS tracking system for birds and small mammals is proposed. The system allows localizing effectively the animals within large areas. However, the project is not focused on data collecting and transmissions, which is required by the PREDNET project. Moreover, redundant coverage of the area is required in the proposed system, which, as we will show, is not always possible in the Kruger park.

Another project proposes a solution to monitor migrating whooping cranes[8]. This solution uses less sensors and has less strict constraints in terms of delivery period (it has to be less than 24 hours, which is much bigger than 15 minutes required in PREDNET project). The size limitations are also different due to the difference of sizes of animals. Also, in this project the authors propose to use GSM cellular technology with another short range 802.15.4 radio to send the data. These solutions are not suitable for PREDNET project due to the short range of 802.15.4 technology and high power consumption of GSM. Moreover, GSM does not allow to manually adjust the communication parameters. The problem of GSM for PREDNET project is related also to not full coverage of Kruger park zone by cellular networks.

Some wildlife animal tracking solutions are based on the satellite technologies (*e.g.*, Argos, Iridium, Globalstar) [40], [28]. Even though these solutions ensure a good coverage of the target area, they have important drawbacks. First, the hardware installed on the animals is very expensive, which makes impossible to equip all the animals in the target area. Second, the energy consumption of these devices is high. That leads to the short lifetime of the nodes, and, thus, makes this kind of solutions unsuitable for the PREDNET project.

## 1.4 LPWAN networks

As mentioned in Section 1.3.1, one of the peculiarities of the PREDNET project context is the huge target area. The proposed solution has to ensure packet delivery from any position of the entire southern part of the

Kruger park. Thus, well known in the WSN short range solutions (*e.g.*, IEEE 802.15.4 based transceivers) will not be applicable in the framework of the PREDNET project due to the small coverage. Indeed, with a given node density (1.7 animals per square km), the use of short range communication can cause a high number of isolated nodes (the nodes which are not in range of any other node). In this case, the delivery of the urgent alarm messages from the animal in danger to the BTS will be impossible even with multihop strategy. Thus, long range communication technology ensuring extended coverage is required. As mentioned before, cellular network (GSM, NB-IoT, LTE-M) and satellite based solutions are not suitable for the project due to both, high energy consumption and the hardware costs. So, the LPWAN technology [87],[54] seems to be the most appropriate to meet functional requirements of the project. Some examples of the LPWAN technologies will be presented in the next section.

### 1.4.1 Sigfox

Sigfox [92] is an operator based LPWAN solution. At the physical layer the Ultra Narrow Band (UNB) signals with the DBPSK (Differential Binary Phase Shift Keying) in the Sub-GHz license-free bands are used. The transmission rate is fixed to 100 bits/s which corresponds, thus, to the 100 Hz of occupied signal bandwidth, which results in high receiver sensitivity and long range transmissions. However, the operator-based model is the important limitation for the PREDNET project. Indeed, the coverage of the area is based on the operator decisions. Thus, the possible coverage of the Kruger park by the Sigfox network is not guaranteed. Moreover, message payload is restricted to 12 Bytes, which limits possible extension of the list of sending measurements.

### 1.4.2 Ingenu (ex. RPMA)

RPMA (Random Phase Multiple Access) is a proprietary technology developed by On-Ramp company renamed to Ingenu [66]. The technology is based on DSSS which uses Gold Code. The used modulation is DBPSK. The time-slotted structure is used. Multiple access is performed by adding a random delay to the transmitting signals, which ensures up to 1000 transmissions per slot. Technology operates in the worldwide available 2.4 GHz ISM band. However, the important drawback of this band for the PREDNET project is high attenuation of the 2.4 GHz signals by water and plants which are abundantly present in the Kruger park.

### 1.4.3 LoRa

LoRa physical layer technology is a proprietary solution based on CSS (Chirp Spread Spectrum) modulation technique. The technology implements also FEC (Forward Error Correction) and CRC (Cyclic Redundancy Check) to ensure high receiver sensitivity (up to  $-148$  dBm) and robustness of communications, which leads to high transmission ranges. Due to the high sensitivity of receiver nodes, LoRa nodes are able to receive signals below the noise floor. Thus, classic CCA (Clear Channel Assessment) based on energy detection (implemented in IEEE 802.15.4 transceivers, e.g. TI CC2420) cannot be used to detect ongoing transmissions. The proprietary CAD (Channel Activity Detection) based on preamble detection is, thus, developed.

The user is able to tune some communication parameters in order to set the optimal values of communication range, energy consumption and data rate to meet the requirements of the specific application. The following settings are available:

- Carrier frequency (CF). Depending on used transceiver model, 3 different radio bands are available: 137 – 175 MHz, 410 – 525 MHz and 820 – 1020 MHz, covering not only the most important Sub-GHz ISM bands, but also the radio amateur and license based bands.
- Radio bandwidth (BW). Depending on the transceiver model, it is possible to choose between up to 10 available values, from 7.8 kHz to 500 kHz. Higher values of BW correspond to higher chip rates and lower receiver sensitivities and have lower requirements for stability of the crystal oscillator.
- Spreading Factor (SF). SF is a parameter representing the ratio between symbol rate ( $R_s$ ) and used bandwidth (BW), as expressed in [1.1](#):

$$R_s = \frac{BW}{2^{SF}} \quad (1.1)$$

Each symbol carries SF bits and chip and sent per second per Hz of bandwidth. Depending on the transceiver model, SF from 6 to 12 can be chosen. Higher SF values correspond to more robust communications but lower data rates. In [88] and [89] the spreading factors are claimed orthogonal to each other, but [16] shows that the orthogonality is not perfect.

- Coding Rate (CR). CR is a parameter of FEC, determining the redundancy of the correction code. It can be chosen between 1 and 4 to determine the coding rate as follows:

$$CodingRate = \frac{4}{4 + CR} \quad (1.2)$$

The CR parameter impacts the transmission bit rate ( $R_b$ ) as expressed in 1.3:

$$R_b = SF * R_s * \frac{4}{4 + CR} \quad (1.3)$$

- Preamble length. It is possible to set the preamble length expressed in number of symbols. The minimal preamble length corresponds to 4.25 symbols. Longer preamble increases the probability of detection of the packet.
- Transmission power. The transmission power can be set between -4 and 20 dBm with a step of 1 dB.

Among different LPWAN solutions, the LoRa radio [1] has been chosen for its flexibility and hardware/software availability. Moreover, this latter allows to deploy a private network with a custom MAC layer protocol. The large number of available parameters listed above provides potential to develop adaptive communication protocols on top of LoRa physical layer.

## 1.5 Contributions of this thesis

In our opinion, the interference will be the most important challenge for WSN and IoT in future 10 years. Indeed, interference is directly related to the number of devices and technologies sharing the same bands. Since the number of connected devices is growing, the pernicious impact of the interference will become stronger rapidly with time. An efficient solution to avoid the impact of interference should be then proposed in priority.

In this thesis we answer the following questions:

- What is exactly the impact of the interference on the lifetime of the WSN nodes?
- What are the available parameters of the WSN nodes to adjust dynamically in order to decrease the impact of the interference?
- What are the indicators that can be used to make a right decision regarding the parameters to adjust?

The contributions of this thesis can be summarized as follows:

- We evaluate experimentally the impact of the interference on the energy consumption of a WSN node,
- We study the evolution of the interference level depending on time, used channel and position of the WSN node,
- We develop, implement and evaluate an adaptable multihop Cognitive Radio (CR) solution for WSN,
- We develop and evaluate WildMAC - an adaptable MAC layer protocol customized for the wildlife animal tracking in the framework of the LIRIMA PREDNET project.

## 1.6 Structure of the thesis

The present thesis is organized as follows:

- In Chapter 2 we present an experimental study of the interference impact on the energy consumption, and, thus, the lifetime of the WSN node.
- Chapter 3 is focused on the study of the multi-armed bandit solutions applied to the WSN Cognitive Radio setup. Different solutions are evaluated via both, simulations and WSN hardware implementation. The Thompson sampling based solution is extended to the multihop WSN scenario and evaluated during the EWSN Dependability Competition.
- Chapter 4 presents the WildMAC protocol for LIRIMA PRED-NET wildlife animal tracking project. The MAC protocol is evaluated via WSNet simulations based on the parameters obtained during the field tests based on the LoRa hardware.
- Finally, Chapter 5 concludes this thesis and presents perspectives for the future works.



## Chapter 2

# Experimental study of interference impact on the energy consumption in WSN

### 2.1 Chapter introduction

In Chapter 1 we mentioned two main issues for WSNs:

- Interference due to growing number of devices and RF technologies operating on the same radio bands
- Limited available energy due to the impossibility or difficulty of battery charging/replacing - the main source of power for WSN nodes

These two problems are related. Indeed, the interference impacts not only the Quality of Service (QoS) and reliability of communications, but also the energy consumption of nodes. Interference causes packet losses. In most of WSN applications, lost packets need to be re-transmitted and every re-transmission is an energy and bandwidth waste. In [85, 109], the authors mention the relationship between interference and energy consumption. To the best of our knowledge, existing works on the impact of the interference on the energy consumption in WSN are mainly based on simulations and theoretical analysis. These methods provide only estimated data based on averaged values of energy consumption from datasheet and cannot take account of the energy consumption behavior of radio devices, which depends on multiple factors. Contrariwise, the hardware measurements provide real and accurate values of the energy consumption. An example of the measured current values is shown in Fig. 2.1 where two independent curves (for radio and microcontroller) are presented. We can notice that the observed level of current is not constant: important fluctuations are present.

In this chapter we present the following contributions:

- we developed an experimental measurement platform which enables to measure the energy consumption of different components of WSN nodes independently as well as the interference level and device state;

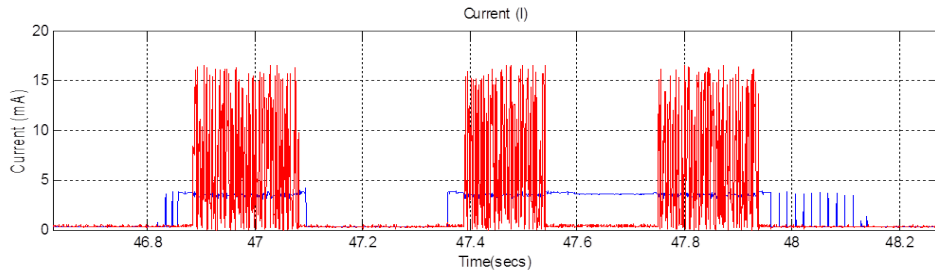


FIGURE 2.1: Example of currents of CC2420 radio module (red curve) and MSP430 micro controller (blue curve) measured by Synergie platform.

- we highlighted and quantified the relationship between interference and energy consumption from an experimental point of view in both ideal (anechoic) and real (office) environments;
- we evaluated experimentally the energy performance of the X-MAC protocol [19];
- we isolated the energy measurements for each component of the WSN node and analyzed exclusively the energy consumption of radio module to exclude the activity of other circuits on the measurements;
- we developed a distributed interference measurement platform and provided the results of a long scale interference measurements (one week).

In Section 2.2 the existing related works will be described. Then, in Section 2.3 the developed measurement platform that we used is described. Section 2.4 details experimental setup and Section 2.5 presents measurements results. In Section 2.6 the long term interference measurements will be described. Then, Section 2.7 concludes this Chapter.

## 2.2 Motivation and Related works

If the impact of interference on the QoS in WSN is described in literature, the consequence on energy consumption is not studied deeply. In this work, we focus on the impact of interference in 2.4-GHz band on the energy consumption of WSN nodes. The coexistence of several wireless communication technologies in the 2.4-GHz band as Wi-Fi (IEEE 802.11), IEEE 802.15.4, Bluetooth, wireless cameras, among others, as well as other sources of interference (*e.g.* microwave oven) in a same environment is a serious issue. In [93] and [59], this problem is studied by calculating the packet reception rate (PRR) according to the interference level and the technology selected. In [55], the impact of the interference from Wi-Fi, Bluetooth and microwave ovens on the PER of ZigBee (IEEE 802.15.4) transmitters is studied. The case of buildings was proposed. Besides, M. Petrova *et al.* present in [82]

an interesting work about the impact of the interference caused by IEEE 802.11g/n technologies on IEEE 802.15.4 networks. In this study, the authors calculate the PRR according to different parameters as the selected IEEE 802.15.4 channel, distance or angle between the nodes and the interference makers. However, in none of these works, the study of the relation between the impact of interference and the energy consumption is done.

In [15], the authors developed the JamLab platform, a low-cost solution to measure and regenerate the interference patterns from real environment. In this work, the energy consumption aspect is related to interference measurements and only simulated using a software solution proposed in [35]. The authors use the PRR as a metric to evaluate the interference impact. However, only final PRR values (after taking retransmissions into account) are provided. Thus, the physical layer frame-level precision is not achieved. In our work, we are able to assess the energy consumption of every physical transmission or retransmission. In [38] the authors also use JamLab to test a multi-hop configuration with 11 nodes and two types of interferers (Wi-Fi and microwave oven) simulated by several nodes, providing a relation between energy and interference, but the energy consumption is estimated by a software tool called "Contiki Powertrace built-in power profile" [34] which cannot provide a high level of accuracy since it is based on average consumption values from datasheet.

The authors of [109] propose a solution to measure the interference level in order to decrease its impact on QoS and energy consumption of WSN nodes. However, the quantitative evaluation of the impact of interference on energy consumption of wireless communication is not provided. As in [15], the energy consumption of interference measurements part is only evaluated theoretically, using a model from [58].

In [85], the increase of energy consumption due to interference is illustrated by calculating the excess energy through a home automation scenario that features a simple retransmission without any radio duty cycle (RDC) protocol, which is important to implement in order to increase the battery life. Moreover, the energy consumption of multiple retransmissions is only estimated as a product of the energy of single transmission by the number of transmissions, which we will show it is not necessarily true. None of

these works either experimentally studied the energy consumption of the node nor combined the energy and interference measurements. Our work experimentally studies the interference from real devices in relation with the energy consumed by the nodes of WSN when the retransmissions and the packet loss happen.

Another contribution we propose is the ability to analyze the energy consumption of each single module of the node independently. It allows us to focus exclusively on the energy consumption of radio module - the main source of energy waste in case of communication problems. In contrary to

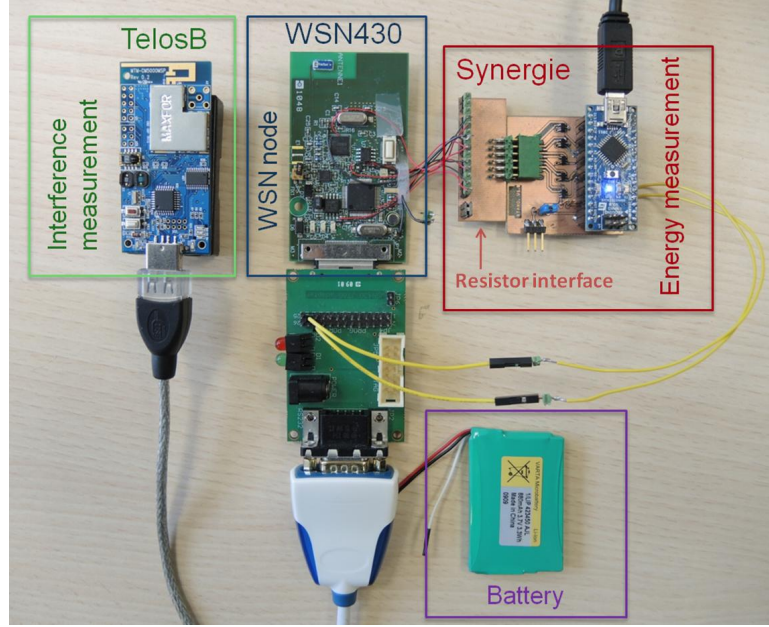


FIGURE 2.2: Elements of the measurement platform.

the works described in [21], [113], [39], [91], we are able to exclude the energy consumption of other modules which are not pertinent for this study and which can alter the results of measurements.

### 2.3 Description of the platform

Two sets of devices have been used to complete the experiments of this work: one for the transmission part (TX) and the other for the reception part (RX). Both sets are composed of three different devices each as shown on Fig. 2.2:

- 1) **WSN430 sensor node** as the node under evaluation, used in FIT IoT-lab testbed [104]. It contains an MSP430 microcontroller, a CC2420 radio [23], luminosity and temperature sensors, a microphone and 3 LEDs. This node can be controlled by embedded operating systems (OS) for WSN nodes, *e.g.* Contiki, TinyOS, FreeRTOS or Riot.
- 2) **TelosB mote** [83] to measure the interference. It features a similar hardware structure as WSN430, programmed with a Contiki [31] code that reads Received Signal Strength Indicator (RSSI) values at the center frequency of the channel used by the WSN430 nodes. This option is implemented in the CC2420 chip, which provides average values of electromagnetic energy measured during  $128 \mu\text{s}$  intervals. In our case, we were able to achieve an operating rate of 4000 samples per second.
- 3) **Synergie platform** [65] developed in IRCICA laboratory to accurately measure the energy consumed by each component of a WSN node. It is based on commercially available low-cost and low-power components and

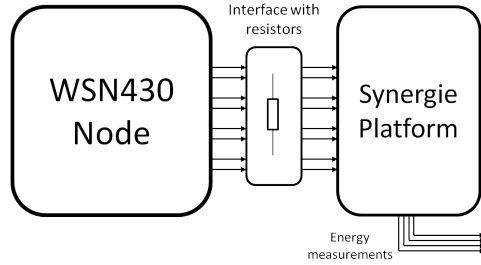


FIGURE 2.3: Connection between the WSN430 node and Synergie platform

consists of a 10-bit Analog-to-Digital Converter (ADC) embedded in an ATmega328p microcontroller and five operational amplifiers ZXCT1086 to enable five independent measurements. To recover the energy measurements from the node, Synergie takes the voltage from the terminals of resistors added before the power supply input of each component of the circuit. The node under evaluation and the measurement platform are connected by the resistor interface which makes the measurement unit compatible with various WSN nodes. The node is also connected to the Synergie platform via General Purpose Input-Output (GPIO) lines in order to synchronize energy measurement data with different states of the device (*e.g.* beginning of the (re-)transmission, dropped packet). GPIO lines provide this information directly from the code programmed in the micro-controller of WSN430. The measured values and GPIO codes are transmitted to a computer through a serial link. Synergie platform is able to acquire the energy measurement data at the rate of 1500 samples per second for the five components in parallel. Then, the synchronized energy measurements from the hardware are analyzed to obtain the current required by each component independently. The energy consumption of the node is finally calculated. For this work, we take the value of the resistors as well as the voltage used in the circuit into account in order to measure the current. These resistors are chosen according to the maximum current value of each electronic component in the node and the characteristics of the ADC included in the micro-controller of Synergie platform. The diagram of the connections between the WSN430 node, the interface of resistors and the Synergie platform is depicted in Figure 2.3.

In the following, we analyze the average values of RSSI and energy consumption for each application layer packet (including retransmissions). These values are calculated between the end of previous packet and the end of current packet which are delimited using GPIO signals. The timestamp values provided by the ExtraPuTTY software [45] are used to estimate the packet duration.

## 2.4 Experimental setup

In this section, we detail our experimental setup (see Figures 2.4a and 2.4b).

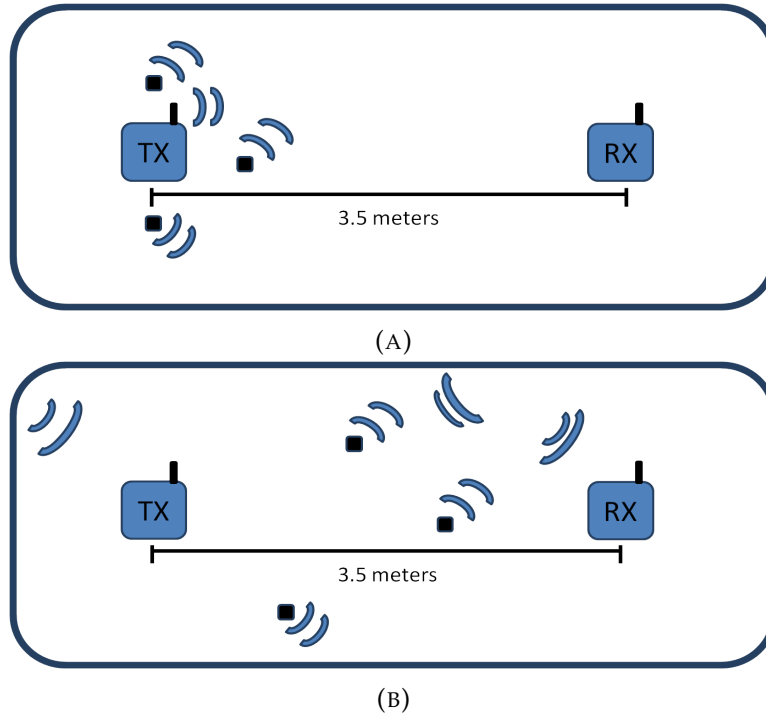


FIGURE 2.4: Scenarios of the experiment: a) in anechoic chamber, b) in office-type lab environment.

We have carried out a unicast communication between two Contiki-driven WSN430 nodes: one sender (TX) and one receiver (RX). Both nodes use Rime protocol [32] on a network layer, X-MAC Radio Duty Cycle (RDC) management strategy and Carrier Sense Multiple Access (CSMA) Medium Access Control (MAC) algorithm as parameters of Contiki communication stack. At physical layer, data are represented as IEEE 802.15.4 [64] packets. The packets are generated every second by TX and include a 19-byte payload, a 6-byte Rime header and 15-byte MAC header (for 16-bit addressing). The total size of each packet is, thus, 40 bytes. Packets to send are stored in a 24-packet capacity buffer.

An example of X-MAC transmission is shown in Fig. 2.5. Following the X-MAC protocol, a transmitting node wakes up when it has a packet to transmit and sends a sequence of beacons (X-MAC preamble) containing the destination MAC address. Once the destination node is awoken, it decodes the MAC address from the beacon and sends an early acknowledgement (ACK) back to TX node to announce its availability to receive the data. TX node can then start to send its data packet, that is acknowledged by RX in case of correct reception. Otherwise, TX repeats the procedure, after a random back-off time, up to 3 times (IEEE 802.15.4). After 3 non-ACKed transmissions, the current data packet is dropped (deleted from the buffer). It is important to mention that the size of an ACK message is 11 bytes [42], which is about 4 times smaller than a data packet and, thus, having shorter on-air time, which means lower probability to loose an ACK packet. A 125 ms duty cycle was set as a parameter of X-MAC protocol. It means that RX

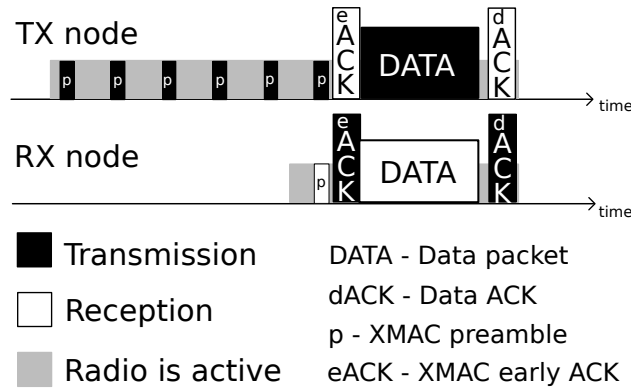


FIGURE 2.5: Example of a successful X-MAC transmission.

wakes up every 125 ms to check whether there is a packet to receive on the medium or not. By default, in Contiki, both RX and TX nodes are able to receive packets, so, both nodes wake up every 125 ms. To exclude the energy impact of listening activity at the TX side, we disabled this ability for the TX node. The TX node, thus, sends packets periodically (every second), listens to the ACK message and then goes to the sleep mode.

We performed two similar sets of measurements in two different scenarios: in the first case, later referred as *ideal case*, the measurements have been carried out in an anechoic chamber whereas the second experiment, referred as *real case*, has been completed in an office environment of IRCICA laboratory. Every case is detailed in following subsections.

In the following, we will call "primary" the useful link under study.

#### 2.4.1 Ideal case scenario

A first set of experiments has been carried out in an anechoic chamber. The first objective is to study the behavior of the primary WSN (TX and RX nodes) without any external sources of interference. Then, we add progressively up to three interfering XBee [108] / IEEE 802.15.4 nodes belonging to another (secondary) WSN. These nodes operate in the same channel as the primary TX and RX nodes. The packets sent by the nodes included in the XBee network contain a payload of 100 bytes, which corresponds to the maximum payload size for a packet according to the IEEE 802.15.4 standard, and they are transmitted every 10 ms. This causes serious interference in the channel because of the big size of interfering packets. Indeed, 128 bytes (for payload and header) of a packet transmitted at 250 kbps is equivalent to a slightly more than 4 ms of on-air time. This channel occupation duration is bigger than the time required to send a smaller primary network packet. In Section 2.5, we show the impact of this interference on the primary nodes under evaluation.

The scenario for the experiment in the anechoic chamber is depicted in Figure 2.4a. In this scenario, the distance between TX and RX nodes is 3.5

meters whereas the interfering nodes are situated near the TX, at a distance of 20 centimeters.

### 2.4.2 Real case scenario

The same primary nodes used in ideal case have been placed in a laboratory environment. In this case, we can find some external sources of interference in the building as Wi-Fi Access Points and microwave ovens situated near the test setup. Interfering network is composed by the same number of nodes as in ideal case scenario: three nodes with XBee modules working in the same channel as the main nodes and sending packets every 10ms with 100 bytes of payload.

The distance between TX and RX nodes is once again set to 3.5 meters as shown in Figure 2.4b, but, in this case, the interfering nodes are situated further from TX node. They are fixed in different places between both nodes. The goal of this change of position in the interfering nodes is to study the behavior of the system in a real scenario, with a secondary WSN situated in realistic positions.

## 2.5 Measurement results

### 2.5.1 Measurement approach

In this subsection, data measurements are described using the ideal case example. During the experiments, we collect packet statistics on the number of retransmissions (on TX side) and the number of received duplicated packets (on RX side) for each generated application layer packet. This information is collected from the WSN430 node via serial connection to the computer.

Statistics for the anechoic chamber scenario are presented in Table 2.1.

Each row in Table 2.1 represents the number of physical transmissions of a single application layer packet on the TX side as follows:

TABLE 2.1: Number of transmissions per packet sent by TX and of received duplicated packets on RX.

		'1' 1 RX	'2' 2 RX	'3' 3 RX	'4' 0 RX
'1'	1 TX	745			
'2'	2 TX	203	24		
'3'	3 TX (success)	131	20	1	
'4'	3 TX (fail)	77	10	0	330

1. Packet type '1' corresponds to the situation when a packet is sent just once, *i.e.* well received by RX and the ACK sent by RX is well received by TX. This is the ideal situation.
2. Packet type '2' corresponds to two transmissions of a packet, whether a data frame or an ACK is lost.
3. The same logic also applies for Packet type '3', TX sends three times the same single packet and TX receives the ACK only after the third transmission.
4. For packet type '4', three transmissions are done but TX never receives the ACK. In this case, two options are possible: either one or several data frames are received by RX but the ACK messages are lost or no data frame is well received by RX.

Each column in Table 2.1 corresponds to the number of times a single packet is received by RX as follows:

1. In the columns, packet type '1' describes the situation when a packet is received once, the best situation.
2. Packet type '2' occurs when a single packet arrives twice to RX due to the loss of an ACK.
3. Then, packet type '3' represents one packet received and two duplicates of the same packet.
4. Finally, packet type '4' corresponds to "no packet received".

The detection of packet retransmissions, duplicates and losses requires an accurate synchronization. This synchronization between TX and RX statistic data was possible thanks to the timestamps created by the ExtraPuTTY software as well as the signals generated by the GPIO lines connected between WSN430 node and Synergie platform. Then, synchronized values enable us to combine the type of packet on TX and RX sides.

Let us further analyze Table 2.1. In this example, most of the transmitted packets correspond to the combination '1'-'1', where the used format is 'TX'-'RX', *i.e.* type of packet on TX and in RX sides respectively, for the same single packet (see the Figure 2.6). Then, '1'-'1' represents the ideal situation, where a packet sent by TX is correctly received by RX after first trial and the corresponding ACK is received by TX. '2'-'2' situation appears rarely because of the short length of the ACK frames. We observe as well that the event '3'-'2' occurs less often than '3'-'1' whereas '3'-'3' appeared only once in this example. Indeed, when the channel occupancy significantly increases because of interfering signals, the probability to lose a data frame is higher than to lose an ACK, due to the difference of size, *i.e.* on-air time. As the case of '3'-'3', the combination '4'-'3' is unlikely to appear since the

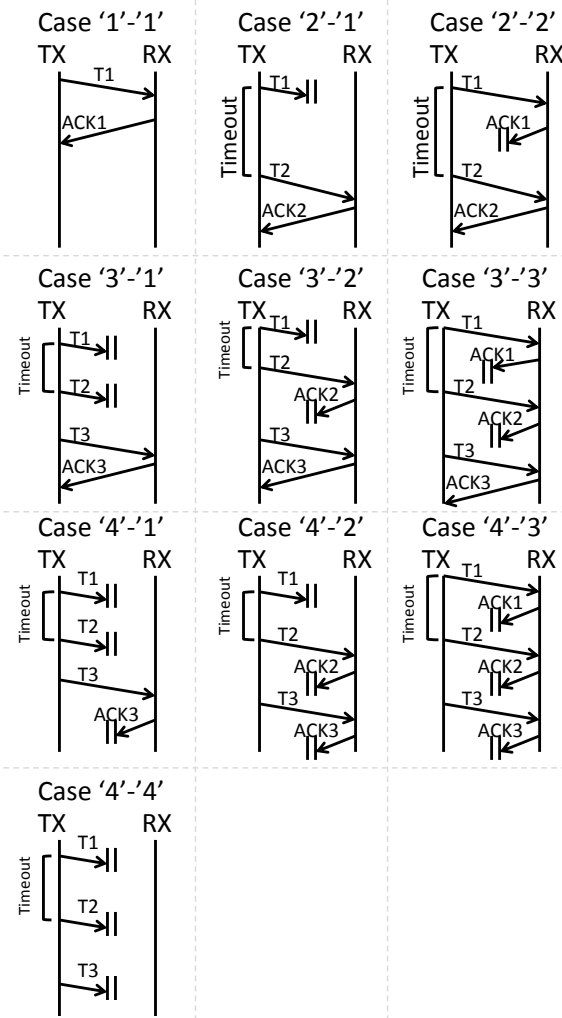


FIGURE 2.6: Examples of combinations of type packets TX-RX.

probability to lose three consecutive ACK messages while receiving three duplicated data frames is very small. Therefore, the case of '4'-'3' never appeared in this experiment. Finally, '4'-'4' corresponds to the situation when the interference in the channel makes the communication impossible. No data packets are received by RX and, then, ACK packets are not sent. We observe that Table 2.1 corresponds to a triangular matrix, since the number of receptions cannot be greater than the number of transmissions.

### 2.5.2 Ideal case

Synchronized measurements of energy consumption of the radio module, interference level and packet transmission statistics are presented in Fig. 2.7. The total number of packets for each type ('1', '2', '3' and '4') is indicated in the legend. Fig. 2.7a represents the average energy consumed by the transmitter radio as a function of the average measured RSSI for each packet. These average values are computed during the whole packet transmission (including retransmissions) for each application layer packet.

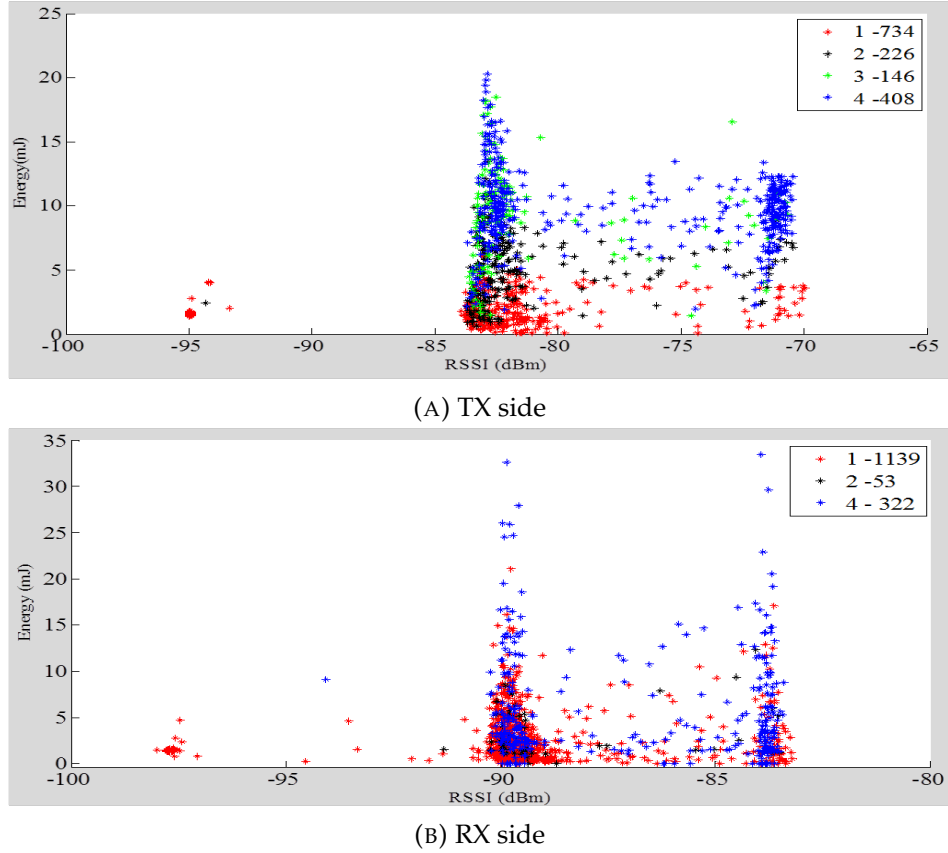


FIGURE 2.7: Energy consumption vs RSSI per packet type in ideal case.

These different packet types of transmissions are presented by different colors (see Table 2.1). We can notice three distinguished sets of points. The first set is situated in the zone of low interference (around  $-95$  dBm) and low energy consumption. This set contains the packets successfully received after one transmission and only one packet retransmitted once. These packets were transmitted during the first part of the experiment, carried out without any interference (thanks to anechoic chamber ideal characteristics), which explains the high transmission success rate. Second set of points is situated around interference level of  $-83$  dBm. So, the gap between these two sets of points is bigger than  $12$  dB. No packets are situated in this zone because the interfering XBee node is switched on suddenly. The second set of points corresponds to the cases when one to two nodes interfere. In this case, due to the increased level of interference, we can observe an important number of packets retransmitted once or twice (types '2' and '3' respectively) as well as dropped packets (type '4'). Average energy consumption is also significantly increased. The third set of points is situated near the interference level of  $-72$  dBm. This set of points is related to the case of three interfering nodes. In this case, we can observe an important number of dropped packets prevailing over other packet types.

A similar graph, presented in Fig. 2.7b, is obtained for measurements on

RX side. In this graph, different numbers of receptions (duplicates) for every packet are represented by different colors (see Table 2.1). As in TX case, three sets of points can be observed. First set is represented by packets received once (without duplication). Second and third sets of points contain important number of never-received packets (packet '4'). The average interference level corresponding to these sets of points is lower than in TX case (-97, -90, -83 dBm vs -95, -83, -72 dBm respectively) due to an increased distance between the transmitter, interference sources and the interference measuring module at the RX side.

### 2.5.3 Real case

Similar graphs are provided for the real case. Fig. 2.8 represents different types of packets as a function of energy consumption and measured RSSI on TX and RX sides. As for the ideal case, we can clearly notice three sets of points. Since the conditions of the experiment are different, these sets of points are shifted in RSSI axis in comparison with the set of points in the ideal case. We can also notice a more significant variance of RSSI values than in the ideal case due to the presence of signal reflections and external sources of interference that we cannot control. The same explanation also holds for the presence of retransmitted and lost packets in the low interference zone, where no XBee module is active. In this case, this zone corresponds to the set of points around -93 dBm RSSI level in Fig. 2.8a. At RX side (see Fig. 2.8b), we can also observe an increased variance of energy and RSSI. Three different sets of points are differentiated, but we can observe a more dispersed scattering of points. However, the gap between the second and the third set (sets situated around -89 dBm and -83 dBm respectively) is not as clear as in the ideal case. This is also due to the external sources of interference.

### 2.5.4 Measurement analysis

#### TX side

Fig. 2.9 represents the distribution of different types of packets as well as the total energy consumed by each type of packet during the experiment at the TX side for ideal and real cases respectively. The total energy consumption per type of packet is calculated from the average energy consumption and the number of packets belonging to this type.

From Fig. 2.9, we can notice that the distribution of the total energy consumed by the TX device is different in ideal and real cases. However, the average energy consumed for each packet type is almost the same in both scenarios. The difference of total energy consumption is due to a higher packet loss rate in the real case. We observe also that in the ideal case, half of

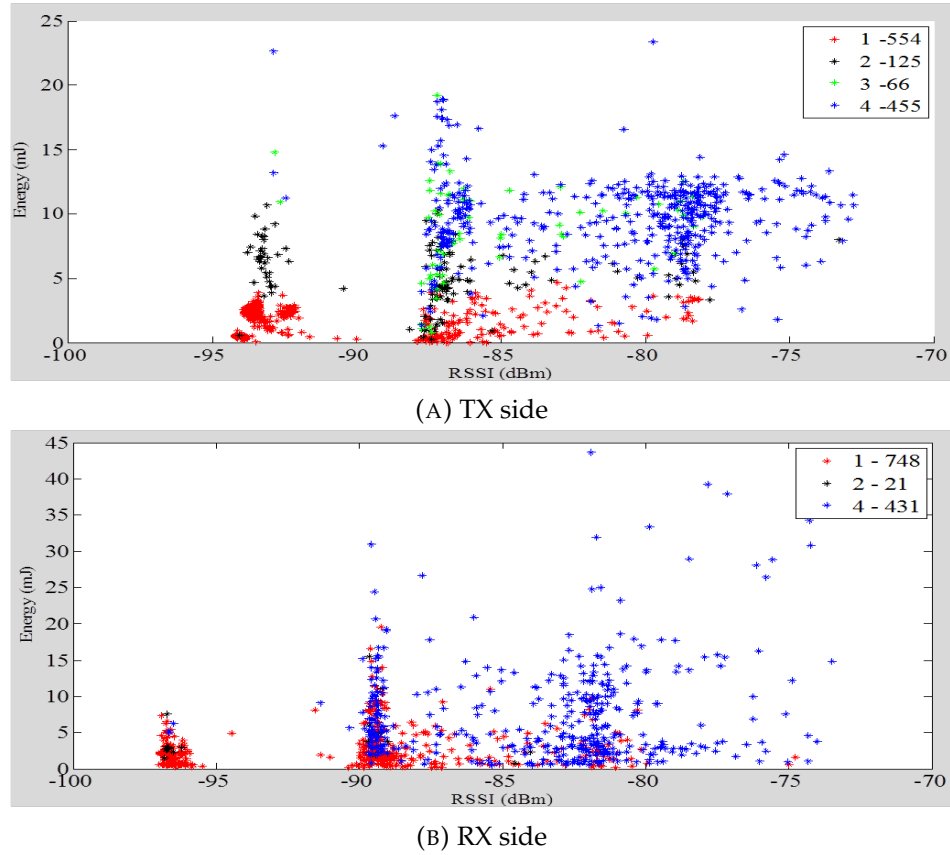


FIGURE 2.8: Energy consumption vs RSSI per packet type in real case.

the total energy (50.6%) used by the radio module during the entire experiment was related to dropped packets (type '4'), *i.e.* the packets which are sent three times but for which the ACK message is never received. According to Table 2.1, there is a high probability that these packets are, indeed, lost. In other words, near 50% of the TX node energy is wasted even though only a quarter of the packets (26.9%) is lost (packet type '4'). The real case is even worse: we observe 65.1% of wasted energy because of this type of packets. On the other hand, we can notice that for both, ideal and real cases, the first-try acknowledged packets (best case) represent almost half of the sent packets (48.5% and 46.2% resp.). Even so this is the largest group of packets, it represents only 17% of the energy consumption in the ideal case and 16.4% in the real case. Another important observation is related to the low percentage of packets successfully acknowledged after three trials (9.8% for ideal and 5.5% for real case). Since the number of transmissions is limited to three, after two trials, the only possible options are success or failure (packet type '3' and '4' resp.). We can notice that the probability of failure after two unsuccessful transmissions is much higher than the probability of success. That impugns the pertinence of a third transmission. The percentage of success after second trial is also relatively low comparatively to first-time acknowledged packets. This questions the efficiency of the re-transmission policy when interference is high.

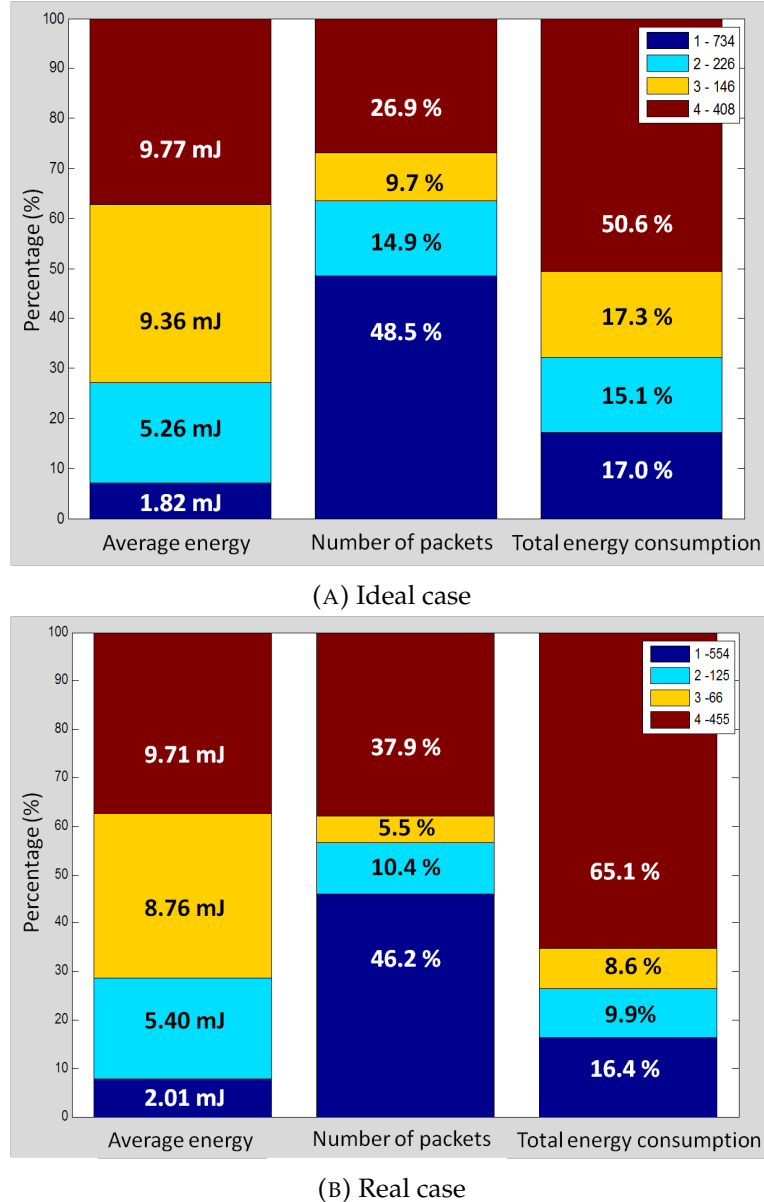


FIGURE 2.9: Avg. energy, total number of packets and total energy per packet type on TX side.

### RX side

Fig. 2.10 represents the distribution of different types of packets as well as the total energy consumed by each type of packet during the experiment at the RX side for ideal case. The total energy consumption per type of packet is calculated from the average energy consumption and the number of packets.

As we can notice from the figure, the packets type '4' do not represent the largest group of packets in contrary to TX side (remember, in case of RX, the packet type signifies the number of duplications for a given application layer packet). Indeed, in our experimental setup the interfering nodes were situated much closer to the TX side. Also, we observe zero packet type '3' packets. In fact, duplications happen when the data packet is received

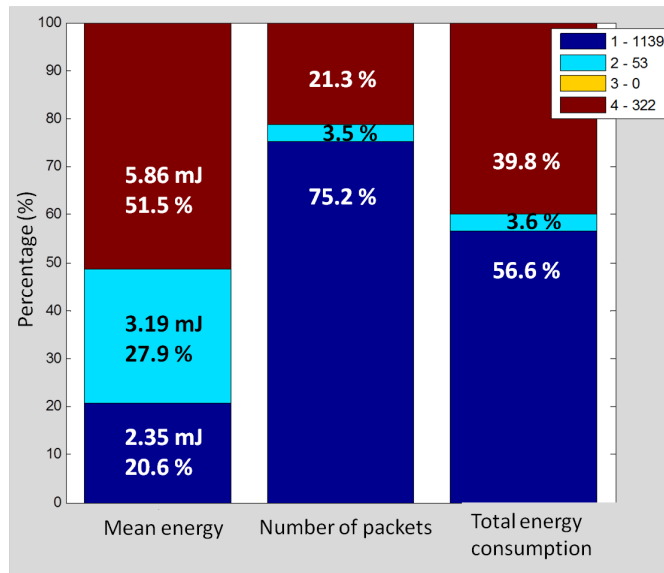


FIGURE 2.10: Energy statistics per type of packet on RX side: average energy, number of packets and total energy consumption. Ideal case.

correctly by the RX device, but the ACK message is lost, thus the packet is retransmitted. Since the size (and, thus, the on-air duration) of the ACK packet is much shorter than the one of data packet, the probability to lose an ACK packet is smaller than the one for the data packet. In case of packet type '3', 3 data packets were received well, whereas 2 small ACK packets were lost, which is unlikely to happen. We can notice also, that the packet type '4' corresponds to the type with the biggest energy consumption. It can be caused by the fact that in case of high interference the RX node receives the same retransmitted packet many times, but each time the packet is dropped due to the bad CRC. However, each reception causes additional energy consumption.

In the following we will focus only in the TX part.

### 2.5.5 Lifetime evaluation depending on RSSI

Based on experimental data, we calculate the relative frequencies for each packet type, with different values of RSSI. In conjunction with the mean energy necessary for a given packet type, this will allow us to determine the lifetime of the node.

#### Ideal case

According to the measurements of energy consumption and RSSI of the packets obtained on TX side for the ideal case, as shown in Fig. 2.7a, we calculate the distribution of the type of packets ('1', '2', '3' and '4') over different RSSI windows. Generally, the windows are chosen by starting from  $-95$  dBm and by increasing with a step of 5 dB. In the ideal case, no packets are situated in the  $[-90, -85]$  dBm window. Consequently we merge this

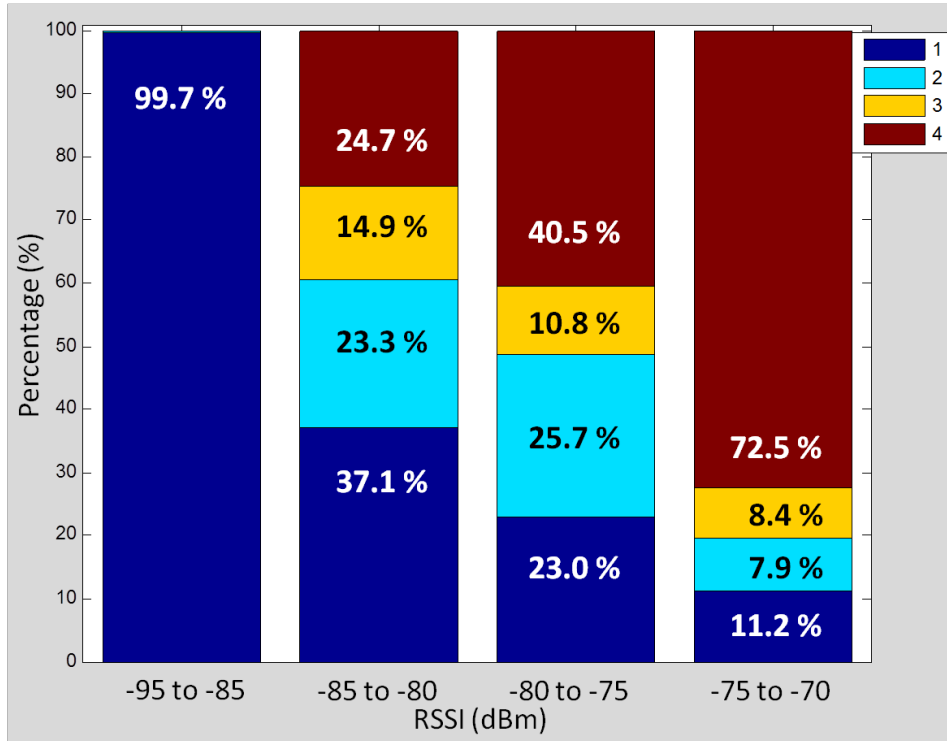


FIGURE 2.11: Packet distribution per RSSI window on TX - Ideal case.

window with the  $[-95, -90]$  dBm window. Fig. 2.11 shows the distribution of the packets with the estimated values of the type frequencies.

In Fig. 2.11, we observe that the type '1' packets (in dark blue) in the  $[-95, -85]$  dBm window correspond to almost 100% of packets. This is coherent because the experiment was completed in the anechoic chamber. In the  $[-85, -80]$  dBm window, the percentage of packets '1' decreases considerably but continues to be the predominant type. The number of other packet types is increased significantly, especially types '2' and '4' with a relative frequency of 23.3% and 24.7%, resp. In the  $[-80, -75]$  dBm window, packets '1' decrease to 23% whereas type '2' and, mainly, '4' continues to increase. The  $[-75, -70]$  dBm window corresponds to the zones where the interference becomes higher due to the activity of the three interfering XBee modules. In this window, the dominant packet is '4' with 72.5%, which means that three out of four packets sent with this level of interference are lost despite three transmission trials. We also observe the low percentage of packet type '3' in all the windows. This constitutes an important issue because the probability to receive a packet successfully after three tries is low while the energy consumed by this type of packet is very high. At this point, we can conclude that having transmission limit set to three is not efficient in case of high interference, since the relative frequency of success at the third transmission is very small while the relative frequency of failure is high (8.4% and 72.5% respectively for a window of  $[-75, -70]$  dBm). So, decreasing the maximal number of transmissions can help to save energy at the price of a small loss in reliability.

The average energy consumption  $E_{\text{RSSI}_k}$  in each RSSI window  $k$  has been calculated from the average energy consumption  $E_{\text{avg}}(n)$  per type of packet  $n$  (obtained experimentally) and from the packet distribution per RSSI window  $p_n$ , as

$$E_{\text{RSSI}_k} = \sum_{n=1}^4 p_n \cdot E_{\text{avg}}(n). \quad (2.1)$$

Based on these results, presented in Table 2.2, we can see that the average energy consumed by a transmitted packet varies according to the level of interference in the channel. A packet transmitted with an interference level situated in the  $[-75, -70]$  dBm window will consume 4.6 times more in average than a packet sent when the RSSI value does not exceed -85 dBm.

TABLE 2.2: Avg. energy, maximum number of transmitted packets and lifetime of the node per RSSI window - Ideal case.

RSSI (dBm)	-95 to -85	-85 to -80	-80 to -75	-75 to -70
Avg. energy (mJ)	1.84	5.71	6.74	8.47
Num. of packets ( $\times 10^6$ )	5.23	1.68	1.42	1.13
Lifetime (days)	46.8	20.2	18.2	16.2

Next, we evaluate the number of packets that TX node is able to send until total discharge of a given battery for every RSSI window to estimate the lifetime of the node. We have chosen a real 850-mAh TCL PL-383562 polymer Li-ion battery modeled by Chen and Rincon-Mora [26]. They give the discharge equation of a real battery and calculate the State-of-Charge (SOC) where the voltage decreases below a threshold which corresponds to near 5% of the SOC. Below that voltage, the circuit is not operational. Then, the maximum amount of energy used to supply circuit corresponds to about 95% of the total energy stored in the battery. Based on this result and the average energy consumption per RSSI window, we calculate the maximum number of packets (with a 19-byte payload) transmitted with respect to the interference level, shown in Table 2.2. Based on the energy stored in the battery, the maximum number of packets transmitted per RSSI window and the average time per packet, it is possible to assess the lifetime of the node depending on the interference level. These results are also presented in Table 2.2. The lifetime of the node decreases dramatically from 46.8 days in the  $[-95, -85]$  dBm window to 20.2 days in  $[-85, -80]$  dBm (more than by half). The lifetime continues to decrease up to 16.2 days if the interference level in the channel stays in the  $[-75, -70]$  dBm window.

### Real case

Fig. 2.12 represents the distribution of the different types of packets in the real case for 5 different interference zones from  $-95$  dBm to  $-70$  dBm with the step of 5 dB. It includes the values of this distribution per RSSI level and

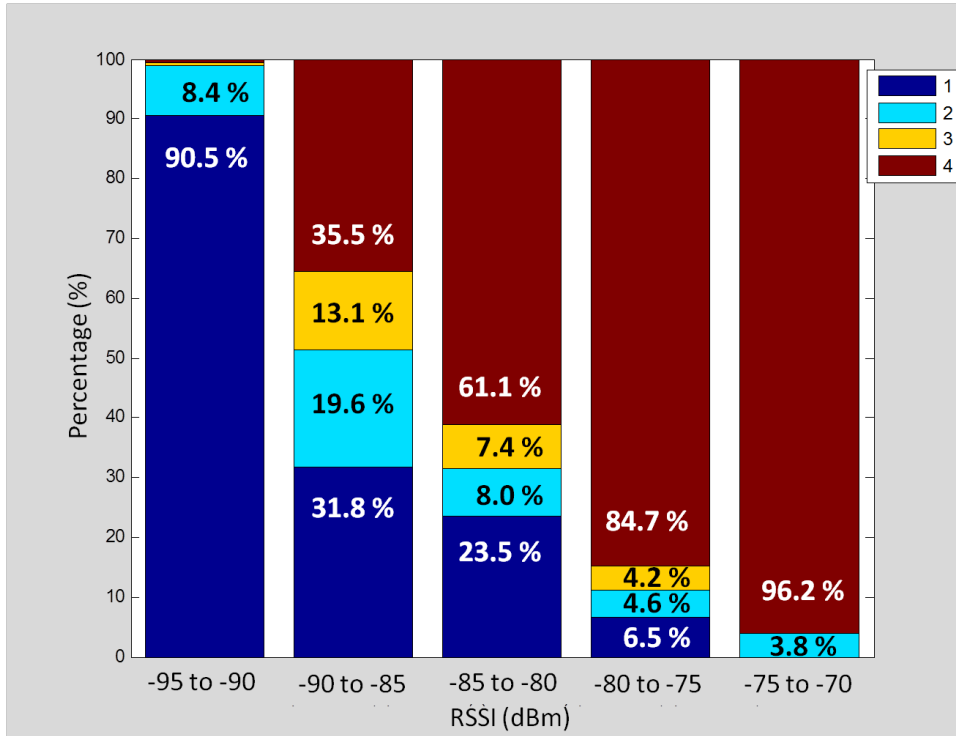


FIGURE 2.12: Packet distribution per RSSI window on TX - Real case.

per type of packet. In this case, as observed in Fig. 2.8a, there are packets situated in all the five RSSI windows.

We observe different behaviors of the system in each window. In the zone with a lower interference level ( $[-95, -90]$  dBm), the percentage of successful transmissions is 99.3% (packets '1', '2' and '3') whereas the percentage of having a successful transmission with only one try (packet '1') is 90.5%. Due to the external sources of interference and radio channel conditions, this percentage is less than in the ideal case, where it reaches 99.7%. The percentage of packets '1' decreases in an exponential manner until it reaches 0% in the highest interference zone. At the same time, the percentage of packets '4' increases. The amount of packet '4' increases slower than the decrease of packet '1' because of the presence of types '2' and '3' in the RSSI windows between  $-90$  dBm and  $-75$  dBm. Other aspect to notice is that packet type '3' represents the packet with the smallest percentage of appearance in all the RSSI windows, as in the ideal case. Also, it is important to take into consideration that the percentage of the packet type '4' in windows with the maximum of interference,  $[-80, -75]$  dBm and  $[-75, -70]$  dBm, are 84.7% and 96.2%, respectively. This means that the relative frequency and, thus, the probability to transmit a packet successfully is very low. Then, we should avoid sending the packets when the interference reaches these levels in order to improve the energy efficiency.

Now, we calculate the number of packets that TX can send with a 850 mAh battery supplying the node, as in the ideal case. The resulting values of the average energy, the number of packets and the lifetime of the node

TABLE 2.3: Avg. energy, maximum number of transmitted packets and lifetime of the node per RSSI window - Real case.

RSSI (dBm)	-95 to -90	-90 to -85	-85 to -80	-80 to -75	-75 to -70
Energy (mJ)	2.37	6.29	7.48	8.97	9.54
Packets ( $\times 10^6$ )	4.04	1.52	1.28	1.07	1.01
Lifetime (days)	34.4	18.8	17.1	15.7	15.2

per RSSI window are presented in Table 2.3. We observe that four times more packets can be sent in conditions of low interference in comparison with the highest interference conditions. The maximum lifetime (34.4 days) is more than the double of the expected lifetime in the case of the highest interference level (15.2 days). Finally, if we compare both, ideal and real cases, lifetime of the node is shorter in all the RSSI windows for the real case due to multipath fading and/or the interference caused by the external sources.

### 2.5.6 Using Wi-Fi as a interfering network

In the previous sections, we used XBee nodes as a source of interference. This kind of nodes uses the same communication technology as the primary network. We performed similar tests but with Wi-Fi as the interfering technology. The configuration for the primary network consisting of a TX and a RX nodes was not changed. The interfering network was organized as follows: 2 laptops with embedded Wi-Fi Network Interface Cards (NIC) were communicating through a Wi-Fi AP installed in the IRCICA TELECOM lab. Both laptops were connected to the AP at the rate of 54 Megabits per second. The PCs were running a "Distributed Internet Traffic Generator" (D-ITG) [17] which contains two parts: sender application (which generates traffic) and receiver application (which receives generated traffic). The laptop running sender application was installed close to the TX node of the primary WSN network under evaluation. This PC was using the IEEE 802.11g standard, so communicating via 2.4 GHz ISM band, and thus was representing a source of interference. However, the second PC was using the IEEE 802.11a standard (5 GHz band). So, the first PC was the main source of interference whereas the second PC could not interfere with the primary network. The duration of the experiment was set to 15 minutes. Different levels of interference were represented in this case by different packet generation rates in the Wi-Fi network. The packet generation rate, thus, was increasing periodically (every 2.5 minutes) during the experiment in the following way: in the beginning of the experiment the packet generator was deactivated for the first 2.5 minutes, then for the following time periods, the rate was set consecutively to 100, 300, 500, 700, 900 packets per

second. The synchronized measurements of energy consumption of the radio module, interference level and packet transmission statistics for both, TX and RX nodes are presented in Fig. 2.13.

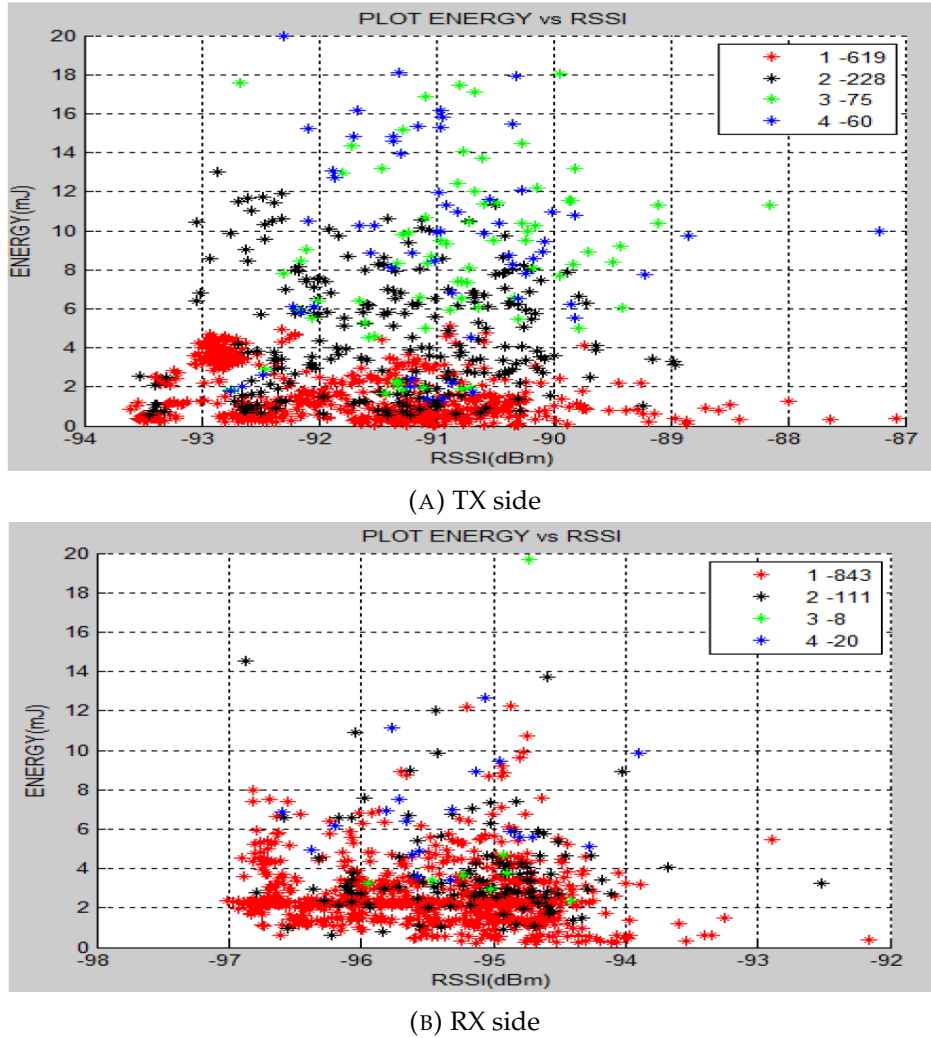


FIGURE 2.13: Energy consumption vs RSSI per packet type (Wi-Fi scenario).

We can notice that the type '1' packets are mostly situated on the bottom of the graphs for both, TX and RX nodes, as it was the case in previous tests with the XBee interfering network. The values with a higher packet type are situated in the zone of higher energy consumption, which features the same behavior that in the previous setup. However, we cannot observe any tendency regarding the distribution of packets over the RSSI values (as 3 sets of points observed in the XBee case). Indeed, we can observe the presence of all packet types both in the low and high interference zones. Indeed, since the packets of the interfering Wi-Fi network are sent at much higher data rate than for primary network, the on-air duration of the Wi-Fi packets is often less than the measuring duration of the TelosB node (128 microseconds). Thus, the RF chip of the TelosB node is unable to detect all the interfering packets, which shows the inefficiency of the used CSMA approach in this case.

The packet statistics collected at the TX node are presented in Table 2.4. From the table, we can observe the similar repartition of the average energy consumption per packet type as in the previous scenario. It confirms our expectations, since in both cases (for XBee and Wi-Fi interfering networks) we used the same sensor platforms (same RF chips).

TABLE 2.4: Results of energy, number of packets and total energy per type of packet on TX side. Real case.

Packet Type	'1'	'2'	'3'	'4'
Avg. Energy (mJ)	1.60	4.76	8.86	9.65
No. packets (%)	63.0%	23.2%	7.6%	6.1%
Total energy (%)	29.9%	32.6%	20.0%	17.4%

## 2.6 Long term distributed interference measurements

In the previous sections, the impact of the interference level on the energy consumption of the nodes was studied. However, in these tests the interference patterns were generated in an artificial way. As we mentioned, in real case our measurements were impacted also by the external sources of interference (*e.g.*, Wi-Fi network, microwave oven). Thus, in real case we were unable to control the level of interference because it is related to the activity of other users of the ISM band. In this section we analyze the evolution of the interference level in time, space and frequency in the long term for an office building environment. To do so, a distributed spectrum sensing platform based on low cost hardware was developed to perform continuous spectrum sensing during one week.

### Description of the platform

The platform was based on Digi XBee S1 [107] radio modules. The system was containing two types of devices: end node device with XBee radio driven by Arduino Nano prototyping board [9] with ATMega328 microcontroller and coordinator device represented by a PC connected to the XBee module via serial communication adapter and storing the received measurements data. The photo of the end node is presented on Figure 2.14. The Arduino boards of end devices were configured in order to send the energy detection commands to the XBee module about every 700 ms. The XBee modules then scan all the 16 IEEE 802.15.4 channels (represented in Figure 2.15) during 30.72 ms each. Thus, the total time of scan is 491.52 ms. After completing the spectrum measurement, the XBee module sends the measured values back to the Arduino which prepares a packet with the collected data to send to the coordinator. Once the packet is ready, the Arduino

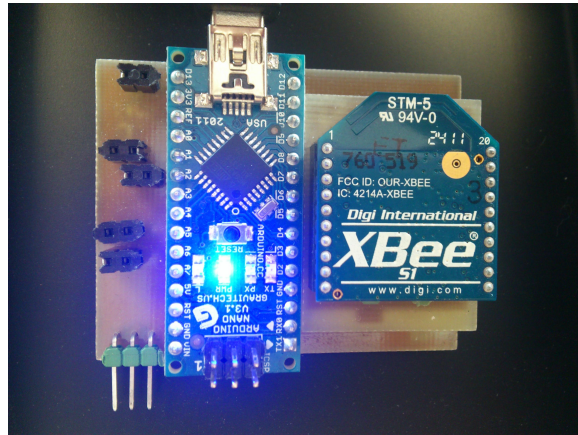


FIGURE 2.14: End node

forwards it back to the XBee module for further transmission to the coordinator by using the channel which was not affected by the Wi-Fi activity (cf. Figure 2.15).

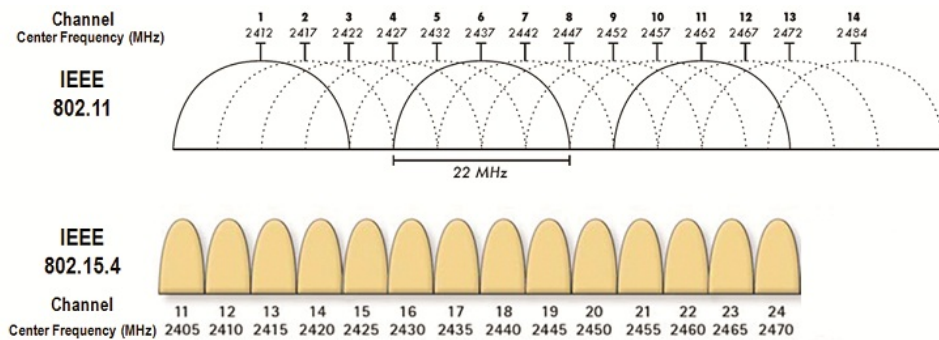


FIGURE 2.15: IEEE 802.15.4 and IEEE 802.11 channels allocation in 2.4 GHz ISM band. Credits: NI

### Experimental setup

The previously described system was deployed in the IRCICA's Telecom platform premises. It is a  $90\text{ m}^2$  room with installed telecommunication equipment. The lab is equipped with a Wi-Fi access point (AP) operating on channel 1. Five end nodes were installed in the premises. The placement of the nodes is represented on the map on Figure 2.16. One node was installed next to the access point at the distance of about 30 cm (node 1), one in the middle of the room within a distance of about 5 m from the AP in line of sight (node 4), one a bit further, in a distance of about 8 m in line of sight (node 5), one in the opposite side of the lab at the distance of about 10 meters behind metallic cases of telecommunication equipments, thus without line of sight (node 3). The last node among 5 (node 2) was installed in the next room, thus without line of sight, but the gypsum board wall between rooms does not attenuate strongly the signal. This node was installed also close to the microwave oven in the cafeteria next door. The end nodes were communicating with a coordinator by using Channel 20 which

was not strongly impacted by the interference from the AP (cf. Figure 2.15). The system was started on a Monday morning and it was collecting the

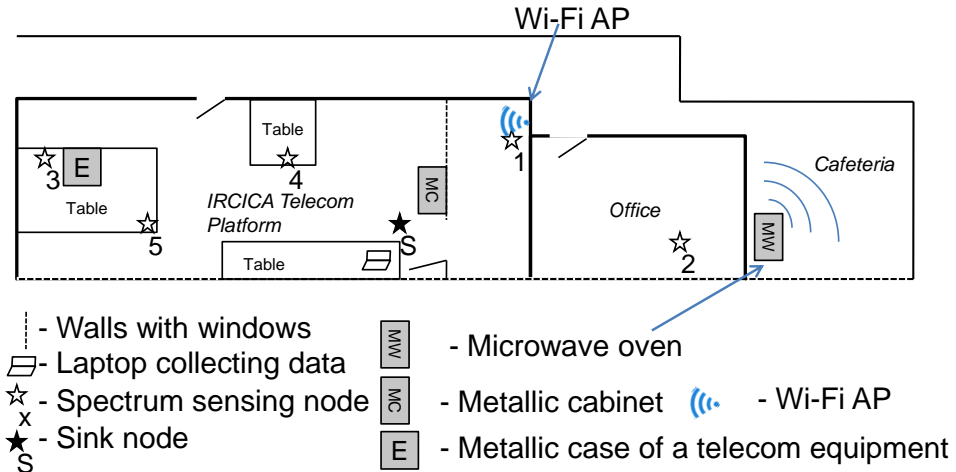


FIGURE 2.16: Node placement map

measurement data during one week. The results of this measurement are described in the next subsection.

## Results

One week interference measurements on the IEEE 802.15.4 channel 12, corresponding to the middle of the Wi-Fi channel 1 used by the AP during the test, are depicted in Figure 2.17.

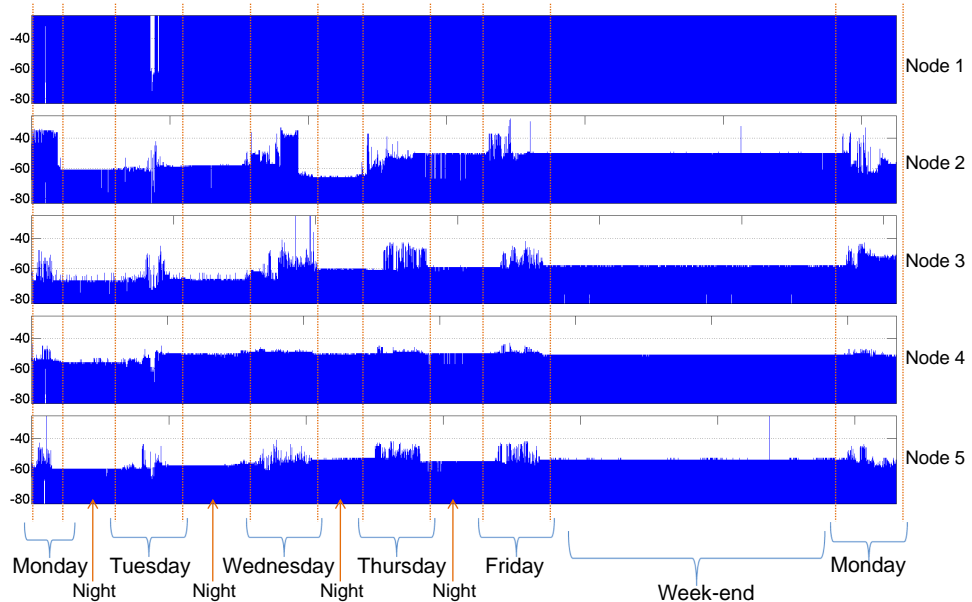


FIGURE 2.17: One week interference measurement.

This figure shows the evolution of the RSSI level measured by each of the 5 nodes in time. We can clearly notice the impact of the daily activity of the Wi-Fi users (6 activity peaks corresponding to 6 working days from Monday to next week Monday). During the week-end the access to the

building is restricted and is forbidden at night. So, there are less (or no for the night time) active Wi-Fi users during these periods of time. That is why we can observe a lower level of interference comparatively to the working days. This behavior can be observed clearly for Nodes 2,3,4,5 in the figure.

We can notice also that each node perceived different levels of interference. Indeed, the nodes are impacted by interference differently depending on their position and neighboring activity. For example, we can observe that the measurements of Node 1 are saturated because of the very close proximity of the Wi-Fi AP - the main source of interference in this context. Moreover, the high interference activity is observed by this node even during the week-end and at night. This is because the AP is periodically sending beacon messages containing the service information about available Wi-Fi networks (*e.g.* Service Set IDentifier (SSID)) whatever the traffic is.

The perceived level of interference also depends on the used channel. Indeed, different parts of the ISM band are impacted by the interference in a different way. Figures 2.18a and 2.18b show that in average the nodes sense a lower interference level when we shift the channel further from the spectrum occupied by the AP in the lab.

Then, to confirm the observed phenomenon, we carried out a similar test in the EuraTechnologies site of the FIT IoT-LAB platform in Lille. This building is situated far away from the IRCICA lab. So, these two experimental setups are independent. Apart from the FIT IoT-LAB platform, the EuraTechnologies building hosts many offices, so, it could be considered as office environment *i.q.* the case of the IRCICA lab measurements. However, it is important to take the activity of other users of the platform into account. Indeed, any user of the FIT IoT-LAB platform can book a number of nodes to perform its communication tests at any time. The signals from other sensor nodes will, thus, increase the level of interference.

We carried out our measurements during 6 days (from Tuesday to next week Monday). In contrary to the previous test setup, in the IoT-LAB scenario we used WSN430 devices (previously described in this Chapter) in order to perform the spectrum sensing, which provided us with a better sampling rate. We observed similar results presented in Figure 2.19.

In this experiment, we can also notice that the interference level is not constant during the week. We observe again the interference level peaks during the day and lower RSSI level during the nights and week-end. This behavior is caused by Wi-Fi users activity in the building, as for the case of the previous setup. We can also notice an increased level on interference on Channel 26 during the week-end, which is probably caused by the activity of other sensor nodes of the platform.

The obtained results emphasize the importance of the factors which cause the actual level of interference impacting the WSN node: time, position, used channel and communication environment.

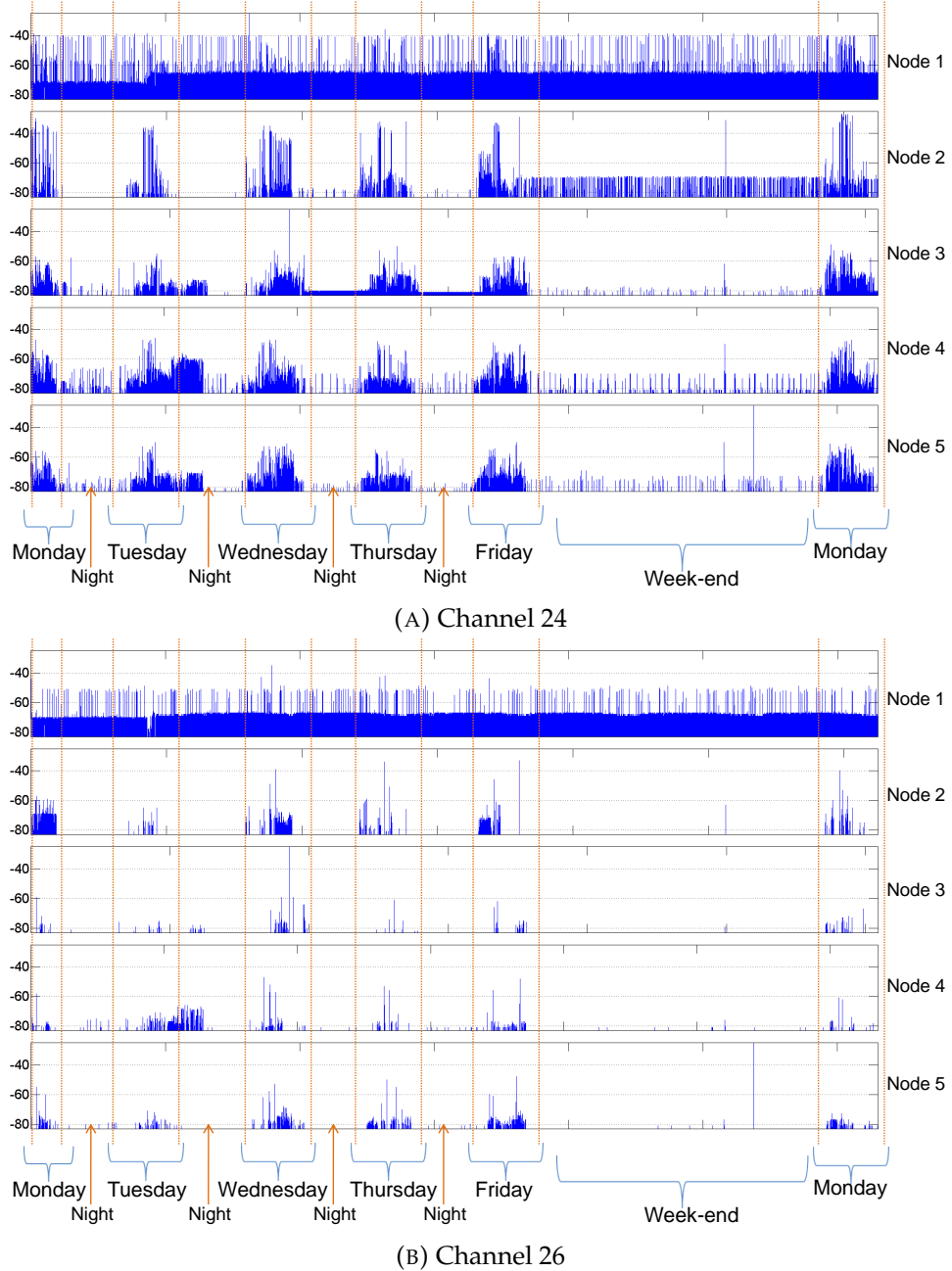


FIGURE 2.18: Evolution of the perceived level of interference depending the used channel (IRCICA TELECOM Lab)

### 2.6.1 Discussion

In [36], Dunkels *et al.* conclude, by using software estimation approach, that the dominating part of energy consumption is due to idle listening. The authors also emphasize the importance of validation of their results by hardware measurements. Our measurements carried out by the Synergie hardware platform confirm the significant impact of idle listening. Indeed, as we explained in previous sections, the type '4' packets cause the biggest energy consumption for both, TX and RX nodes. In the case of RX, the type '4' packets correspond to packet non-reception, so, idle listening. One of the results in [14] is the experimental evaluation of success rate of data packet

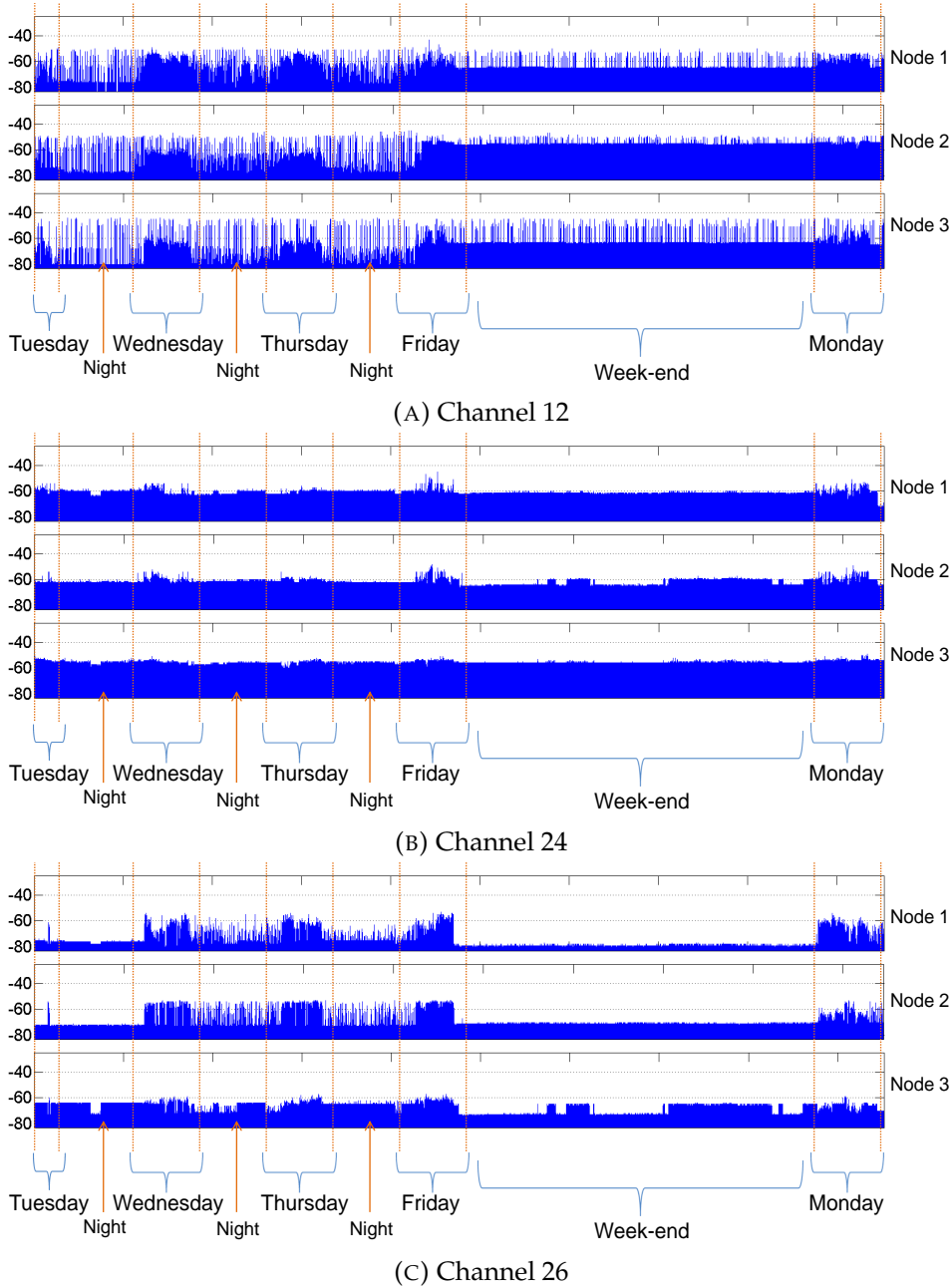


FIGURE 2.19: Evolution of the perceived level of interference depending the used channel (FIT IoT-LAB)

transmission after failed X-MAC early ACK handshake. For this case, the authors observe a very low success rate of 2%. In our work, we notice similar results, but in case of successive transmissions after fails. From Fig. 2.9b we observe the success rate of 5.5% after two unsuccessful transmissions (type '3' packets). This observation is also related to the second conclusion in [14]: X-MAC preamble interruption after noise perception could decrease significantly the packet loss rate (from 50% to 33%). Thus, postponing of the data transmissions towards the periods with low level of interference could increase the success rate and decrease the energy consumption of the nodes. However, this technique is not suitable for some applications with real-time constraints, *e.g.* an event-driven alarm.

As we show in this chapter, if the accuracy of the spectrum measurements based on CC2420 RF chips (used in WSN430 and TelosB nodes) is sufficient to observe in general the evolution of the perceived interference in a large time scale (during a week), the measurements are still not precise enough to detect the interfering signals for each packet transmission and, so, to perform correctly the CSMA MAC strategy. Thus, it is important to use a feasible RF solution which can guarantee the detection of all interfering signals (even with a very short duration).

## 2.7 Chapter conclusion

In this work, we have experimentally evaluated the impact of interference on the energy consumption of both receiver and transmitter nodes with the example of X-MAC RDC protocol and CSMA MAC strategy. According to the IEEE 802.15.4 standard, transmitter node can carry out up to three transmissions for each application layer packet. Never acknowledged packets at the transmitter side as well as never received packets on the received side (packet type '4' in our study) increase dramatically the energy consumption of the devices and, thus, decrease the lifetime. We show that the maximum number of three transmissions of an application layer packet is not energy-efficient because the energy consumed by the transmitter node for three tries is much higher than for one and two tries. Moreover, the results show that the probability to have a well-received packet after two unsuccessful tries is close to 5% in average and very small in highest interference window (zero observed packets) for real case. Then, the third transmission can be removed in order to reach a longer lifetime of the node at the expense of slightly lower packet delivery rate.

We note that the broadly used actual CSMA MAC strategy completed by X-MAC RDC protocol cannot solve this problem and avoid useless and energy inefficient unsuccessful transmissions. Development of a dynamically adaptable MAC protocol is, thus, required. For example, the current RSSI value can be used as input information for the algorithm to dynamically modify the communication parameters (*e.g.* max. number of retransmissions, CCA threshold, communication channel) before sending a packet.

In our IRCICA TELECOM lab experimental setup for 1 week spectrum sensing, we observed the decrease of the interference level when we shift the used channel to the other side of the ISM band, away from the spectrum occupied by a Wi-Fi AP installed in TELECOM lab. That is because other Wi-Fi APs of the building were situated far from the test site. We can use this observation in this particular context in order to choose the best channel to communicate and also when possible to decide the best positioning of nodes. However, in other cases we can have many sources of interference with a spectrum distributed all over the band in a random way. Moreover,

as we show, the level of interference can change depending on time and position of the nodes. It can also be different depending on the environment. For example, the evolution of the perceived interference level in outdoor urban or rural scenario may be very different from the results presented in this chapter for indoor office environment. It will change also depending on the number of users in the WSN network. An adaptive MAC protocol, which can take all these aspects into account and choose the best channel for the WSN nodes at the specific time and position will then considerably increase the performances of the network.

## Chapter 3

# Thompson Sampling based Cognitive ratio solution for Multihop WSN

### 3.1 Chapter introduction

As we have shown in Chapter 2, the interference level in the ISM bands changes depending on the time, the position of the node and the used channel. Since high level of interference can decrease significantly the lifetime of the WSN, it is important to develop an efficient adaptable MAC protocol, which will dynamically choose the least interfered channel based on local RSSI observations. This task could be completed by applying the Cognitive Radio (CR) approach. Even though the CR approach was developed originally to detect and use the whitespaces in the license based spectrum, this approach can be applied to WSNs. As it was mentioned previously, WSNs mostly operating in ISM bands have to deal with increasing level of electromagnetic interference. At the same time, studies show that the license based spectrum is under-utilized in both spatial and temporal domains [49]. This has led to tremendous research on optimizing the spectrum access methods [4, 110, 3]. The Dynamic Spectrum Access techniques [110] sense the available spectrum in order to find less interfered frequency band and use it for transmissions. This technique is used in Cognitive Radio (CR) approach [79]. This approach allow CR devices to use a part of licensed frequency bands under certain conditions. CR is a promising approach to improve spectrum efficiency [79, 57]. The main goal of the cognitive radio devices is to use the so-called white spaces (see Fig 3.1) in the licensed spectrum opportunistically [110]. In other words, a cognitive radio device is allowed to access the licensed spectrum as a secondary user where and when it is not being used by the primary user (which has the exclusive right to use it), conditioned on the limited interference [57], which will decrease the occupancy of the saturated ISM bands. In addition, cognitive radio schemes could be utilized in the next generation heterogenous networks where different tiers of the network use spectrum white spaces to transmit [41]. In this scheme, although all network tiers have the same privilege to access the

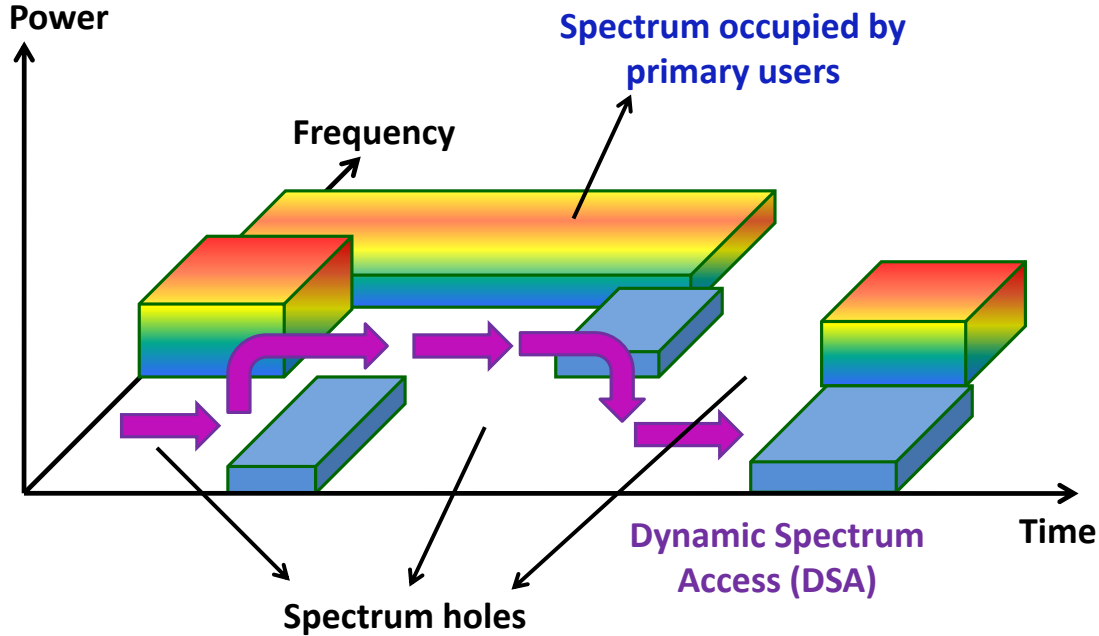


FIGURE 3.1: Dynamic spectrum access.

spectrum, it is highly desirable to keep the level of interference in different tiers below a certain threshold. To maintain the desired interference limit, the spectrum access has to be managed precisely. An efficient cognitive radio device must be able to choose the channel with the highest probability of availability and access the channel after sensing the availability of the channel correctly [74].

Cognitive radio approach can be applied not only to the license based bands, but also to the unlicensed spectrum [2, 3]. Indeed, since the usage of ISM bands is not strictly controlled the estimation of the unlicensed spectrum users behavior is important task. The application of the CR technique to the ISM bands allows improving the efficiency of the spectrum sharing and facilitate the coexistence of different standards, which is particularly important for energy constrained WSNs (as it is studied in the Chapter 2). It is important to note that in ISM bands all the users have the same priority to access the medium. However, CR approach applied to unlicensed bands will help CR users to avoid the most interfered parts of available spectrum.

In [2] and [68] CR is proposed as a solution for WSN, which leads to the specific kind of WSN: Cognitive Radio Sensor Networks (CRSN) or Cognitive Radio Wireless Sensor Networks (CR-WSN). Even though Cognitive Radio can enhance the performances of the WSNs, multiple challenges have to be addressed in order to enable the implementation of the CR-WSN. We believe that the most important challenges in the field of CR-WSN are spectrum decision process [3] and multihop communications. Indeed, it is impossible to dedicate an interference-free Common Control Channel in ISM bands, since the entire band is always available for other technologies. So,

the cooperation between nodes by sharing the observed locally spectrum availability data is complicated. Thus, an independent distributed algorithm, that will decide which channel to use based only on the local observations should be developed. Moreover, in the ISM bands the channel utilization statistics for other users of the band are unknown. Also, in contrary to the Cognitive Radio solutions based on IEEE 802.22-2011 standard [61] (where one-hop communications only are supported) in WSNs multihop capabilities could be required for some applications. Even though the IEEE 802.22 Amendment 2 (2015) describes the possibility of multihop communications, they are possible only through advanced less constrained devices which are not common in WSNs. In the 802.22 standard the receiver (base station) is able to listen to all the available channels simultaneously. So, the end node device can choose any available channel and be sure that the receiver node is listening. However, the WSN nodes are often based on low cost hardware and, thus, do not have the multichannel capabilities. So, it is not trivial to estimate which channel is used at the receiver side on CR-WSN operating in the ISM band.

In this chapter we propose a Thompson sampling based Cognitive Radio approach and we develop a multihop extension for WSN.

The CR spectrum management process consists of four major steps [3]:

- Spectrum sensing. The CR devices have to observe the spectrum activity to be able to analyze it further and make a decision about the channel to use.
- Spectrum decision. The node analyzes results of the spectrum sensing in order to determine the best channel to use. The channel is selected and set at this step.
- Spectrum sharing. In case of the presence of multiple CR users, they have to follow specific rules in order to share the available spectrum between them.
- Spectrum mobility. The CR users should take account of the fact that other CR users can move from one part of available spectrum to another.

Different approaches exist at the spectrum sensing step [2, 3]. Some examples are presented below:

- Matched filter. This is optimal solution in the case when the information about primary user is known by CR devices in stationary Gaussian noise. However, *a priori* knowledge of the primary user channel usage statistics, required for this method, are not always available. Moreover, in the ISM band, it is impossible to guarantee the feasible statistics on the other users of the band, since this kind of bands in

available to any device without license. So, this solution is unsuitable in our context.

- Feature detection. This technique uses cyclostationarity of the modulated signals, which can be detected by analyzing a spectral correlation function. Despite the robustness of this method, we cannot use this solution due to its high computational complexity. In fact, the WSN nodes are in general equipped with a low cost low power MCU which do not have sufficient computational resources to perform the feature detection technique.
- Energy detection. The simplest method which can be based on the RSSI measurements provided by the off-the-shelf RF chip. Even though this solution neither requires a high computational capabilities nor requires strong assumptions on knowledge of other user statistics, the performance of this method highly depends on the variations of the noise power level. Thus, false alarms could be detected. However, this issue could be managed by a well defined RSSI threshold. In this work we have chosen this spectrum sensing strategy.

Further in this work we focus mostly on the spectrum decision step. In fact, as in our case, the last two steps could be managed at the spectrum decision level. As mentioned previously, it is impossible to guarantee an interference free Common Control Channel in ISM bands, which enables centralized approaches for spectrum sensing and spectrum decision processes. Thus, each CR-WSN node operating in the ISM bands has to execute a distributed spectrum decision process independently. Development of such an approach is a complex task. Since the energy constrained secondary network devices (or CR-WSN nodes in our context) have to avoid the energy waste, it is crucial to identify the best available channels as soon as possible. A naive approach is to scan the whole band and identify the available channels. Naive approach imposes large latency and energy cost on the network specially when the number of accessible channels is large. In addition, to the best of our knowledge, advantages of multihop CR-WSNs running independent distributed spectrum decision techniques has not been exploiting with existing off-the-shelf WSN motes operating in the ISM bands. As a result, finding the best channel with minimum time and energy cost and apply cognitive scheme to multihop communications are still two open problems.

We address, thus, the non-trivial channel exploration-exploitation dilemma [77] in cognitive radio in an experimental setting and extend it to multihop communications. For the case of classic cognitive radio networks, the problem is defined as follows. A large number of channels are available for potential usage by secondary network users. The channels are occupied with different rates by primary user which has the exclusive right to

use it. In our scenario, we apply the cognitive radio approach to the WSN operating in the 2.4 GHz ISM band. Thus, there are neither primary nor secondary devices, since all the users have the same priority to access the channel. However, we assume a 802.11 network as a primary network and a 802.15.4 based network as a secondary network for our tests. On one hand, it allows us to mimic closely the real CR setup. On the other hand, this model can improve the coexistence between different standards using the same ISM band *e.g* IEEE 802.11 and IEEE 802.15.4. In fact, the IEEE 802.11 signals have a larger bandwidth than the signals of IEEE 802.15.4 networks (22 MHz for IEEE 802.11b/g standard vs 2 MHz for IEEE 802.15.4, as shown on Figure 2.15 in Chapter 2. For IEEE 802.11n the channel bandwidth can be even larger). Moreover, the maximum transmitting power of Wi-Fi APs is much higher than for IEEE 802.15.4 devices (20 dBm in Europe and 30 dBm in United States vs 0 dBm for commercially available TI CC2420 IEEE 802.15.4 transceiver). Clearly, the DSSS technology implemented in IEEE 802.15.4, which helps against narrow band interferers, will not be able to completely protect the WSN transmissions against the Wi-Fi interference due to a much larger band of the IEEE 802.11 signals. Contrariwise, the IEEE 802.11 signals should not be considerably impacted by IEEE 802.15.4 transmissions, since the latter are considered as narrow band interfering signals. Despite the IEEE 802.11 and IEEE 802.15.4 users have the same priority to access the 2.4 GHz ISM spectrum, assuming Wi-Fi as a primary network technology will force the IEEE 802.15.4 users to avoid the parts of the spectrum occupied by Wi-Fi, and, thus, decrease the probability of packet losses. In both scenarios (a classic cognitive radio and CR-WSN case), the problem is to find and exploit the channel with the best rate as soon as possible. We model the channel selection process as a multi-arm bandit and compare different learning approaches in terms of throughput in an experimental test-bed. Although modeling the channel selection dilemma as a multi-arm bandit problem has been investigated theoretically in literature, performance of this model in practical implementations is not addressed. The contributions presented in this chapter can be summarized as follows:

- we model the channel selection dilemma (spectrum decision step of the CR spectrum management) as a multi-arm bandit problem applied a Thompson [24] sampling-based approach;
- we provide an experimentation of our approach and compare its performances to the most efficient and simply implementable learning approaches in terms of throughput both by simulation and experiments on real hardware platform.
- we propose a multihop cognitive radio extension together with an experimental proof of concept.

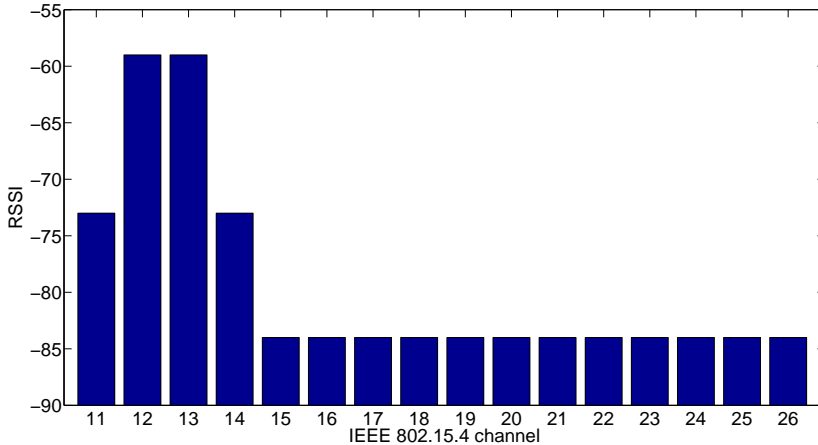


FIGURE 3.2: A sample from one week interference measurements. The node is situated in the middle of the lab.

We show that the Thompson sampling formulation finds the best channel significantly faster and the most efficient among the other algorithms in a practical cognitive radio setting. This results in smaller latency in transmission and less energy consumption for channel exploration.

In the next section the existing works in the field of the spectrum decision process will be reviewed.

### 3.2 Related works

Spectrum decision process is analyzed based on a channel model. Channel selection is addressed in [111]. The optimal strategy is derived using a partially observable Markov decision process (POMDP) framework. In this framework, the channel is modeled as a  $2^N$  state Markov chain where each state is represented by a binary N-tuple indicating the availability of each channel. The model is reduced into  $N$  two-state Markov models where the transition probabilities are constant and based on the statistics of the primary user assuming independence between the channels. However, these assumptions are not realistic. The available channels are not always independent, especially in the ISM bands. Indeed, as we mentioned in the previous section, the Wi-Fi technology uses more bandwidth than IEEE 802.15.4. Thus, the activity on one IEEE 802.11b/g channel impacts four consecutive IEEE 802.15.4 channels at the same time. This case is depicted in Figure 3.2 which represents a sample from the one week interference measurements at the IRCICA TELECOM lab, described in Chapter 2. Recall that in this setup, the Wi-Fi AP was configured to use the channel 1 with 20 MHz of bandwidth. From the figure we can clearly notice that the first four IEEE 802.15.4 channels are impacted by the Wi-Fi activity, which shows the correlation between WSN channels. Note, that in case of IEEE 802.11n which can

use 40 MHz channels, eight consecutive IEEE 802.15.4 channels simultaneously, which represents the half of all the IEEE 802.15.4 channels available in the 2.4 GHz band. Thus, the correlation between the channels used by WSNs could be very strong. In [52] and [53], co-existence of a cognitive radio system a IEEE 802.11 primary network is investigated. The channel is modeled by a four state continuous-time Markov model where the states of the Markov chain represent data packet transmission, acknowledgment transmission, short inter-frame spacing time and idle channel. The transition probabilities are obtained from measurement data. The sojourn time is defined as the time that the process spends in each state and estimated by a generalized Pareto distribution. In [75], a comprehensive study on the holding time distribution for idle and busy channel states in ISM band is provided. This study also suggests generalized Pareto distribution for holding times for all considered bands. However, these works require expensive equipment with high energy consumption, which makes impossible the integration of these approaches in a large-scale WSN (and IoT) networks, containing billions of nodes.

The channel selection dilemma is formulated as a multi-arm bandit in [69] and [51]. Algorithms based on upper confidence bound (UCB) algorithm suggested in [11] are applied to identify the channel with the best availability rate. In [69], the performance of UCB based algorithm in terms of regret is investigated for different numbers of accessible channels. Regret is the throughput missed due to not choosing the best channel compared to an oracle who knows and exploits the best channel from the beginning. In [51], dependencies are considered between the channels and a UCB based algorithm is proposed and analyzed in terms of regret. In [56] a cognitive scenario with two competing networks with jamming capability is considered. The decision on jamming or communicating on the channel for each network is modeled in a Bayesian setting for Thompson sampling. In this adversarial scenario, it is shown that the Bayesian framework outperforms UCB based algorithms. Channel decision problem is modeled as a restless multi-arm bandit problem in [105]. The probing time to find an available channel is minimized using the model. The performance of the method is numerically evaluated and is shown to have advantage over previous methods.

As it will be shown in later in this chapter, the multi-arm bandit based solutions could be implemented on real low-cost hardware used in WSNs. Thus, potentially it can be a solution enabling the cognitive radio capabilities for existing and future WSN and IoT networks. However, even though multi-arm bandit model has been studied extensively in theory, the performances of it have not been evaluated yet on real WSN hardware in cognitive radio context. The experimental evaluation and validation of the multi-armed bandit solution is required before the commercial evaluation. Indeed, in practice, the perfect theoretical assumptions are often not valid,

which can affect the performance of the algorithms. In our work we implemented the theoretically efficient algorithms in a practical setting of a WSN operating in the 2.4 GHz ISM band. Also, we developed a multihop extension for the proposed scenario, which is, in our best knowledge, was not done yet. The details of the simulations and experiments are given in the following sections.

### 3.3 Optimal Algorithms for Multi-Armed Bandit

In this section, we formulate the channel selection and exploration dilemma in cognitive a radio context as a multi-arm bandit problem. Then, we describe efficient and simple learning algorithms commonly used to solve the multi-arm bandit problems and adapt them into the cognitive radio context.

#### 3.3.1 Channel selection modeling

In a multi-arm bandit problem, an agent tries to obtain as much reward as possible by playing the most rewarding arm among  $N$  arms. However, each arm rewards randomly upon being played according to an unknown distribution. Hence, the objective is to minimize exploration to find the most rewarding arm. A policy  $A$  is an algorithm that defines the actions of the agent usually based on the previous observations. We assume  $n_j$  to be the number of times the  $j^{th}$  arm has been played after  $n$  steps and  $\mu_j$  to be the expected reward of the  $j^{th}$  arm. In other words, channel  $j$  is found available in average  $\mu_j n_j$  times in  $n_j$  measurements.  $\mu_j$  is associated with the statistics of the primary user of the channel. The regret of the policy  $R_A$  is defined to indicate how much reward is lost on the average due to the exploration,

$$R_A = \mu^* n - \sum_{j=1}^N \mu_j E(n_j) \quad (3.1)$$

$$\text{where } \mu^* = \max_{1 \leq j \leq N} \mu_j$$

where  $E(\cdot)$  indicates the expected value. Minimizing the regret is desirable as it will maximize the average reward.

In [73], authors have derived a logarithmic lower bound for the regret function in a multi-arm bandit problem,

$$R(n) = \ln(n) \left[ \sum_{i=1}^N \frac{p^* - p_j}{D(p^* || p_j)} + o(1) \right], \quad (3.2)$$

where  $p_j$  are the reward densities of the arms and  $p^*$  is the density of the arm with the maximum average reward ( $\mu^*$ ).  $D$  is the Kullback-Leibler divergence between the two densities and  $o(1) \rightarrow 0$  as  $n \rightarrow \infty$ .

In cognitive radio setting, the user must find the best available channel among  $N$  accessible channels as fast as possible considering its time and energy constraints. A naive policy is the exhaustive search for an available channel. Despite its simplicity, this policy incurs large energy and latency overhead on the secondary user network.

Here we assume changes in the statistics of the primary user are slower than the convergence time of the algorithms [72, 56]. To keep track of the primary user statistics, an expiration time can be defined to trigger the search for a new channel. Another criterion to trigger the search for a new channel is to define a threshold for the number of consecutive unsuccessful channels access after which the user will search for a new channel.

In [11], policies based on upper confidence index are investigated and shown to achieve optimal regret uniformly over time. In this work, we evaluate the performance of learning algorithms in [11] with  $\epsilon_n$ -greedy and Thompson sampling, an old algorithm which has recently gained interest in research community due to its simplicity and efficiency. In the following algorithms, values for the parameters of the algorithms were analyzed numerically and are assigned to optimize the performance of the algorithms.

### 3.3.2 Adaptation of UCB approach

Upper confidence bound (UCB) algorithms are based on empirical mean obtained through observations and a term related to the upper confidence interval of the empirical mean. UCB1 based algorithm chooses the channel with the highest upper confidence bound defined as,

$$c_j = \bar{x}_j + \sqrt{\frac{2\ln(n)}{n_j}}, \quad (3.3)$$

where  $\bar{x}_j$ ,  $n$ ,  $n_j$  are the empirical means of channel  $j$  states, the total number of channel accesses and the number of times channel  $j$  is accessed so far. The values are updated in every iteration based on the observations. The decision criterion is proportional to the empirical average of the obtained rewards and is known as the exploitation factor. A second term triggers the exploration and is inversely proportional to the square root of the number of times the channel is accessed ( $n_j$ ). Further details and proofs of optimality are presented in [11].

We adapted the described above UCB1 algorithm for the cognitive radio context as presented in Algorithm 1.

UCB2 is an improved version of UCB1 is presented in [11]. In UCB2 based channel access, the channel access is divided into epochs. At each epoch, the best performing channel is selected according to the selection criterion defined as:

---

**Algorithm 1** UCB1

---

**Parameters:**

$K$ : total number of accessible channels  
 $j$ : channel index  
 $n$ : total number of channel access  
 $n_j$ : number of times channel  $j$  is accessed so far  
 $s_j$ : current state of the channel  $j$   
 $\bar{x}_j$ : empirical mean of the channel  $j$  states  
 $c_j$ : UCB1 criterion for selecting the best channel defined in Equation 3.3  
TRANSMIT(): Packet transmission function

**Initialization:**

```

1: for all  $j$  do
2:   if channel  $j$  is busy then
3:      $s_j = 0$ 
4:   else
5:      $s_j = 1$ 
6:   end if
7:   update  $\bar{x}_j, c_j$ 
8: end for

9: while True do
10:    $n = n + 1$ 
11:    $m = \arg \max\{c_j\}$ 
12:   if channel  $m$  is busy then
13:      $s_m = 0$ 
14:   else
15:      $s_m = 1$ 
16:     TRANSMIT()
17:   end if
18:   update  $\bar{x}_m, c_m$ 
19: end while

```

---

$$c_j = \bar{x}_j + a_j(n, r_j), \quad (3.4)$$

where  $a_j(n, r_j)$  is defined as,

$$a_j(n, n_j) = \sqrt{\frac{(1 + \alpha) \ln(\frac{en}{\tau(r_j)})}{2\tau(r_j)}} \quad (3.5)$$

and,

$$\tau(r_j) = \lceil (1 + \alpha)^{r_j} \rceil. \quad (3.6)$$

$r_j$  is the number of epochs channel  $j$  is acceded. In each epoch, the channel is accessed  $\tau(r_j + 1) - \tau(r_j)$  times.  $\alpha$  is a parameter of the model and should be tweaked based on the setting. Theoretical solution does not define  $\alpha$

---

**Algorithm 2** UCB2

---

**Parameters:**

$K$ : total number of accessible channels  
 $j$ : channel index  
 $n$ : total number of channel access  
 $r_j$ : number of epochs channel  $j$  is accessed so far  
 $s_j$ : current state of the channel  $j$   
 $\bar{x}_j$ : empirical mean of the channel  $j$  states  
 $c_j$ : UCB2 criterion for selecting the best channel defined in Equation 3.4  
 $a_j(n, r_j)$ : model parameter defined in Equation 3.5  
 $\tau(r_j)$ : model parameter defined in Equation 3.6  
 $\alpha$ : model parameter (optimally set as 0.01 based on simulations)  
TRANSMIT(): Packet transmission function

**Initialization:**

```

1: for all  $j$  do
2:   if channel  $j$  is busy then
3:      $s_j = 0$ 
4:   else
5:      $s_j = 1$ 
6:   end if
7:   update  $\bar{x}_j, c_j$ 
8: end for

9: while True do
10:    $n = n + 1$ 
11:    $m = \arg \max\{c_j\}$ 
12:   iterations =  $\tau(r_j + 1) - \tau(r_j)$ 
13:   for all  $i=1$ :iterations do
14:     if channel  $m$  is busy then
15:        $s_m = 0$ 
16:     else
17:        $s_m = 1$ 
18:       TRANSMIT()
19:     end if
20:     update  $\bar{x}_m, c_m$ 
21:   end for
22: end while

```

---

specifically. The value of  $\alpha$  is tuned experimentally based on the context. Our simulation results show that  $\alpha = 0.01$  optimizes the performance of the UCB2 algorithm in our experimental setting. Algorithm 2 represents our adaptation of the UCB2 algorithm from [11] to the cognitive radio scenario.

### 3.3.3 Adaptation of $\epsilon$ -greedy

Another well-known and simple policy in bandit problems is  $\epsilon$ -greedy algorithm. The agent chooses the most rewarding arm based on the previous observations with probability  $1 - \epsilon$  and a random arm with probability  $\epsilon$ .

$0 \leq \epsilon \leq 1$  is exploration factor. As shown in [11], decreasing  $\epsilon$  proportionally to  $\frac{1}{n}$  bounds the regret function logarithmically. The  $\epsilon_n$ -greedy based channel selection algorithm ( $\epsilon \propto \frac{1}{n}$ ) is given in Algorithm 3.

---

**Algorithm 3**  $\epsilon_n$ -greedy

---

**Parameters:**

$K$ : total number of accessible channels  
 $j$ : channel index  
 $n$ : total number of channel access  
 $s_j$ : current state of the channel  $j$   
 $\bar{x}_j$ : empirical mean of the channel  $j$  states,  
 $\epsilon$ : exploration factor,

$$\epsilon = \min\{1, \frac{cN}{d^2 n}\} \quad (3.7)$$

$c, N, d$ : parameters of the model  
TRANSMIT(): Packet transmission function

**Initialization:**

```

1: for all  $j$  do
2:   if channel  $j$  is busy then
3:      $s_j = 0$ 
4:   else
5:      $s_j = 1$ 
6:   end if
7:   update  $\bar{x}_j$ 
8: end for

9: while True do
10:    $n = n + 1$ 
11:   if  $\frac{cN}{d^2 n} < 1$  then
12:      $\epsilon = \frac{cN}{d^2 n}$ 
13:   else
14:      $\epsilon = 1$ 
15:   end if
16:   Select a random value  $r$  in  $[0, 1]$ 
17:   if  $\epsilon \leq r$  then
18:      $m = \arg \max \{\bar{x}_j\}$ 
19:   else
20:     randomly choose  $m$  from  $\{1, \dots, K\}$ 
21:   end if
22:   if channel  $m$  is busy then
23:      $s_m = 0$ 
24:   else
25:      $s_m = 1$ 
26:     TRANSMIT()
27:   end if
28:   Update  $\bar{x}_m$ 
29: end while

```

---

We found the optimum values for the model parameters,  $c = 10^{-4}$ ,  $d = 10^{-2}$ ,  $N = 5$ , through simulation.

### 3.4 Thompson Sampling Based Learning Algorithm

This section incorporates Thompson sampling into a learning algorithm for channel selection problem. Thompson sampling [24] is best understood in a Bayesian context. Assume we observed  $S_j$ , the observation vector, after accessing channel  $j$ ,  $n_j$  times. Assuming Bernoulli distribution for each access trial with parameter  $\mu_j$ , the parametric likelihood function for observation vector  $S_j$  is as follows,

$$p_j(S_j|\mu_j) = \mu_j^{t_j} (1 - \mu_j)^{n_j - t_j}, \quad (3.8)$$

where  $t_j$  is the number of successful transmissions on  $j^{th}$  channel in  $n$  trials. Without loss of generality, we use Beta distribution as the prior for the distribution of parameter  $\mu_j$ . This is because Beta distribution is conjugate prior for the likelihood function in Equation (3.8), which simplifies the derivations [29]. Using Bayes rule we can write,

$$p_j(\mu_j|S_j) = \frac{p_j(S_j|\mu_j) \frac{\Gamma(\alpha+\beta)}{\Gamma(\alpha)\Gamma(\beta)} \mu_j^{\alpha-1} (1 - \mu_j)^{\beta-1}}{p_j(S_j)}, \quad (3.9)$$

where,

$$\Gamma(\alpha) = \int_0^\infty x^{\alpha-1} e^{-x} dx \quad (3.10)$$

and  $\alpha$  and  $\beta$  are the shape parameters of the Beta distribution; as we assume no prior information on  $\mu_j$ , we initialize  $\alpha = \beta = 1$ , which yields to uniform distribution. Substituting (3.8) in (3.9) yields,

$$p_j(\mu_j|S_j) = \frac{\Gamma(\alpha+\beta)}{\Gamma(\alpha)\Gamma(\beta)} \mu_j^{t_j+\alpha-1} (1 - \mu_j)^{n_j-t_j+\beta-1}. \quad (3.11)$$

$\alpha' = t_j + \alpha$  and  $\beta' = n_j - t_j + \beta$  can re-write (3.11) as:

$$p_j(\mu_j|S_j) = C \mu_j^{\alpha'-1} (1 - \mu_j)^{\beta'-1} \quad (3.12)$$

where  $C = \frac{\Gamma(\alpha+\beta)}{\Gamma(\alpha)\Gamma(\beta)}$ . Using the fact that,

$$\int p_j(\mu_j|S_j) d\mu_j = 1, \quad (3.13)$$

and the following equality,

$$\int x^{\alpha-1} (1-x)^{\beta-1} dx = \frac{\Gamma(\alpha)\Gamma(\beta)}{\Gamma(\alpha+\beta)} \quad (3.14)$$

we obtain,

$$p_j(\mu_j|S_j) = \frac{\Gamma(\alpha' + \beta')}{\Gamma(\alpha')\Gamma(\beta')} \mu_j^{\alpha'-1} (1 - \mu_j)^{\beta'-1}, \quad (3.15)$$

which is the beta distribution with parameters  $\alpha'$  and  $\beta'$ ,

$$p_j(\mu_j|S_j) = \text{beta}(\alpha', \beta'). \quad (3.16)$$

The use of the beta distribution facilitates the implementation of the Thompson based solution in the hardware, since the existing mathematical libraries could be used to generate beta distributed random numbers. Thompson sampling Channel selection algorithm is described in Algorithm 4.

---

**Algorithm 4** Thompson Sampling

---

**Parameters:**

$K$ : total number of accessible channels  
 $j$ : channel index  
 $n$ : total number of channel access  
 $s_j$ : current state of the channel  $j$   
 $t_j$ : number of successful transmissions so far  
 $\bar{x}_j$ : empirical mean of the channel  $j$  states,  
 $\alpha$ : *a priori* (beta distribution) model parameter  
 $\beta$ : *a priori* (beta distribution) model parameter  
 $\alpha'$ : *a posteriori* (beta distribution) model parameter

$$\alpha'_j = t_j + \alpha_j \quad (3.17)$$

$\beta'_j$ : *a posteriori* (beta distribution) model parameter

$$\beta'_j = n_j - t_j + \beta_j \quad (3.18)$$

TRANSMIT(): Packet transmission function

**Initialization:**

```

1: for all j do
2:   if channel  $j$  is busy then
3:      $s_j = 0$ 
4:   else
5:      $s_j = 1$ 
6:   end if
7:   update  $t_j$ ,  $n_j$ ,  $\alpha'_j$  and  $\beta'_j$ 
8: end for

9: while True do
10:   for all j do
11:     sample  $r_j \sim \text{beta}(\alpha'_j, \beta'_j)$ 
12:   end for
13:    $m = \arg \max\{\bar{r}_j\}$ 
14:   if channel  $m$  is busy then
15:      $s_m = 0$ 
16:   else
17:      $s_m = 1$ 
18:     TRANSMIT()
19:   end if
20:   update  $t_j$ ,  $n_j$ ,  $\alpha'_j$  and  $\beta'_j$ 
21: end while

```

---

As there is no prior information about the channels, we set  $\alpha = 1$  and  $\beta = 1$  which yields to uniform distribution in  $[0, 1]$ .

### 3.5 Performance evaluation

To evaluate the performance of Thompson sampling based solution in comparison with other techniques described in this chapter (UCB1, UCB2,  $\epsilon_n$ -greedy), we used three different approaches:

- simulation based on generated channel samples,
- simulation over the real channel measurements,
- experimentation via real WSN hardware implementation.

For each approach, we used the relative throughput as an evaluation metric. This metric can be derived from the average throughput as follows: the average throughput of algorithm  $A$  ( $\bar{T}_A$ ) is obtained as the ratio of the cumulative number of transmitted bits ( $N_b(A)$ ) to the time passed since the beginning of the transmission  $t$ ,

$$\bar{T}_A = \frac{N_b(A)}{t}. \quad (3.19)$$

The relative throughput of  $A$  was obtained as the ratio of the average throughput of  $A$  to the average throughput of an oracle agent ( $\bar{T}_O$ ) that always operates on the best channel,

$$\overline{RT}_A = \frac{\bar{T}_A}{\bar{T}_O}. \quad (3.20)$$

Note that the relative throughput of the oracle algorithm is always one. The relative throughput enables us also to estimate the gain in terms of energy saving, which is very important for WSNs. Indeed, the algorithm which helps to find the best channel faster will decrease the time spent in the exploration process and transmissions over interfered channels. This will lead to energy savings.

In the following subsections the proposed evaluation approaches will be described along with the experimental setup details.

#### 3.5.1 Simulation based on generated channel samples

The channel observations are modeled and created as Bernoulli trials with parameter  $\mu$ . In other words,  $\mu$  is the probability that the channel is available. We created  $N = 10k$  samples for 10 channels with  $\mu$  values randomly distributed in  $(0, 1)$ . The sampling rate is assumed 1500 samples per second to match the measurements detailed in the next subsection. Algorithms are implemented in MATLAB and numerical analysis are performed to find the

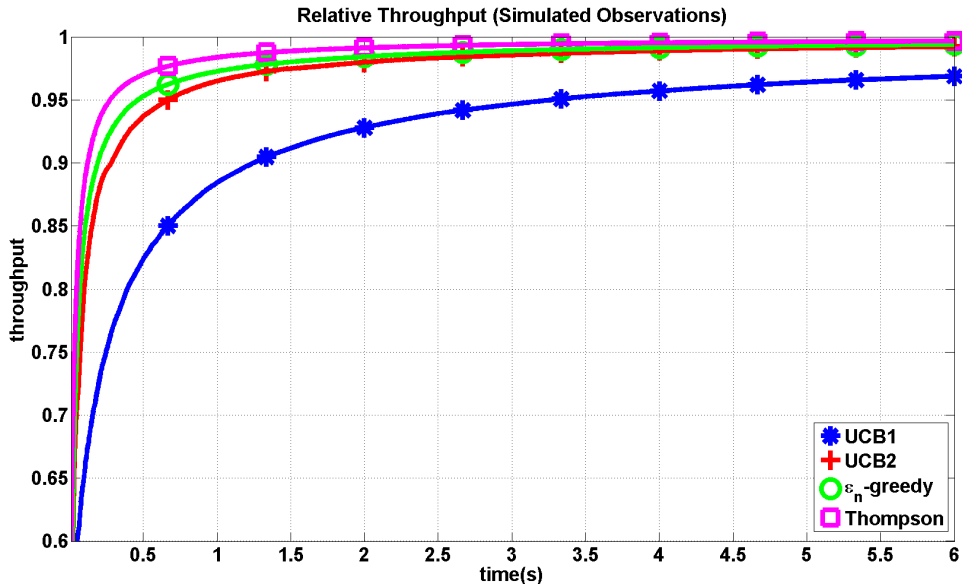


FIGURE 3.3: Relative throughput comparison of different algorithms on 10 accessible channels ( $\mu = 0.80$ ). Oracle (The user that knows the best channel from the beginning) has relative throughput 1.

optimum values for the parameters of the algorithms. To do so, simulations are run for 100 iterations and averaged to yield the relative throughput defined by (3.20). Figure 3.3 shows the relative throughput for different algorithms vs. time in seconds. In the exploration phase, the throughput of all algorithms is significantly lower than the oracle agent. However, all algorithms eventually find the best channel and start exploiting it almost all the time and hence reach a throughput close to the oracle. As seen in the figure, Thompson sampling based algorithm converges to the best channel in fewer steps than the other policies. In addition, it achieves higher average throughput as it spends less time on exploring the channels and converges to the best channel faster. This results in smaller latency in transmission and lower energy consumption for channel exploration.

### 3.5.2 Simulation over the real channel measurements

To make our scenario more realistic, we used real-time measurement of the channel to compare the performance of different algorithms. To approximate a realistic scenario, we used TelosB node (IEEE 802.15.4) as the secondary user of a Wi-Fi channel which is considered as the primary user channel, as it was discussed in the Section 3.1. The schematic of the test bench is depicted in Figure 3.4.

The IEEE 802.11g Wi-Fi access point (AP) as well as the primary user client equipment, a laptop with a Wi-Fi interface card, were on the line of sight at the distance of 4.5 m. The Wi-Fi network was configured to use the channel 6 of Wi-Fi, because it was the available part of the spectrum. The AP was connected by wire (Ethernet) to the PC running the Apache

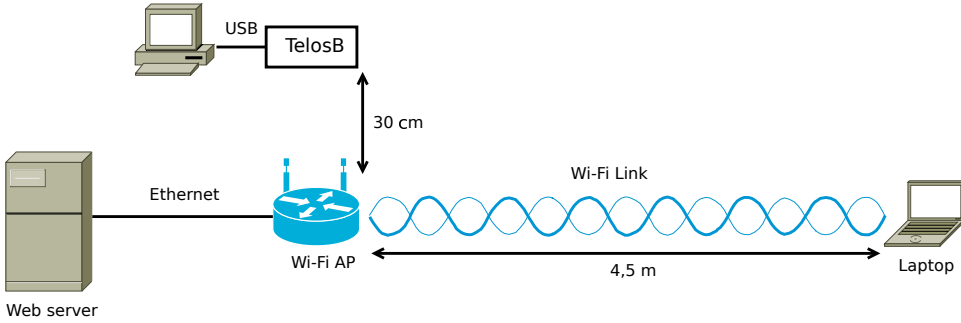


FIGURE 3.4: Schematic of experiment setup.

web-server providing the access to a web-page and a big data file (about 1 GB). The laptop was using the web browser either to perform the web-surfing, or to download the data file. The measurements were performed by the TelosB node which was situated near the Wi-Fi AP at the distance of 30 cm. The TelosB node was driven by Contiki operating system running the code to read the Received Signal Strength Indication (RSSI) values of the channel 17 of IEEE 802.15.4 (the center frequency 2435 MHz) that overlaps with the channel 6 of IEEE 802.11 (the center frequency 2437 MHz) used by the AP. The TelosB node was performing measurements at the sampling rate of about 1500 samples per second and sending the measured values to another PC via the USB link.

Figure 3.5 shows the RSSI values received by the secondary user when only one primary user is connected to the network. Figure 3.5(a) shows the RSSI when the user is idle and most of the traffic is coming from the control frames and beacons of the base station. As expected, the channel is available most of the time. In Figure 3.5(b), the user is browsing Internet pages frequently. Figure 3.5(c) shows the RSSI values when the user is downloading a large file (Approx. 1 GB). Average Availability rate of the channel ( $\mu$ ) is obtained by dividing the number of idle samples to the total number of observations where idle channel was obtained by applying a threshold of  $-44dBm$  to the RSSI measurements. The average availability rates for the setting depicted in Figure 3.5(a-c) are  $\mu = 0.99$ ,  $\mu = 0.92$ ,  $\mu = 0.12$  respectively.

### 3.5.3 Experimentation via real WSN hardware implementation

In the final evaluation step, we implemented the algorithms in TelosB node to compare their actual performance in real-time. In our setup, we used 3 pairs of laptops occupying 3 orthogonal Wi-Fi (IEEE 802.11g) channels, 1, 6 and 11 overlapping with standard 802.15.4 channels, 12, 17 and 22 respectively. As in cognitive radio scenario, we suppose that the TelosB communicates with a multi-channel receiver, which is able to receive the messages from all available channels simultaneously. The traffic in the Wi-Fi network was generated using "Distributed Internet Traffic Generator" [17] in single flow mode with packet size 500 bytes which is the average packet size on

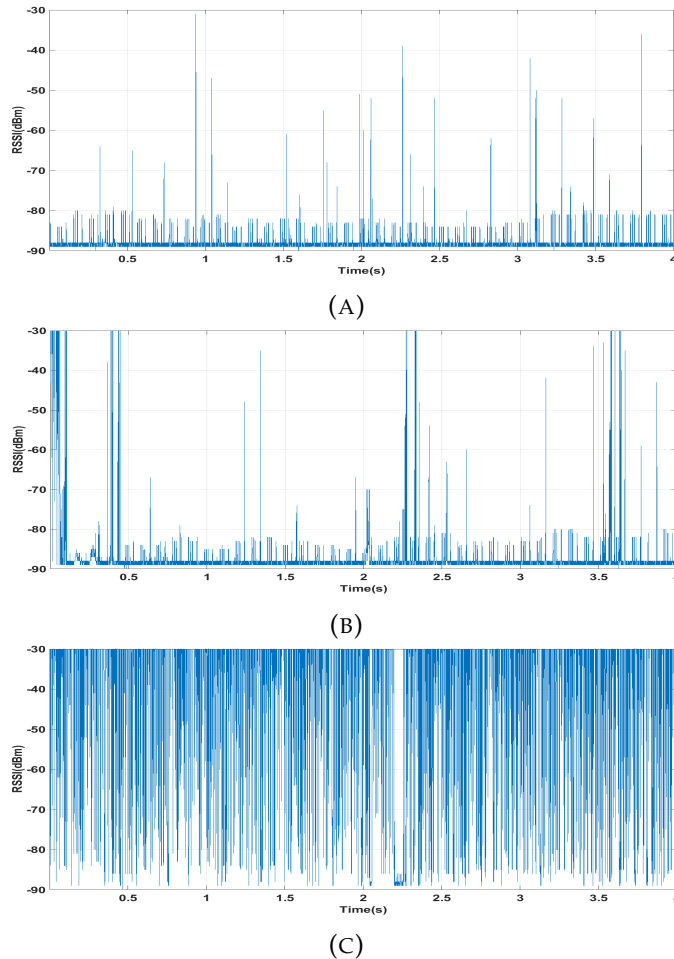


FIGURE 3.5: Spectrum measurements: a) No user activity.  
b) One user browsing the web. c) One user downloading a large file.

the Internet [99]. Two TelosB nodes were programmed in Contiki operating system one with a learning algorithm and one as oracle fixed on the best channel. To generate samples of Beta distribution used in Thompson sampling algorithm we used "GEN\_SEQUENCE" open-source library [71]. Our experimental setup is shown in Figure 3.6.

To monitor the availability rate of the channel we programmed one TelosB node as monitor which just sampled the channel. The availability rate obtained as the average number of samples the channel is detected available. The RSSI sensitivity of TelosB node was set to  $-40\text{dbm}$ . This relatively high threshold was set to suppress the RSSI received from other networks present in the building. With this sensitivity, the monitor node registers approximately 90% availability rate for the channels. The availability rate of channel 6 drops to approximately 40% when the traffic generator is activated at  $2000\text{pkt/sec}$  and packet size of 500 bytes. The availability rate of the channel 1 drops to approx. 60% when the traffic generator occupies the channel with  $500\text{pkt/sec}$ . Channel 11 is left without traffic although the server and client were connected. The monitor shows approx. 90% availability on the channel. Note that the channel occupancy rate is affected by

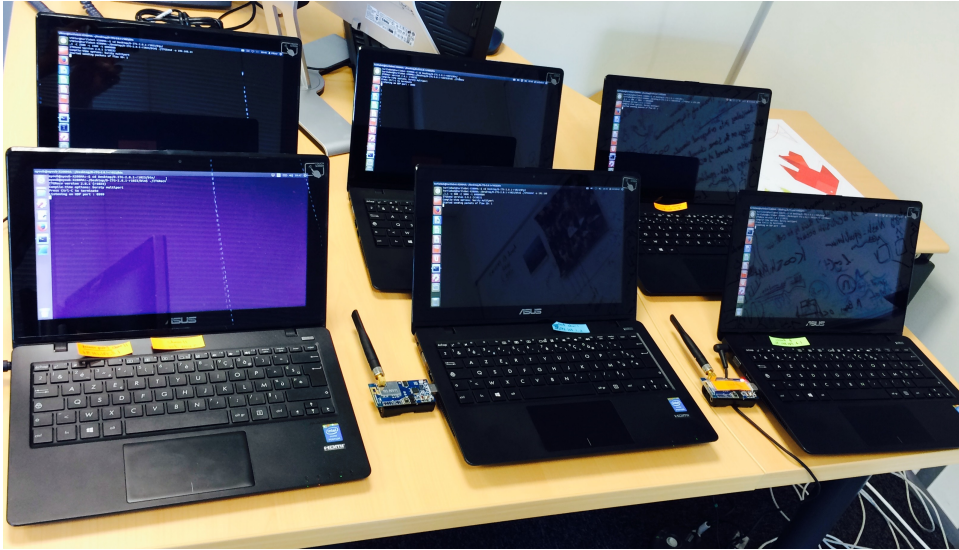


FIGURE 3.6: Experimental setup: 3 pairs of laptops occupy  
3 orthogonal channels of Wi-Fi (1, 6, 11)

our traffic, other networks traffic and noise. However, it was roughly constant during the experiment at the given rates.

We programmed two TelosB nodes; one as an oracle which always operates on the channel with the best availability rate. The other node was programmed with the implementation of a learning algorithm to find and use the best channel. In our results, we considered an available channel as a successful transmission. In reality, the packet transmission can be disrupted in the middle of the transmission and cause the transmission to fail. However, the collision will affect the throughput results of all algorithms including the oracle the same way. Hence the comparison results would not be affected.

### 3.5.4 Evaluation results

In this subsection we compare the results obtained by the three approaches presented above for all described techniques: UCB1, UCB2,  $\epsilon_n$ -greedy and Thompson. All these three evaluation approaches were adapted to the scenario of three IEEE 802.15.4 channels (described before): 12, 17 and 22, which are situated close to the center frequencies of the three non-overlapping Wi-Fi channels in the 2.4 GHz ISM band: 1, 6 and 11 (cf. Figure 2.15 in the Chapter 2). In fact, this scenario is quite common in the office buildings with multiple Wi-Fi AP installed to cover the entire building. The best practice in this case is to distribute the non-overlapping channels between the APs in the way to get the advantage of the spacial reuse. This will causes different spectrum occupancy in different parts of the building (as in was mentioned in the Chapter 2). Moreover, multiple Wi-Fi networks can operate in all the 3 orthogonal channels within the same area. The channel activity could be different for each network and depends on the user activity. The used traffic generator allows us to reproduce this scenario.

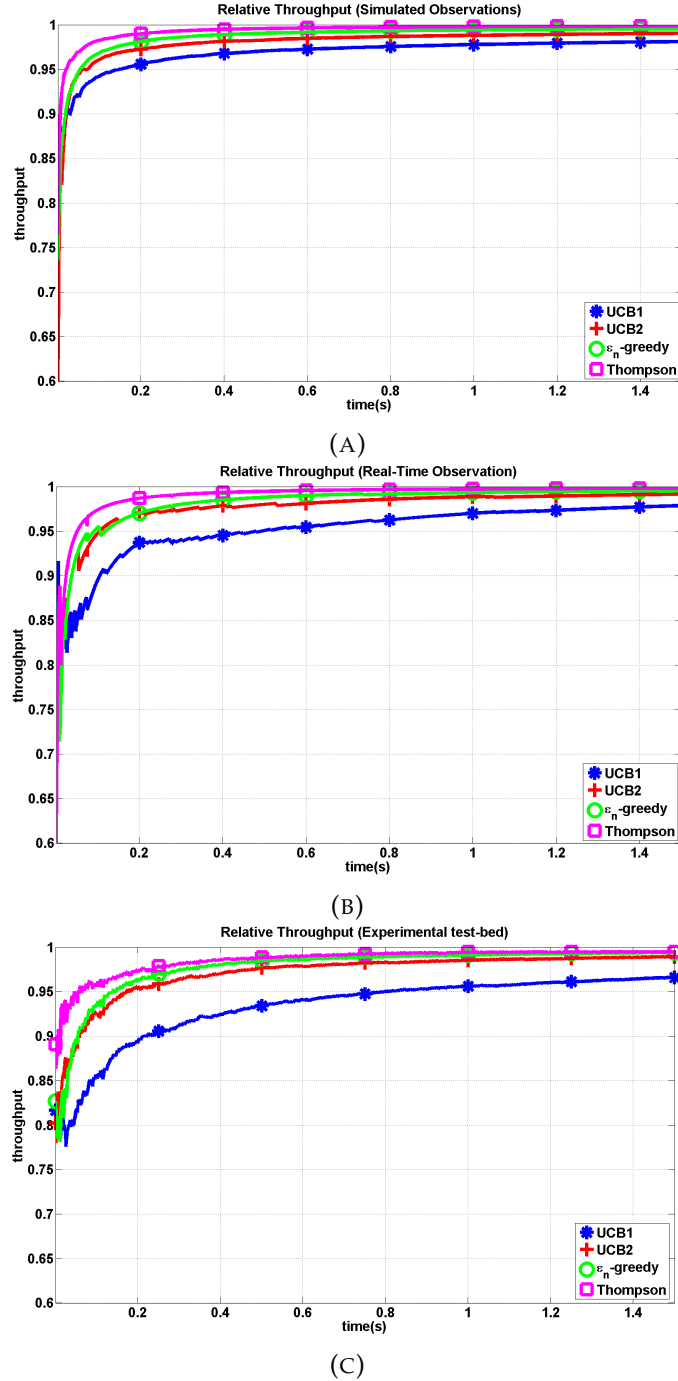


FIGURE 3.7: Relative throughput on three accessible channels using a) Synthetically generated channel observations. b) Real-time measurements c) Empirical real-time test-bed.

The simulation results with the samples generated for the 3 channels with 3 different values  $\mu$  corresponding to the values measured in the section 3.5.2 (0.99, 0.92 and 0.12 respectively) are presented in the Figure 3.7(a).

Then, we used the real-time channel observations instead of synthetically generated data to compare the performance of the learning algorithms. The results are shown in the Figure 3.7(b). As seen in the figures, the comparison results using real-time data is similar to the results obtained through synthetic channel. The real-time measurements results show that

Thompson sampling algorithm reaches 99% of the oracle throughput after 0.26s (390 samples) approx. 57% faster than the next best algorithm ( $\epsilon_n$ -greedy) which achieve the same throughput in 0.60s (900 samples).

Finally, we obtained results for the tests with real hardware implementation. In each set of experiments, we performed 3 experiments where occupancy rate of the channels were permuted. We repeated each experiment 3 times. The relative throughput of each algorithm in each experiment is divided by the oracle performance of the best channel and then averaged over all the experiments for each algorithm.

The results are shown in Figure 3.7(c). As seen in the figure, similar results are obtained in empirical evaluation of the algorithms where Thompson based method achieves the best performance followed by  $\epsilon_n$ -greedy and UCB2 algorithms which performed similarly in this context.

## 3.6 Multihop extension

In some cases the multihop capabilities of WSN are required. Multihop communications allow to increase the coverage of the network and the reliability when the sink node becomes unreachable in one hop. Enabling the multihop capabilities in CR-WSNs is not a trivial problem. In fact, the main challenge in multihop multichannel wireless networks is to ensure that both sender and receiver nodes use the same channel at the same time. In this section we propose a solution to implement the described before Thompson based cognitive radio solution in a multihop wireless network operating in the 2.4 GHz ISM band.

### 3.6.1 Test application scenario: EWSN 2016 dependability competition

Our solution was proposed in the framework of the EWSN dependability competition. The competition proposes to all contestants to implement their solutions on the specifically designed testbed and compare their performance in the interfered environment. The schematic of the experimental case is represented in the Figure

Twelve to fifteen user controlled TelosB nodes were deployed in the different rooms of a building in different rooms on a total surface of about  $150m^2$ . The exact number of the nodes as well as their position were unknown in advance. There were three possible categories of user controlled nodes: intermediate (forwarding) node, sensing node and sink node. The sensing node had to monitor the binary light switching activity (on/off states) of a LED controlled according to an unknown binary pattern and report the detected light changes to the sink node. The sink node had to repeat the light pattern of the source node by changing a GPIO pin. The nodes were deployed in the way that the direct communication between

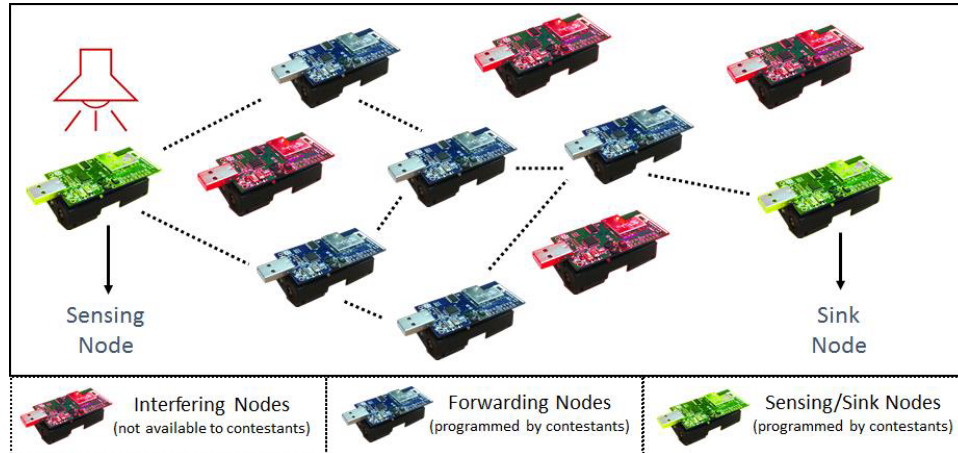


FIGURE 3.8: Dependability competition scenario description. Credits: Carlo Alberto Boano

the sensing and the sink nodes are impossible even at the maximum transmission power. Thus, the intermediate nodes had to be used as multihop relays. The challenging factor of the dependability competition was the presence of the interfering TelosB nodes which were generating dynamically unknown patterns of interfering signals using JamLab [15]. These nodes were controlled by the organizers of the competition and, thus, were unavailable for contestants. The contestants did not have physical access to the user controlled nodes, but they had to provide a firmware, which is uploaded automatically on the nodes. The aim of the competition was to propose a multihop communication solution in order to report the measured at the source node light changes to the sink with the best reliability (the total number of correctly reported light changes), lowest latency and overall energy consumption during the entire 35 minutes test slot dedicated to each contestant. During the first 20 seconds, no light changes were possible. This time could be used by contesting solutions to adjust the parameters or run a learning algorithm. The platform was measuring the evaluation parameters as follows: the reliability and latency were measured by using the GPIO output from the sink node. The energy consumption was measured at each user controlled node by a specific hardware platform connected to the TelosB node. This platform was also in charge to program the node with a provided by contestant firmware. Then, all the individual values of measured energy consumption were summed up in order to obtain the overall energy consumption of the entire system, which was used as an evaluation criterion. The structure of the user controlled node attached to the hardware measurement platform is depicted in Figure 3.9.

In 2016, the dependability competition held in the Institute for Technical Informatics of the Graz University of Technology. The experimental area map is represented in the Figure 3.10.

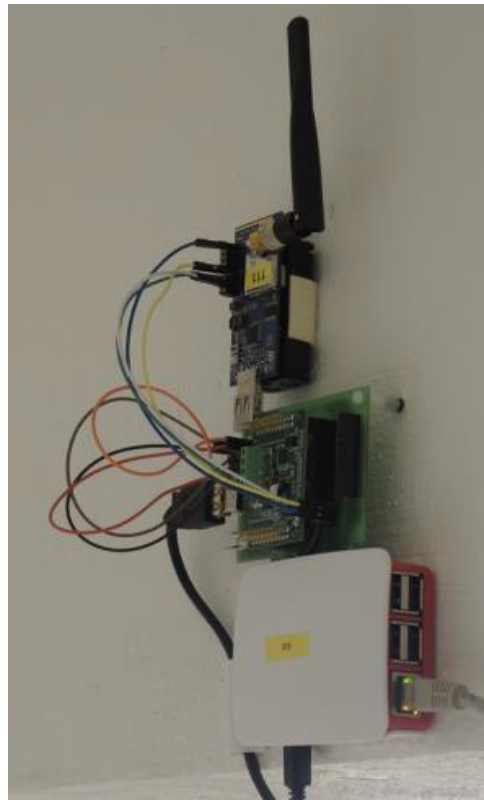


FIGURE 3.9: TelosB node connected to the control platform.  
Credits: Carlo Alberto Boano



FIGURE 3.10: Experimental area map at the Institute for Technical Informatics of the Graz University of Technology. The source and the sink nodes are represented by dark blue stars, whereas the intermediate nodes are represented as blue spots. Credits: Carlo Alberto Boano

We can notice that the sink and the source nodes are situated in different rooms in the opposite corners of the experiment area. The multihop communications are required in this setup. It is important to notice, that the rooms and offices in this building were separated by thick concrete walls, which makes the communication even more challenging. However, to ensure the repeatable experiments, the surrounding Wi-Fi networks of the building operating in the 2.4 GHz band were disabled during the competition.

### 3.6.2 Proposed multihop solution based on Thompson sampling approach

As mentioned before, an important challenge for the multihop CR-WSN networks is to ensure that the receiver and transmitter nodes use the same channel at the same time. Indeed, the classical cognitive radio networks suppose a heterogeneous structure. Indeed, it is often assumed that the sink node (or base station) of the cognitive radio network has multichannel capabilities. It means that it is able to constantly listen to all available channels, which ensures that the end node is always on the same channel as the sink node. In the dependability competition scenario, the single radio TelosB nodes are used, which do not have the multichannel capabilities. Thus, if our Thompson sampling based algorithm is implemented "as is" (as it described in section 3.4) in the dependability competition scenario, there is a high probability that the nodes choose the different channels. Indeed, the interference patterns generated by the interferers nodes running Jam-Lab are random. So, the best channel according to the Thompson sampling approach could be different in each node location.

It is important to note that configuring the nodes to send the messages on the locally best channel is inefficient in a multihop scenario, since this channel could be strongly impacted by interference at the receiver side (sink or next hop). If it happens, the message will be lost. We propose thus to use the best channel found locally by each node using Thompson sampling approach to receive the messages to be forwarded. Then the message is forwarded on all the available channels, which will increase the probability of successful reception of the packet by the next hop at the expense of increased energy consumption. The proposed communication mechanism is depicted in Figure 3.11.

As in the previous test scenarios, we propose to limit the number of available IEEE 802.15.4 channels to 3: channel 12, 17 and 22 which are situated close to the center frequencies of the 3 orthogonal Wi-Fi channels in the 2.4 GHz ISM band. The TelosB nodes was configured as follows:

- The Sensing node was constantly measuring the light conditions. In case of detected change of LED state (on/off), the message containing the current state of the LED (1 or 0 for on and off states respectively)

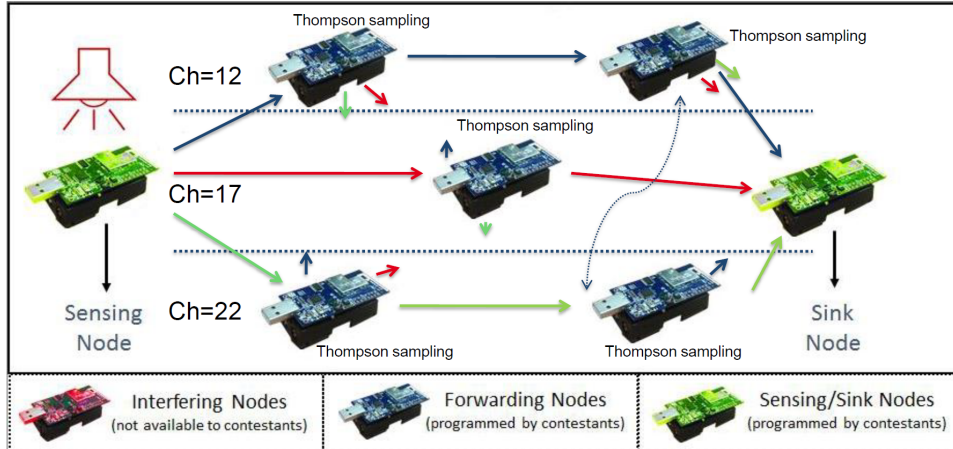


FIGURE 3.11: Proposed Multihop solution

was broadcast following ContikiMAC [33] RDC protocol along with CSMA MAC strategy in each of 3 available channels consecutively. The channel is switched after 0.1 second to let the CSMA strategy the time to perform backoff operations if necessary. The broadcast packets contain also a packet ID to avoid forwarding of the duplicated packets and a TTL value to limit the maximum number of hops. That enables to avoid loops and limits the packet forwarding in the wrong direction. The TTL value was set to 9. Note that ACK messages are not used in the system, since broadcasting strategy is in use.

- Forwarding nodes were running the Thompson sampling cognitive radio algorithm proposed in this chapter in order to determine locally the best channel. During the first 20 seconds the initial sensing was performed. The nodes, thus, determine the best channel and switch to this latter in order to listen for incoming packets to forward. The Radio Duty Cycle period for the intermediate nodes was set to 62.5 ms (16 Hz) in the aim of energy savings. Once the message is received, after TTL and packet ID check, the packet is broadcast all 3 available channels during 0.1 second on each (as at the sensing node side). After each physical transmission during the forwarding, the nodes update the channel statistics which are used by Thompson sampling algorithm. This enables the forwarding node to change the current reception channel, which is important, since the generated interference patterns could be changed dynamically during the test. It ensures that the forwarding nodes always listen on the best channel, which minimizes the probability of packet losses.
- The Sink node keeps the radio always on. It listens to all the 3 channels consecutively with a period of 0.018s. If the packet is received on one of the channels, the sink node checks the packet ID value and changes the GPIO status if needed.

### 3.6.3 Performance evaluation results and discussion

The results for both, preliminary test run and final test run are presented in Table 3.1. In contrary to the final test scenario, the preliminary test duration was set to 5 minutes. The Wi-Fi access points operating in the building in the 2.4 GHz band were active. Another difference between these test setups is the active debug serial interface. Indeed, this interface is useful to adjust some parameters before the final test. However, the use of this interface increases significantly the energy consumption of the TelosB nodes. Thus, this interface was disabled during the final test.

As we can observe, in both scenarios, we achieved relatively high reliability rates (up to 80%), which confirms the efficiency of the first implementation of the proposed multihop cognitive radio technique.

The proposed solution could be adjusted depending on the application scenario by modifying available parameters. For example, the reliability could be increased by extending the list of available channels. However, it will lead to the increase of the latency and energy consumption because of the need to broadcast the messages on more channels. On the other hand, the latency can be decreased by decreasing the broadcasting time on each available channel (0.1 second in our case). However, it can decrease the reliability. Similar effect can be obtained by modifying the RDC period.

One of the directions for future work is the development of the solution which will dynamically adapt the described parameters in order to tune the performance of the algorithm in real time.

The solution can be extended to the efficient mesh scenario by adding the number of the best locally defined channels in the header of the message.

## 3.7 Chapter conclusion

In this chapter, we have studied the performance of the Cognitive Radio as a possible adaptable communication solution for WSN. We observed that a Thompson sampling based solution shows a good performance in terms of reliability even in a non-trivial indoor multihop scenario under jamming. However, the redundancy of the proposed multihop extension (multiple ContikiMAC broadcast transmissions in many channels) could represent a drawback for some solutions, due to possible increased energy overhead.

TABLE 3.1: Evaluation results in multihop scenario

Test scenario	Reliability, %	Latency, ms	Energy, J	Test duration, min
Preliminary test	80.00	1710	307	5
Final test	76.74	1260	988	35

A possible direction of the future works in this topic is further adaptability of the presented solution in order to find a trade-off between the latency, reliability and energy consumption. To do so, additional metrics (*e.g.*, battery state of charge) should be used in order to make decision on parameter adjustment.

Another possible research direction is the development of the Cognitive Radio communication solutions for LPWANs. As we mentioned in Section 3.1, the first step in the Cognitive Radio spectrum management process is the Spectrum sensing. The most simple way to implement this operation is the RSSI based Energy detection approach. However, in LPWAN, the messages are often received with the power under the noise floor, thanks to the high sensitivity of the RF modules. That makes the RSSI based Spectrum sensing approach inefficient, since the measured values in this case will be equal or greater than the noise floor level. An alternative Spectrum sensing technique, thus, should be developed. For example, the number of successfully received packets can be used as indicator of channel availability.

Even though the Cognitive Radio solutions were developed initially for license based spectrum operation, it can be, indeed, used also in the unlicensed ISM bands. Thus, it is a promising adaptable solution for the existing and future IoT networks.

## Chapter 4

# Distributed adaptive MAC protocol for WSN-based wildlife protection

### 4.1 Chapter introduction

As mentioned in Chapter 1, the WSNs as a part of the IoT can be used in a wide range of applications. One of the possible applications is wildlife animal tracking. This scenario is associated with several challenges:

- *Large monitoring area*: the habitat area of wild animals can cover large zones. The coverage of this area must be provided, which is difficult, since the network infrastructure in these zones is generally poor or nonexistent.
- *Mobility of the animals carrying the WSN nodes*: in the natural conditions, wild animals are free to move over their habitat area. Their mobility patterns cannot be controlled. As we showed in Chapter 2, the radio environment can significantly change as a function of current position of the node. It is important to note also that some zones could be uncovered by sink node(s).
- *Weight and size limitations*: limitations hold to ensure comfort and safety of animals carrying the WSN nodes. That is why size and weight limitations (which impact the battery size and capacity) must be respected.
- *Limited access to the animals*: placing nodes and replacing batteries can be expensive and challenging.

To respect the limitations listed above and to meet functional requirements provided in Chapter 1 the following technical requirements must be considered to design an efficient communication strategy:

- *Long range transmissions*. To ensure the expected coverage of the target area, the communication technology has to provide long range communication capability at physical layer. Moreover, due to the low

density of the rhinoceros in the Kruger park, the short range based multihop solutions are inappropriate since the animals could often be out of range of each other in this case.

- *Multihop communications.* Huge size of the target area (as mentioned previously) and lack of electric power in the Kruger park do not allow installing a number of Base Station Transceivers (BTS) sufficient to guarantee a seamless radio coverage. Moreover, the direct communication between a sensor node and a BTS can be impossible in some areas due to the harsh environment conditions. The multihop communications should be considered to allow the full coverage of the target zone.
- *Multi-channel operation.* Long range communication technology will cause a presence of significant number of nodes within a communication range. Moreover, the long range communications often require to use low rate transmissions in order to increase the sensitivity of the receiver and, thus, the Signal to Noise Ratio (SNR), which increases the on-air time of transmitted packets. Indeed, to limit the noise power at the receiver, we need to have relatively narrow bandwidth transmission, and, consequently, a long on-air time. As it will be shown in Chapter 4, single channel capacity could not be sufficient to let all the nodes within a communication range respect the limitations of the data send period in the framework of the PREDNET project. As a consequence, multiple channel will be needed to ensure the full connectivity.
- *Two operation modes.* Both, normal mode and alarm mode must be supported. Each node generates data packets periodically or alarm messages in case of emergency and sends them to the BTS directly or through intermediate nodes. The alarm messages have a more constrained delay and stricter reliability requirements than in the regular packet messages.
- *Low energy consumption.* Limited size and weight of devices impose limitation of capacity of the battery, and, thus, available energy. Moreover, the respect of the minimal duration of lifetime is also required. Therefore, the proposed communication solution must take energy saving into account.

We will show later that existing MAC layer solutions cannot meet all the functional and technical requirements defined by the PREDNET project. Thus, the development of a new MAC layer protocol is needed. As mentioned before, the LoRa technology was chosen as physical layer technique for the PREDNET project scenario. LoRa allows both long range transmissions and low energy consumption. Moreover, this technology let us

develop and implement a custom MAC layer protocol. Indeed, the off-the-shelf LoRaWAN protocol does not support multihop communications, thus, does not meet PREDNET technical requirements. It is important to note also that the GPS modules are used in the project in order to localize the animals in the Kruger park. These modules can also be used to synchronize the nodes, which can be useful in development of a MAC protocol.

In this chapter we study the wildlife animal tracking usecase in the framework of the LIRIMA PREDNET project.

### 4.1.1 Existing MAC protocols

As it was mentioned in the previous subsection, the LoRaWAN[97] MAC layer protocol proposed by LoRa is not suitable for the PREDNET scenario. LoRaWAN is a simple sender initiated ALOHA-based MAC protocol. The advantage of this solution is that it does not require development of any RDC strategy: the nodes can start their transmissions at any moment. Since, the sink node (the Base station) is always on and listening to all the available channels, the message could be received immediately, without any connection establishment process. However, this approach requires the full coverage of the target zone, which, as we will show in the Section 4.3.4, is not possible in our case. Different MAC protocols are proposed in literature. Well known MAC protocols used in WSN with IEEE 802.15.4 compatible radios (*e.g.* X-MAC[19], ContikiMAC[33]) cannot be used in the PREDNET scenario due to their single-channel nature. However, some concepts from this protocols can be reused in our scenario.

The Glossy solution is proposed in [48]. This solution enables to increase the robustness of the transmissions by using the simultaneous concurrent transmissions. In this case multiple nodes send the same data message, which is not energy efficient in our context. However, we can reuse the idea of concurrent transmissions and the capture effect phenomenon in the short control message exchange aiming to reserve the transmission opportunity.

The ORPL[37] proposes a ContikiMAC based solution to decrease the overall energy consumption of the WSN, comparatively to Glossy. This solution is based on the anycast transmissions. The messages are accepted and ACKed only by nodes, situated closer to the sink node. However, to define, whether the node is closer to the sink or not, the RPL routing protocol is used to define the rank (the number of hops that the message should pass to arrive to the sink). RPL is designed for static topologies, thus will not perform well in our case. Moreover, it is resource consuming in terms of memory. However, in our case the rank based approach could be reused to determine the distance to the sink.

In [13] authors propose a Slotted Seeded Channel Hopping (SSCH) protocol. This protocol uses multiple channels to increase the capacity of the network for both single-hop and multi-hop scenarios. The SSCH protocol

is designed to be used with only one radio module per node, while a number of multi-channel MAC protocols need to use 2 radios [12], [6]. However, this protocol is originally designed for IEEE 802.11 wireless cards which are supposed to stay in active mode all the time. So, the SSCH protocol could not be used even with low-power radios because of a lack of the sleep mode (energy constraint). Moreover, the SSCH protocol suppose to be used with high throughput wireless links of 802.11 cards which enables to use up to 35 maximum length packets within a one timeslot. These communication rates are not available for long range low power transceivers.

The Timeslotted Channel Hopping (TSCH) is a mode of IEEE 802.15.4e[63] standard describing time-slotted communications between WSN nodes with channel hopping. This standard focuses on communication mechanisms, but do not describe strategies to build and maintain communication schedules. Communication schedules maintaining for mobile networks is challenging. The schedule can vary in different locations. Indeed, the same time-slots can be reused in different geographical zones. We believe that time-slotted structure, as proposed in TSCH, is useful for PREDNET project application, since it helps to decrease energy loss due to the connection establishment process and, as it will be described later, helps to manage contention based access to the medium. However, the channel hopping approach as a solution against interference is questionable because of the long on-air time for long range transmission technologies which leads to long time-slots along with long application layer packet generation period (15 minutes in our case).

Amouris propose Space-Time Division Multiple Access (STDMA) protocol [7] for mobile *Ad-hoc* networks. This protocol was designed only for WSN whose nodes have a GPS module. The disadvantage of this protocol is related to the need of significant amount of flash memory to store the map of cells with geographic coordinates.

The A-MAC protocol[80] propose to adapt the WSN node duty cycle in according to the current battery State of Charge. It can be useful in our case. Indeed, nodes with higher amount of available energy can wake-up more often in order to forward messages from neighbors, which will decrease the end-to-end delay. At the same time, the nodes with less energy available wake up less often in order to save energy.

## 4.2 Our contribution : the WildMAC protocol

WildMAC is a multi-channel distributed slotted Aloha-based protocol with slot reservation and multi-hop capabilities. It is a synchronized TDMA based solution providing the long-term time-slot reservation for the nodes in the proximity of the sink nodes and on-demand one-time slot reservation for the nodes which are not the neighbors of the sink. The TDMA approach enables to decrease the competition between the nodes in the proximity

of the base stations (BTS) or sink nodes. It is important, since these nodes have to forward the messages from all other nodes which are out of range of the BTS. Thus, the synchronization is required to maintain the time-slotted structure.

The protocol ensures the awareness of the nodes regarding their network depth which we call *rank*. The rank is defined as the minimal number of hops needed to send message to the BTS. Each BTS has a Rank=0. Then, the nodes follow the gradient strategy: the messages are propagated via nodes with a Rank smaller than source node's one, to reach the BTS with the smallest number of hops. The protocol is able to adapt the behavior of the nodes based on their forwarding buffer queue size. WildMAC could also take account of the current node's State Of Charge (SOC) – amount of energy left in the battery, which helps to maximize the individual lifetime duration and enables the integration of the energy harvesting techniques developed in the framework of the PREDNET project. The protocol is tuned to be used with the LoRa technology, but its generic design allows its implementation on top of any other kind of radio (*e.g.*, IEEE 802.15.4g compatible transceivers).

The proposed protocol ensures multihop capabilities which are not provided by off-the-shelf MAC solutions for LPWAN (*e.g.*, LoRaWAN). Moreover, the WildMAC supports mobility which is required in wildlife animal tracking scenario.

#### 4.2.1 General Time division structure

The Time division structure designed for the protocol is presented in Fig. 4.1. Time is divided in Super Frames (SFr) containing a fixed number of timeslots (TS) (common for all nodes). The duration of a Super Frame is equal to the application data generation period, in our case 15 minutes or 900 seconds, as mentioned in Section 1.3.1. Thus, the number of TS in each SFr depends on the duration of each TS. Nodes are synchronized within timeslots but not mandatorily within Super Frames, *i.e.*, all nodes know the time of the beginning and the end of each timeslot, but each node can have its own local TS counter. In our case the nodes are equipped with a GPS module due to the application requirements (see Section 1.3.1). This module can be used also to guarantee the synchronization, which is required to maintain the slotted structure. Nevertheless, the protocol can be used also within nodes which do not embed GPS or other GNSS module. In this case, the problem of the synchronization could be solved as proposed in IEEE 802.15.4e standard [63], by including the phase drift information in the ACK or derived from a beacon frame.

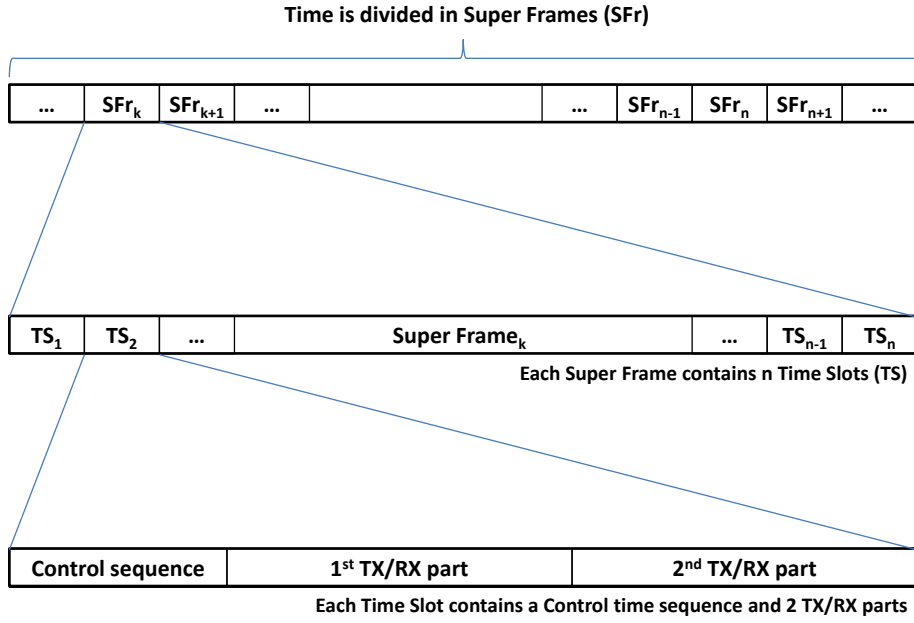


FIGURE 4.1: Slotted Aloha based algorithm with reservation. Global flowchart

#### 4.2.2 Timeslot structure

An example of the general structure of Timeslots is presented in Fig. 4.2 where a sequence of 3 consecutive timeslots is presented. Each timeslot is divided in 3 parts: Control part, First data exchange part (1st TX/RX) and Second data exchange part (2nd TX/RX).

##### Control part

The control part ensures four main functions:

- Rank discovery
- Network synchronization (if needed)
- Alarm message transmission
- Opportunity to transmit ACK messages

These functions are described below in more details. During the control part of the timeslot, all the nodes switch to the control channel, known by each node.

**Rank discovery.** The control part of the timeslot allows the broadcasting of short beacon messages by each node in order to let all surrounding nodes determine their Rank. The fixed offset is defined to send a beacon message for each specific Rank. This offset is proportional to the Rank value, *i.e.* the

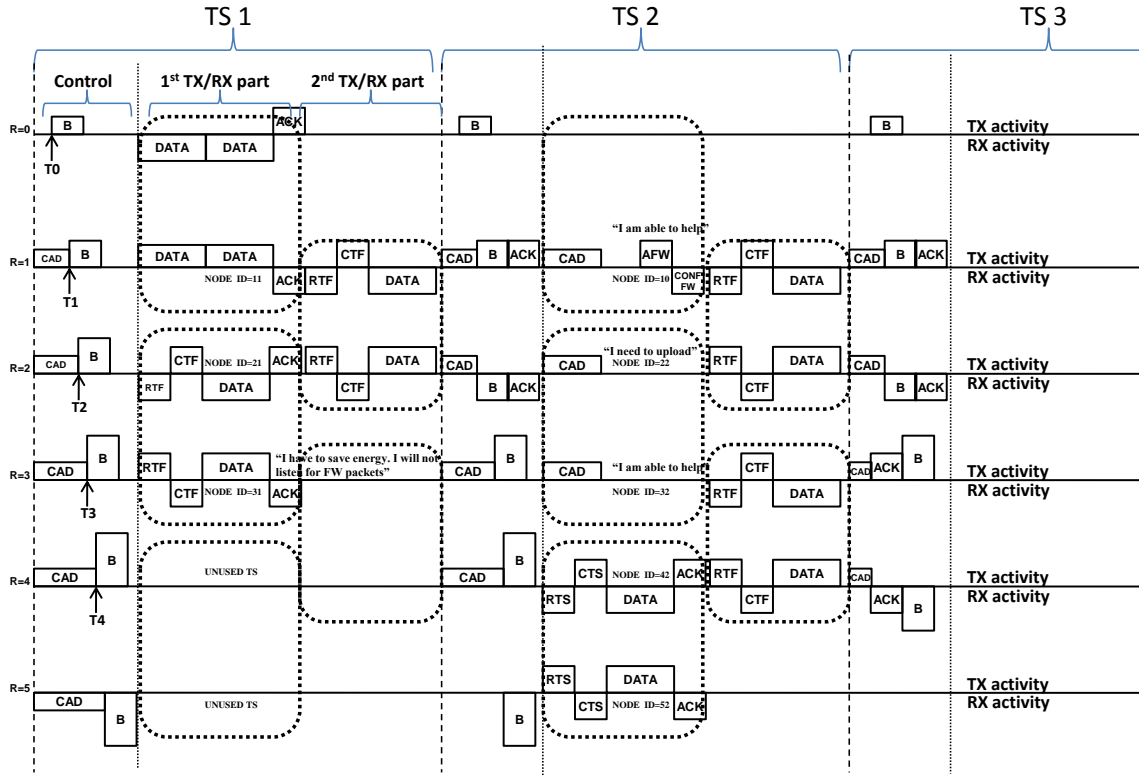


FIGURE 4.2: General Timeslot structure

beacons from lower ranked nodes are sent before higher ranked nodes. In the case of use of a generic radio, the offset step between differently ranked nodes could be set to the duration of the beacon message. In this case, the beacon messages will be sent consecutively starting from BTS nodes (Rank=0) to the furthest nodes (in our case, nodes with Rank=5).

An example of rank discovery process is given in Figure 4.3.

Supposing a new node (Node C in the Figure), situated 3 hops away from the BTS, wishing to join the network. To determine its Rank the node C switches to the channel used for control part of each timeslot and listens for beacon messages. The node is able, thus, to receive the beacon messages from Rank 2 nodes (Node B), other Rank 3 nodes (Node D) and Rank 4 nodes (Node E) since these nodes are in the communication range of C. The Rank is defined then by the earliest received beacon message. In this example, the beacon message from a Rank 2 (Node B) node will be received first due to its lowest offset. Node C sets its Rank as the Rank of earliest received beacon plus one (in the present case, the nodes Rank=2 + 1 = 3).

Since a unique offset for each Rank is defined, the new node is able to define its Rank via preamble or Start Frame Delimiter (SFD) detection (see CAD part in the Fig. 4.2). Besides, the decoding of the entire beacon frame is not necessary, which helps to save energy.

It is clear that the maximum number of supported hops depends on the duration of the Control part of the timeslot. To increase the number

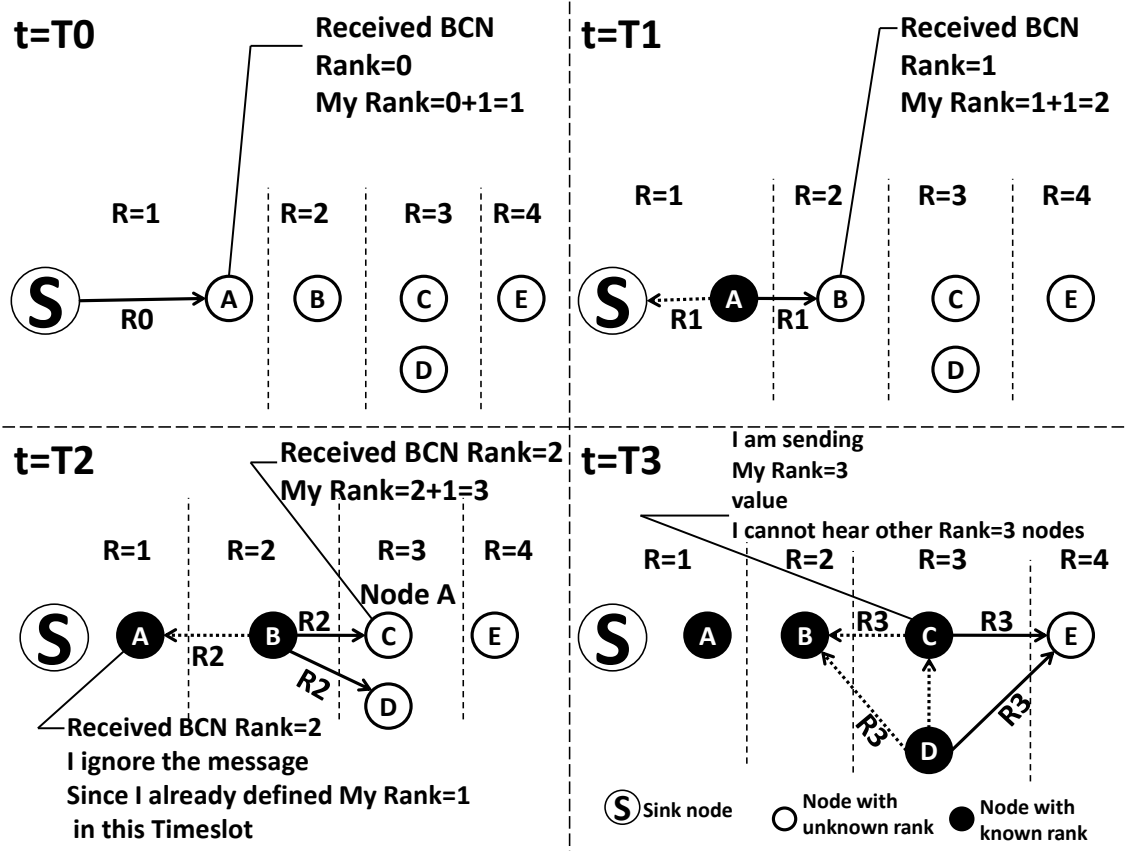


FIGURE 4.3: An example of rank discovery process

of supported hops it is possible to increase the duration of the Control part. However, it will also increase the overall duration of the timeslot which will decrease the total number of timeslots in the Super Frame and, thus, lower the network capacity. Some alternative methods to increase the maximum supported number of hops are described at the end of this Section.

**Network synchronization.** The described method of beacon message detection based on SFD detection of CAD operation with a given offset allows also the network synchronization function. However, in this case the beacon message has to be decoded in order to get the information about the rank. Then, since the offset for each beacon message is known, the time of reception can be used to adjust the clock of the node. This method can be used as alternative to the ACK based and GNSS based methods mentioned before.

**Alarm message transmission.** As can be noticed from Fig. 4.2, the offset of the Rank 0 (BTS) beacon message is greater than zero and equals to the duration of the preamble, as the offset in other cases. This enables the third function of the Control part of the timeslot – transmission of the urgent alarm messages. Indeed, the fact of letting the alarm messages to be transmitted earlier than all beacon messages, gives to these alarm messages a high priority at the physical layer due to the capture effect described above.

The alarm message can be confirmed by an Acknowledgment message in order to ensure reliable transmissions.

**Opportunity to transmit ACK packets.** The ACK messages for normal priority data messages in some cases also can be transmitted during the Control part of the timeslot which constitutes fourth function of the Control part. These cases will be described in Section 4.2.2.

**Methods to increase the maximum supported number of hops** To increase the number of supported hops, it is possible to increase the duration of the Control part. However, it will increase the overall duration of the timeslot which will decrease the total number of timeslots in the Super Frame and, thus, decrease the network capacity. To increase the maximum number of hops in the network without increasing the duration of the Control part, two techniques are proposed. The first technique is related to the capture effect peculiarity of LoRa communications. In fact, when 2 LoRa packets are sent to the same receiver with the same communication parameters (CF, SF, BW) and overlap in time, only the first packet will be received if the transmission of the second packet starts after the end of the preamble of the first one. The second packet in this case will be ignored and but the first packet can still be correctly decoded. This phenomenon happens even if the Received Signal Strength (RSS) of the second packet at the receiver side is higher than the RSS of the first packet until a specific limit which depends on the used SF. *E.g.* for the SF=12, the first packet can be successfully received if the RSS of the second packet is up to 21.5 dB greater than the first one. We propose then to use this phenomenon to optimize the use of the Control part of the timeslot in our system. As we can notice in Fig. 4.2, the beacon messages overlap, but the chosen offset ensures that the beacon message of the node with higher Rank (*e.g.*, ID=21) will be sent after the end of transmission of the preamble of the lower Rank node (*e.g.*, ID=11). In our case (up to 5 hops) this technique allows lowering the duration of the Control part by 36% comparatively to the consecutive sending of non overlapping beacons. Another technique consists of assigning additional channels for the communications in the Control part. *e.g.*, in our case the beacons from the nodes with Ranks between 0 and 4 (up to 5 hops) could be sent via channel 1, beacons from the nodes with Ranks between 6 and 10 (up to 11 hops) could be sent via channel 2 etc. In this case the maximal Rank is proportional to the number of available channels for Control part communications. As will be shown in Section 4.3, these techniques ensure sufficient number of hops to provide communications for the present scenario (animal tracking in the Kruger park). However, the limitation of number of hops can be removed by implementing a simple flooding strategy for nodes with Rank greater or equal to the maximum available Rank. This option is left for future work.

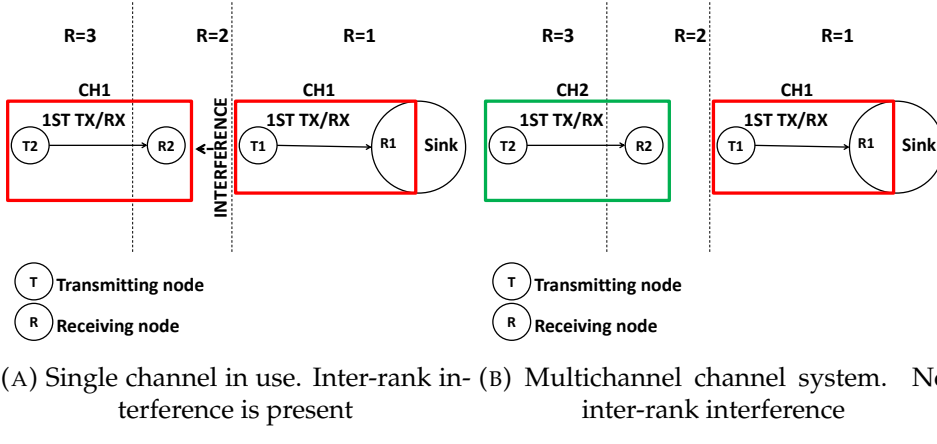


FIGURE 4.4: Inter-layer interference.

### First and Second TX/RX parts

Each node uses one of the TX/RX parts to transmit data and another to receive. The decision about the purpose of the TX/RX parts is based on the node's Rank. In the example presented in Figure 4.2, the nodes with the even Rank values (0,2,4) receive data packets from the upper ranked nodes during the first TX/RX part (reception function) and transmit packets to lower ranked nodes during second TX/RX part (transmission function). For odd ranked nodes (1,3,5) the functions are opposite: transmission function for the first TX/RX part and receive function for the second one. The access to the timeslots for Rank 1 nodes is mainly based on the permanent reservations. It is possible also to request an on-demand timeslot reservation. For the nodes with a Rank greater than 1, the access to the timeslot is only based on the one-time on-demand timeslot reservation. These reservation mechanisms are defined below. The data messages sent during first or second TX/RX parts are acknowledged by ACK messages. We can notice that in Figure 4.2, the First TX/RX part is slightly longer than the second one. The second TX/RX part is shorter due to the ACK message which was moved to the Control part of the next timeslot, as mentioned before. It helps to optimize the timeslot duration.

### 4.2.3 Multichannel operation structure

The multichannel operation of the protocol is proposed in order to improve communication performance and meet technical and functional requirements. To enable multichannel operation, we assume that the BTS is able to receive messages from multiple channels simultaneously. More in details, the requirement to use multiple channel will be explained in Section 4.3. As mentioned in Section 4.2.1, the use of multiple channels in the Control Part of the timeslot increases the maximal number of supported hops. We also propose to use multiple channels during first and second RX/TX parts.

From Figures 4.2 and 4.4, we can notice that the nodes receiving data packets from higher ranked nodes can overhear transmissions from lower ranked nodes (in Figure 4.4 the Rank 2 node (R2) receiving the packet from the Rank 3 (T2) node is impacted by the data transmission between Rank 1 (T1) node and BTS (sink node) during the 1st TX/RX part). This situation leads to the inter-rank interference which will decrease the success rate of transmissions. To overcome this problem, we propose the frequency division structure presented in Figure 4.5.

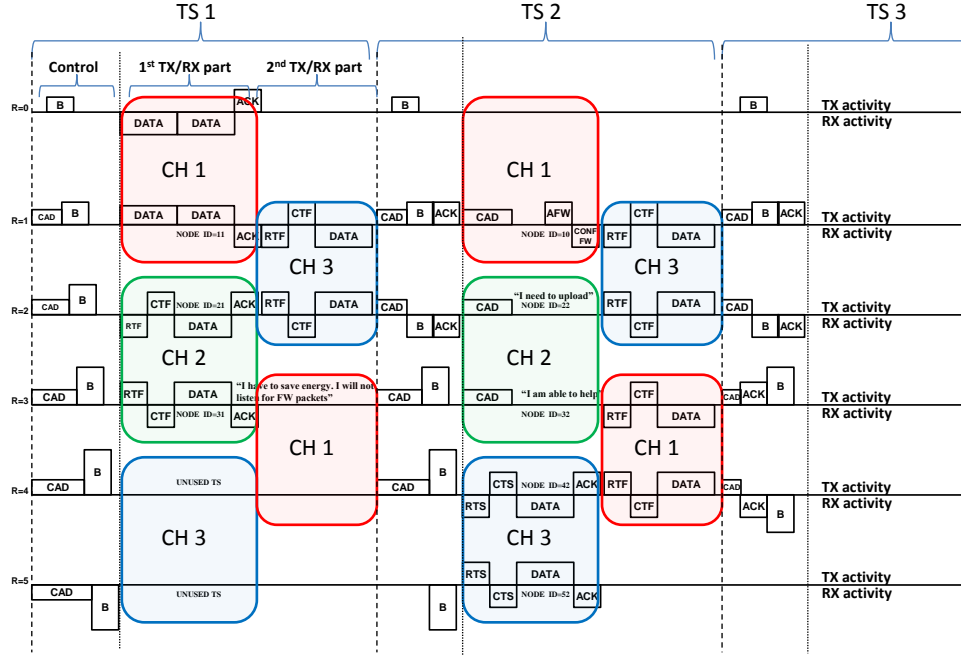


FIGURE 4.5: Inter-rank frequency division structure

In Figure 4.5, different channels are represented as different colors. The presented structure enables a separation between parallel inter-rank transmissions in a pairwise way, enabling spacial reuse. Thus, for the mentioned example, Rank 2 node (ID=21) receives the packet from Rank 3 node (ID=31) via the channel 2 during the 1st TX/RX part. The transmission of a neighboring Rank 1 node (ID=11) to the BTS in this case will not have any impact on Rank 2 node (ID=21), since Rank 1 to 0 transmission is isolated in the other channel - Channel 1. In the same way the transmission between Rank 5 and 4 is isolated from Channel 3. Similar logic applies to the 2nd TX/RX part of the timeslot. Two different channel distribution combinations with the same effect are available and represented in Figure 4.6.

The channel repartition schemes presented in Figures 4.5 and 4.6 can be combined to enable channel hopping. However, the interest of channel hopping in case of long timeslot used (about a few seconds long) is questionable.

The use of multiple channels with the combination of a specific timeslot structure also helps to increase the capacity of the network. Indeed, in

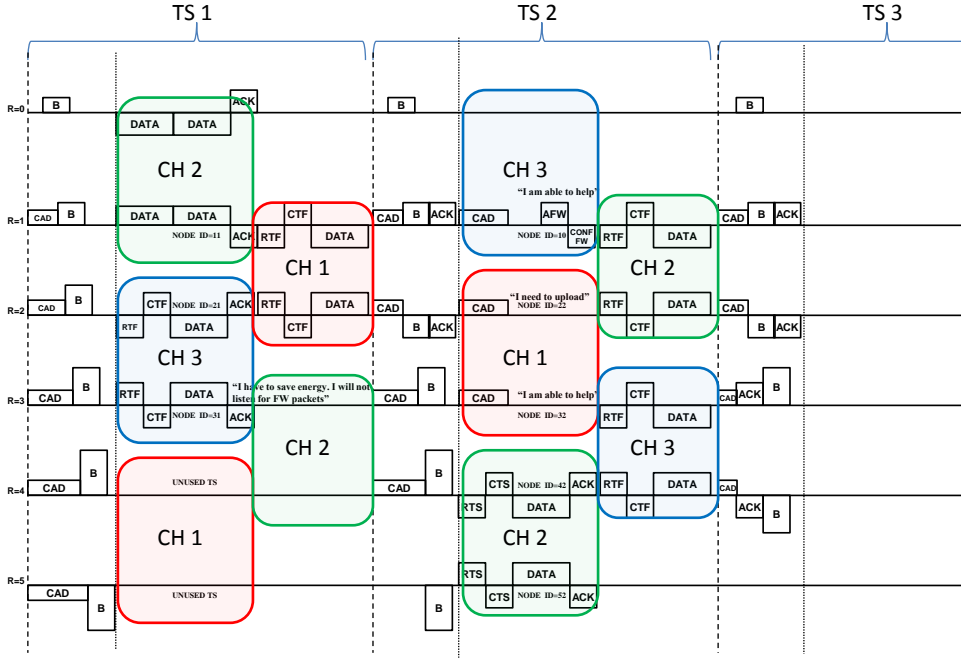


FIGURE 4.6: Combination of Time/frequency division techniques

Figures 4.5 and 4.6, the timeslot structure proposed in the previous subsection is used (see Figure 4.2). However the functions of 1st and 2nd TX/RX parts can be switched in the opposite way, which will lead to the structure represented in Figure 4.7.

These two structures are orthogonal, thus, can be used simultaneously, which will enable two nodes to use the same timeslot and finally will double the capacity of the network. The combination of these 2 structures is presented in Figure 4.8

The implementation of this technique can be done by assigning the first strategy to the nodes with odd ID and the second one to the nodes with even ID.

#### 4.2.4 Timeslot reservation and channel access

If the problem of inter-rank interference can be solved by implementing the multichannel strategy (as described in Section 4.2.3), the intra-rank interference issue must be addressed. To do so, we propose a timeslot reservation mechanism for Rank 1 nodes and competition based channel access strategy for the nodes with a Rank greater than 1. We can call this challenge based channel access as One-time timeslot reservation. The competition is based on Request To Forward/Clear To Forward (RTF/CTF) messages exchange. Let's suppose two Rank 3 nodes willing to send data message up to the neighboring Rank 2 node (see Figure 4.2). Since the network is synchronized, both Rank 3 nodes will send the RTF messages at the same time (concurrently). Even in case of use of a generic radio (not LoRa one)

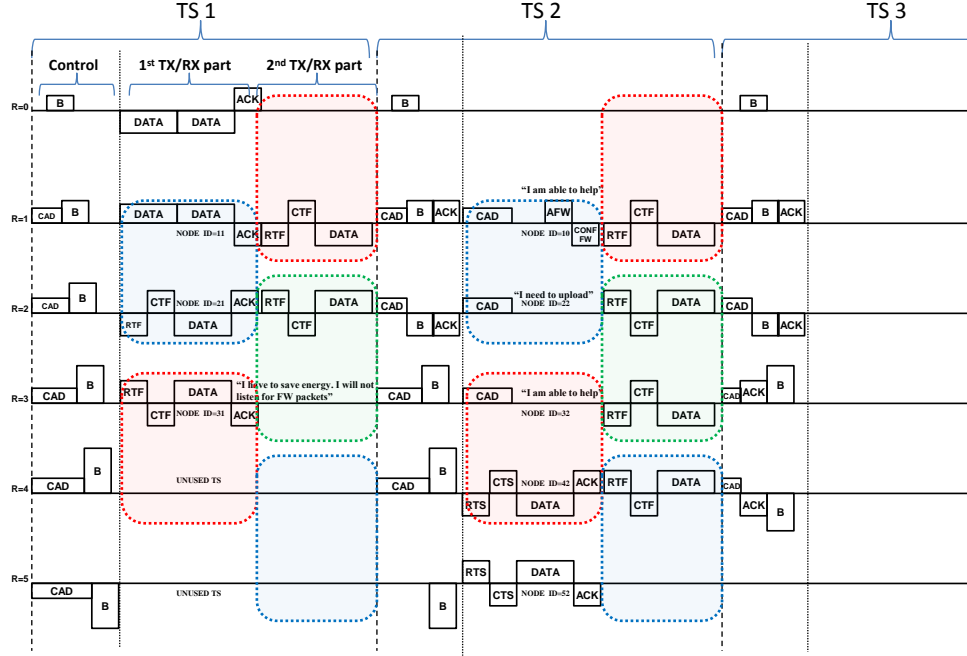


FIGURE 4.7: Opposite time-division structure

the capture effect will happen, as described in [47]. A collision will occur but it is possible that Rank 2 node will successfully decode the message received with the strongest RSS. Then, Rank 2 nodes will send a CTF message containing the address of the node whose RTF message was successfully decoded. This address corresponds to the address of the winner of the competition. Since all Rank 3 nodes participating in the competition receive the CTF message, each participant is aware whether it can send the data packet or it has to retry the competition in a latter timeslot. All nodes with a Rank greater than 1 have to participate in the described competition each time they need to transmit a packet. It means that RTF/CTF message exchange must be always carried out before data transmission. To avoid the bottleneck problem at Rank 1 nodes due to failures in competitions along with buffer overflowed by lower ranked nodes messages, we propose a long term timeslot reservation technique. After timeslot reservation, Rank 1 nodes do not need to exchange the RTF/CTF messages each time they need to transmit data to the BTS. The on-air-time which is not used now for RTF/CTF messages can be reused for additional data packet transmission, which will help to free the packet buffer quickly and avoid the bottleneck problem (see Figure 4.2). The reservation process is depicted in Figure 4.9

First, the node reserving the timeslot has to check if the timeslot is not already reserved by another Rank 1 node. To do so, the CAD mechanism is executed. The occupied timeslot can be easily detected since the host of the timeslot can start transmission at the beginning of the timeslot without any delay. In the first example of Figure 4.9, the reserving node detects the

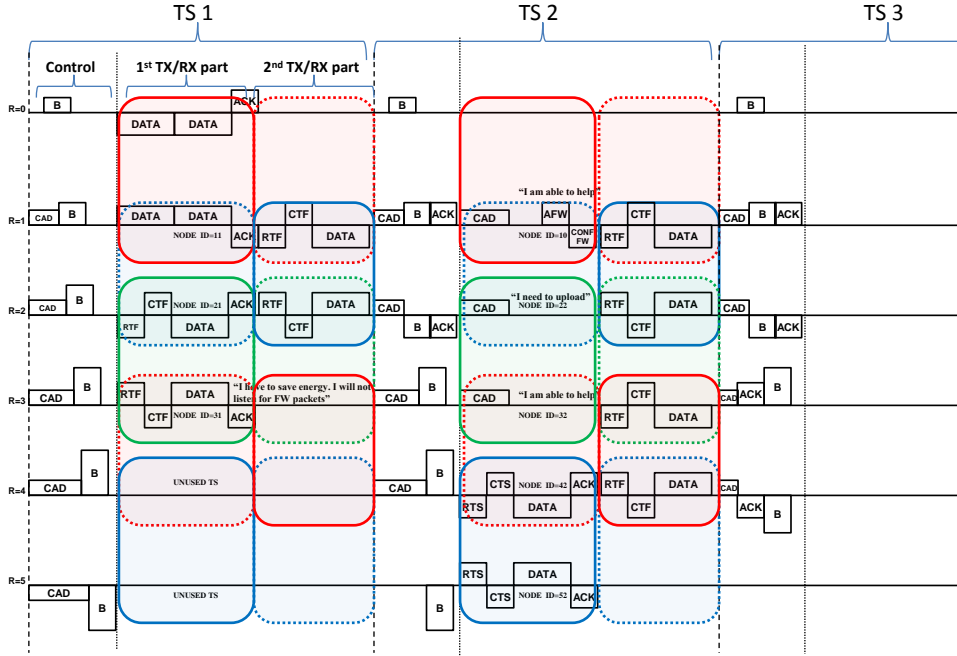


FIGURE 4.8: Inter-rank frequency division structure with hopping

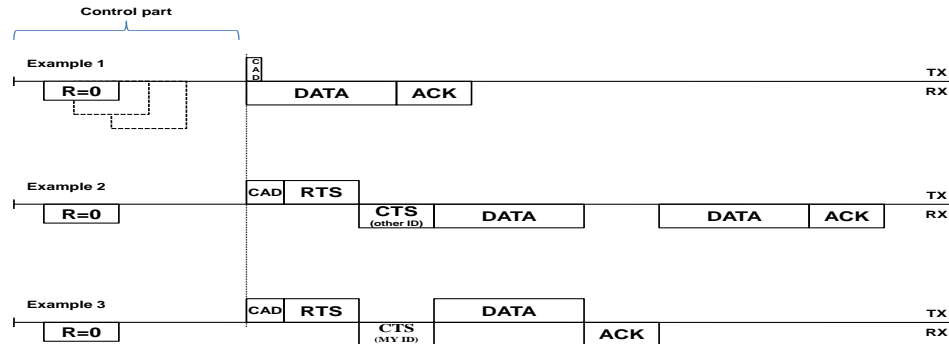


FIGURE 4.9: Long term timeslot reservation for Rank 1 nodes

preamble of the message sent from the timeslot host which reserved it previously. The reserving node, thus, has to retry the reservation in another timeslot. If the preamble is not detected during a defined time, all nodes willing to reserve the timeslot enter the competition similarly as described before. All the reserving nodes, then, send the Request To Send (RTS) messages concurrently to the BTS. As in the previously described competition scheme, the winner of the competition will be defined on the physical layer thanks to the capture effect. The winner will be announced as before by the Clear To Send (CTS) message. In the second example of Figure 4.9, we can observe the case of the lost competition and the third example represents successfully reserved timeslot.

Considering high communication range of BTS (when LoRa technology is used) and mostly settled behavior of rhinoceroses, we can consider the

mobility as relatively low. It means that the reservation renewal will not happen often. However, Rank 1 nodes can also request one-time use timeslot based on the competition similar to the one for higher ranks. To avoid the interference problems, a specific channel and time offset should be used for this purpose, as depicted in Figure 4.10. WildMAC uses the same channel for one-time timeslot reservation transmission of Rank 1 node and communication between Rank 2 and 3 nodes. However, the offset ensures that even though Rank 1 node (node ID 10) and Rank 2 node (node ID 21 in the figure) are within the communication range and sharing the same channel, the transmissions are always carried out in the opposite directions. As shown in the picture with a dotted line, when Node 10 sends an RTF message to the BTS and Node 21 sends a CTF message back to Rank 3 node (ID 31), neither BTS, nor Node 31 are impacted by opposite transmission since Rank 3 and Rank 0 nodes are not in the communication range. A similar situation is valid for the reception: Node 10 cannot receive messages from Node 31, as well as BTS cannot receive messages from Node 21 since these nodes are far from each other. The communications, thus, are isolated.

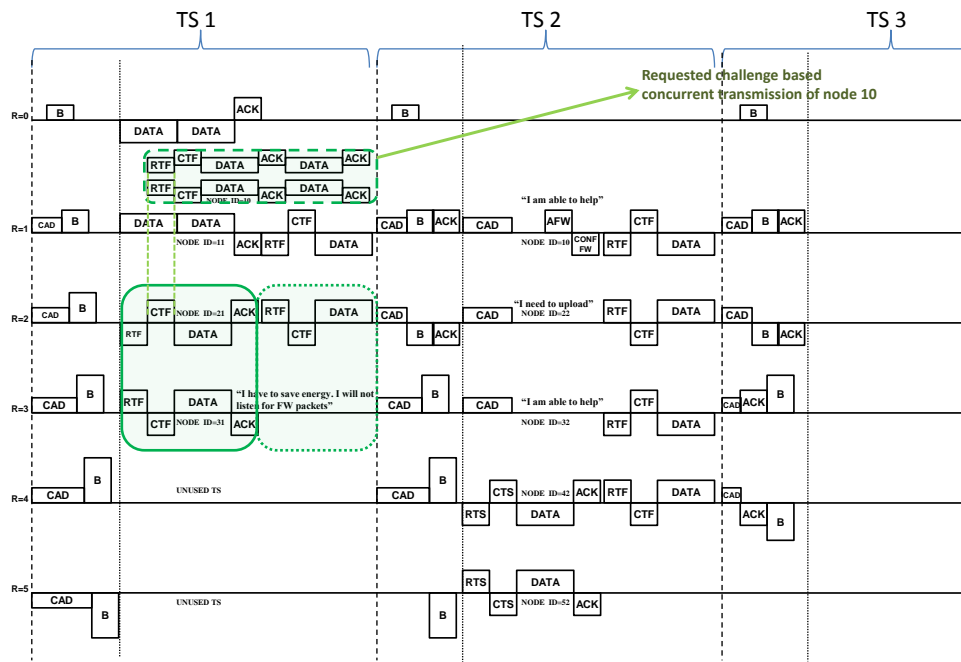


FIGURE 4.10: One-time on-demand timeslot reservation for Rank 1 nodes

The one-time on-demand timeslot reservation for Rank 1 nodes allows the node to send up to 2 data packets with ACK messages. In this case, both 1st and 2nd TX/RX parts are used. This option also helps to avoid a bottleneck problem at Rank 1 nodes, as it gives the opportunity to offload the packets from the buffer in case of overload.

#### 4.2.5 Communication example

In Figure 4.11, an example of communication is provided in order to help the understanding of the WildMAC protocol.

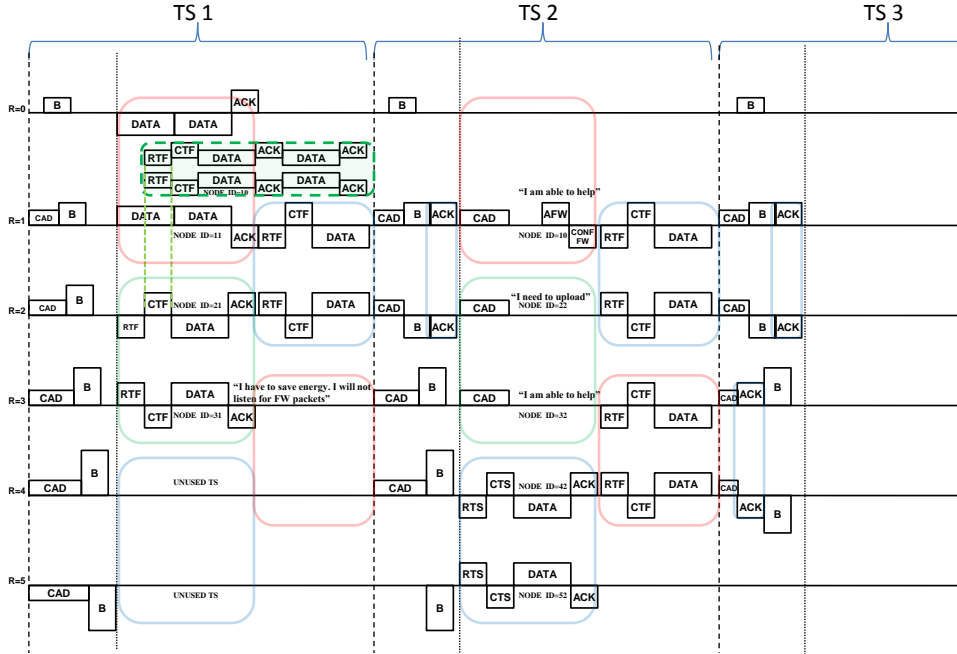


FIGURE 4.11: Inter-rank frequency division structure with hopping

For the sake of simplicity, only one time division structure is shown in this example. We suppose also that all the nodes in the figure have already determined their rank and Rank 1 nodes have reserved their timeslots.

In the figure, Node 31 (Rank 3) is willing to offload the data from its buffer during the 1st TX/RX part of the timeslot 1. It thus requests an access to the timeslot via the competition mechanism described before. Node 21 (Rank 2) confirms the success of Node 31 by sending back a CTS message. Then the data are sent to Node 21 and confirmed by an ACK message. As defined, this communication was done on Channel 2. During the 2nd TX/RX part of the timeslot, Node 21 switches to Channel 3 in order to forward the received packet, or a packet with its own data to Rank 1 node. Node 21 participates in the competition as done by Node 31, and Node 11 confirms the success of Node 21 and receives its data packet. This time the ACK message is sent during the Control part of the next timeslot (TS2). As we can notice, Node 11 sent 2 data packets during the 1st TX/RX part, since it reserved its timeslot, as it was described in the previous section. Also, during Timeslot 1, Node 10 (Rank 1) offloaded the data from its overloaded buffer through one-time on-demand slot reservation. As it was mentioned in the beginning of this chapter, the proposed MAC protocol is able to take the current battery level (SOC) of the device into account. Since

Node 10 offloaded all data from its buffer and has enough energy to forward new packets from higher ranked nodes, during the next timeslot, it listens to the channel (CAD) in order to determine whether this timeslot is reserved by another Rank 1 node. After confirming that the timeslot is free, Node 10 announces its availability to forward new packets by sending an AFW (Available to forward) message to the BTS, which confirms its candidature by a forward confirmation message (CONF FW) to define one Rank 1 node per timeslot in case of multiple nodes available to forward messages. Node 22 did not receive any request to forward message, however it had its own data to send. This node used, thus, the opportunity to forward its data via Node 10. In opposition to Node 10, which had enough energy to forward additional packets, Node 31 faces a low energy issue. It cannot, thus, receive messages from the others and after transmitting its own data, it sleeps. Since the nodes take advantage of the energy harvesting module, after some time, the battery will be charged and Node 31 will be available to forward other packets.

## 4.3 Performance evaluation

### 4.3.1 Chosen LoRa communication parameters

Communication parameters which allow the achievement of the required coverage (long range transmissions) determine transmission rate, packet on-air time and, thus, TS duration. The following parameters have been chosen in order to ensure relatively long range transmissions and acceptable communication rate:

- Center Frequency (CF): 434 MHz;
- Transmit power: 14 dBm;
- Bandwidth (BW): 31.25 kHz;
- Spreading Factor (SF): 9;
- Coding Rate (CR): 4/8;
- CRC disabled.

These parameters will be used in the following sections.

### 4.3.2 Range test and coverage simulation

#### Range test

At the first step of performance evaluation, we carried out a range test. These tests will help to evaluate the performance of the chosen LoRa physical layer technology, estimate the coverage in the target area (Kruger park) and estimate the number of nodes in each cell. The experimental setup was

organized as follows: two Semtech SX1276 based cards were used to establish a point-to-point connection between a fixed receiver side node (RX) and mobile transmitter side node (TX). Both RF modules were configured according to the parameters described above. The RX node was installed on the roof of the Engineering Faculty building of Stellenbosch University (as shown in Figure 4.12).



FIGURE 4.12: Fixed receiver side node

The mobile TX node was installed in the car. During the experiment, the RX node was listening for the incoming request messages from the TX node. Once the message is received, the RX node measures the RSSI and sends this value back to the TX node. The TX node, thus, receives the answer of the RX node containing the measured RSSI at the RX side and also measures the RSSI at the TX side. It enables to collect the RSSI values measured at both, TX and RX sides. When TX node receives the answer from the RX node, it stores both RSSI values in the file and complete them by the current GPS position and timestamp. Then, the obtained file is converted to the .kml format in order to show the measured values on the map using Google Earth software.

### Coverage simulation

The hardware based range test results were compared with the radio coverage simulation carried out with the RadioMobile [84] simulator. This simulator is based on the Irregular Terrain Model (ITM) also called Longley-Rice model [60]. The following simulation parameters were chosen in order to fit the nodes configuration used during the described above range test:

- Base station location: 33.92845S, 18.86606E (120.3m elevation)
- Frequency: 434MHz
- Surface refractivity (N-Units): 301 (default)
- Ground conductivity (S/m): 0.005 (default)
- Relative ground permittivity: 15 (default)
- Mode of variability: Spot, 70% of situations
- Climate: Continental temperate
- Additional loss: City, 100%
- Antenna Polarization: Vertical
- Antenna type: omni
- Antenna gain: 2.15dBi (0dBd)
- Transmit power: 14dBm
- Receiver threshold -136.6dBm
- Line loss: 0.5dB (losses in cable, filter, connectors)
- No additional cable loss
- Mobile station antenna height above ground level: 2m
- Base station antenna height above ground level: 20m

### Obtained results

The results of the both, range test and radio coverage simulation are presented in Figure 4.13.

In the Figure the colored squares represent the RSSI values obtained during the hardware based range test. At the same time, a big filled area depicts simulation results. The range test shows the maximum communication distance of 13 km. We can notice also that the obtained results during the range test fit the simulated coverage area, which means that chosen simulation parameters could be used to estimate the coverage in the other areas.

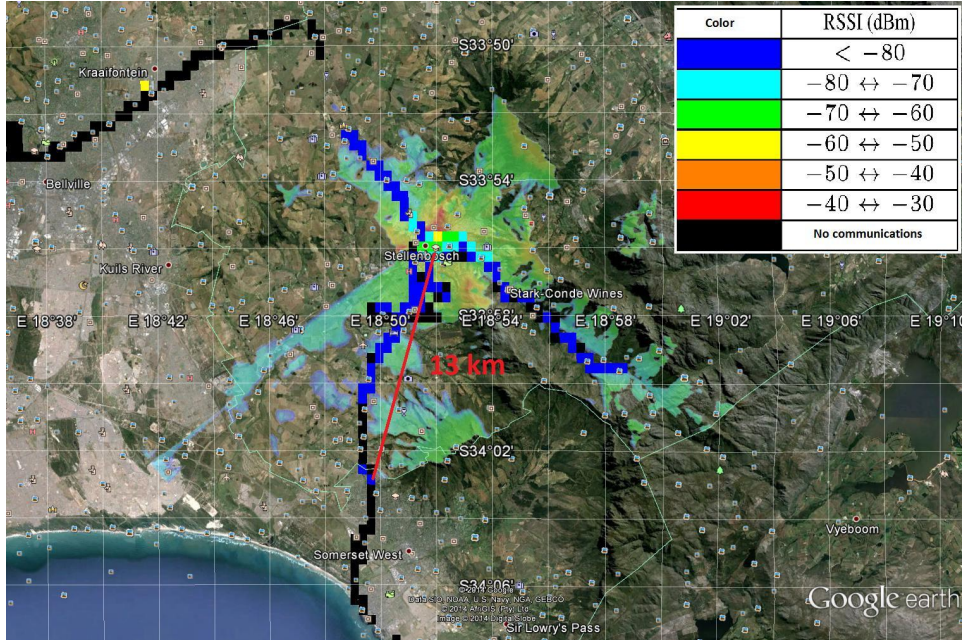


FIGURE 4.13: Coverage map

### 4.3.3 Cell capacity estimation

In the following sections, we use the obtained range test best case communication distance of 13 km. In this case the area covered by one LoRa cell can be approximately calculated as follows:  $A = \pi r^2 \approx 3.1415 \cdot 13^2 \approx 531 \text{ km}^2$ , where  $A$  is an approximated area of the LoRa cell and  $r$  is the communication range. Supposing the animals are distributed randomly in the cell according to a Poisson Point Process (PPP) with a density  $\lambda = 1.7$  (as defined in Section 1.3) animals per  $\text{km}^2$ , we obtain, in average,  $531 \cdot 1.7 \approx 903$  rhinoceros per cell.

An example of the distribution of the animals in a LoRa cell with mentioned above parameters is depicted in Figure 4.14.

The 12-byte data packet payload size was chosen in order to transmit the requested information collected on the body of the animals. The 3-byte control message size was also defined. These values along with the communication parameters described in Section 4.3.1 lead to the following timing configuration:

- On-air duration of a 12 byte data packet: 495.62 ms;
- On-air duration of a control message with 3-byte payload: 233.47ms,
- LoRa preamble duration: 102.4 ms.

The duration of TS was set to 3 seconds, which allows:

- 2 packet transmissions up (to the BTS) and 1 packet reception from higher ranked nodes per TS for Rank 1 devices;
- 2 transmissions up (to the BTS) for Rank 1 nodes in the one-time reserved extra slots;

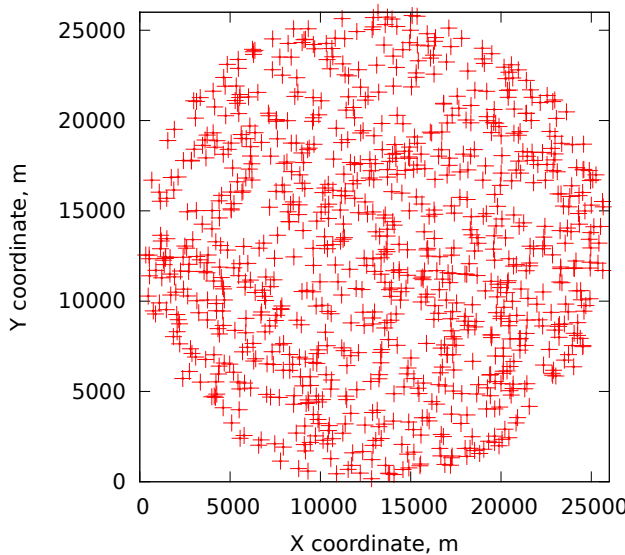


FIGURE 4.14: Example of rhinoceros distribution in a 13 km cell

- one transmission up and one reception from higher ranked devices for other nodes.

As we can notice, Rank 1 nodes have more opportunities to transmit messages in order to avoid the bottleneck problem due to the messages aggregated from the higher ranked devices.

If the Superframe duration is 15 minutes (900 s), 3s TS will lead to  $900/3=300$  TS in a Superframe. Since the number of available TS in one channel is less than the number of animals in a cell, the use of multiple orthogonal channels is required in order to ensure communication for all the nodes. Additional techniques which help to increase the network capacity will be useful.

Adding 3 more frequency domain channels would double the capacity of the network. Then, as discussed in Section 4.2.1, the superposition of 2 time division schemes also would double the capacity. It is also possible to use 2 different combinations of SF and BW with similar range characteristics: BW 62.5 kHz and SF 10; BW 125 kHz and SF 11, which ensures orthogonal communications. Using all these methods will enable us to obtain the following network capacity:

300 TS (Number of TS with one channel)

\* 2 (Double due to TX/RX part shift and superposition)

\* 2 (use of 3+3 channels)

\* 3 (3 BW-SF orthogonal combinations)

= 3600 available TS per cell, which is about 4 times greater than the estimated number of animals per cell. The application of these techniques will reduce the density of the animals in each channel and give a new density  $\lambda_1 = 1.7/4 = 0.425$  animals per  $km^2$ , which corresponds to approximately  $531 \cdot 0.425 \approx 226$  animals per cell.

#### 4.3.4 Kruger park coverage estimation

In this section we used the obtained range test results to estimate the possible coverage in the Kruger park. In fact, in our case the base stations cannot be installed in any point of the Kruger park due to the poor infrastructure, lack of electric power and administrative restrictions. Moreover, the access to some places is difficult, which makes difficult the maintenance of the base stations. Thus, we found the camp positions, which can be used to install the Base station devices safely. We present in Figure 4.15 a coverage estimation for a best case scenario where the BTS (sink) devices are installed in the known camps.

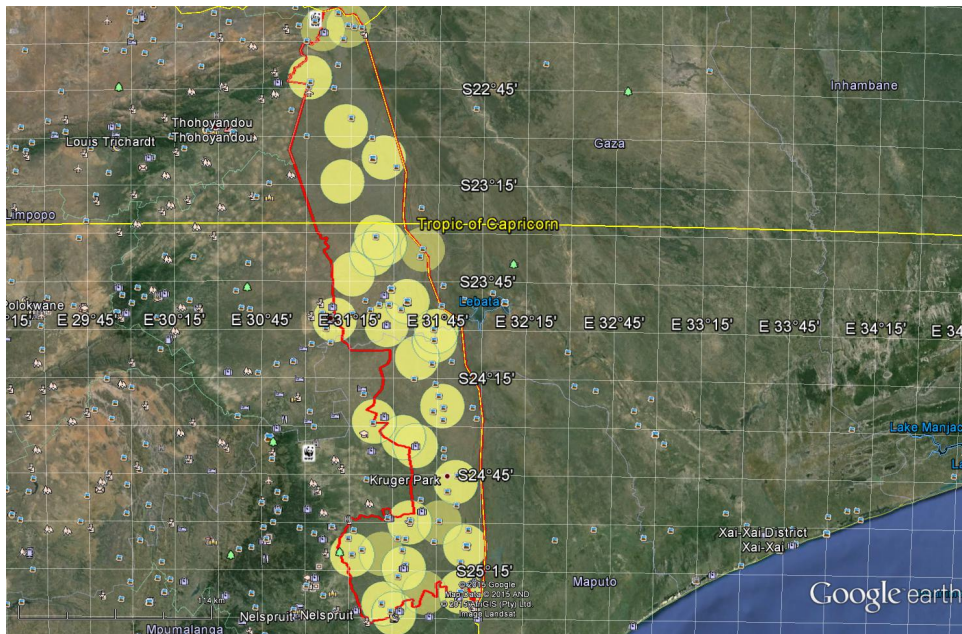


FIGURE 4.15: Estimated coverage in the Kruger Park

From the figure we can observe that even in the best case scenario the target area is not fully covered. Thus, the multihop communications are required in order to meet the functional and technical requirements and ensure the communications in the whole area of the Kruger park.

#### 4.3.5 WSNet implementation and simulation results

The massive deployment of the sensor nodes in the wilderness area on animals is a costly and hard task. The performance of the WildMAC protocol must be evaluated before field implementation. To do so, we implemented the WildMAC protocol in the WSNet<sup>1</sup> event-based simulator. The performance of the WildMAC protocol is evaluated in both, one hop and multi-hop scenarios.

<sup>1</sup><http://wsnet.gforge.inria.fr/>

### One hop scenario

In this scenario we measured the number of successful channel reservations for Rank 1 nodes and the PER as a function of number of occupied timeslots. The nodes arrives to the network one-by-one. Each node tries to reserve the timeslot 100 times (one time per superframe) following the timeslot reservation scheme described in Section 4.2.4. After 100 trials the node switches to the last successfully reserved timeslot and sends its data messages in it during each following superframe to occupy it. Then, the number of successful trials is calculated for each node corresponding to different superframe occupancy values.

As explained before, we suppose 300 available timeslots. The number of nodes is increments from 1 to 320.

We ran 1000 simulations in order to obtain results shown in Figure 4.16. For each simulation the nodes distribution was regenerated according to the PPP with the high value of density and then the first 320 nodes are chosen.

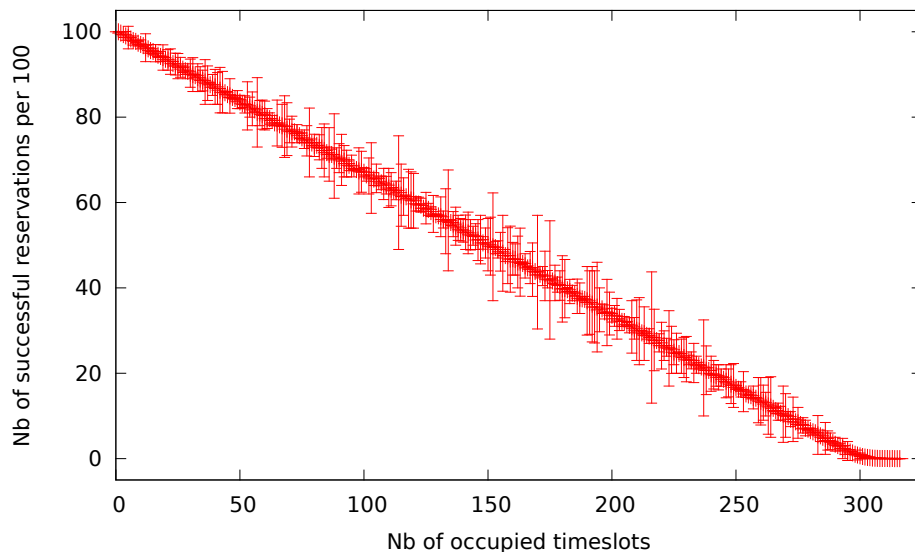


FIGURE 4.16: Number of reservation successes versus number of occupied timeslots

From the figure we can notice that the number of successful timeslot reservations decreases linearly from the maximum value of 100 to the 0, which corresponds to the theoretical values of the probability of successful timeslot reservation which can be obtained as follows:

$$P_s = 1 - \frac{N_b}{N_t}, \quad (4.1)$$

where  $P_s$  is the probability of successful timeslot reservation,  $N_b$  is the number of occupied timeslots and  $N_t$  is the total number of timeslots.

In this scenario we also evaluated the packet error rate (PER). The PER was calculated as follows:

$$PER = 1 - \frac{RX}{TX}, \quad (4.2)$$

where  $RX$  is the total number of received packets from all the transmitting data nodes and  $TX$  is the total number of the transmitted data packets by all transmitting nodes. Only the nodes which have completed their reservation process can contribute to the PER statistics. Also, only the data packets are considered to calculate the PER. The obtained values of PER as a function of number of transmitting nodes is presented in Figure 4.17.

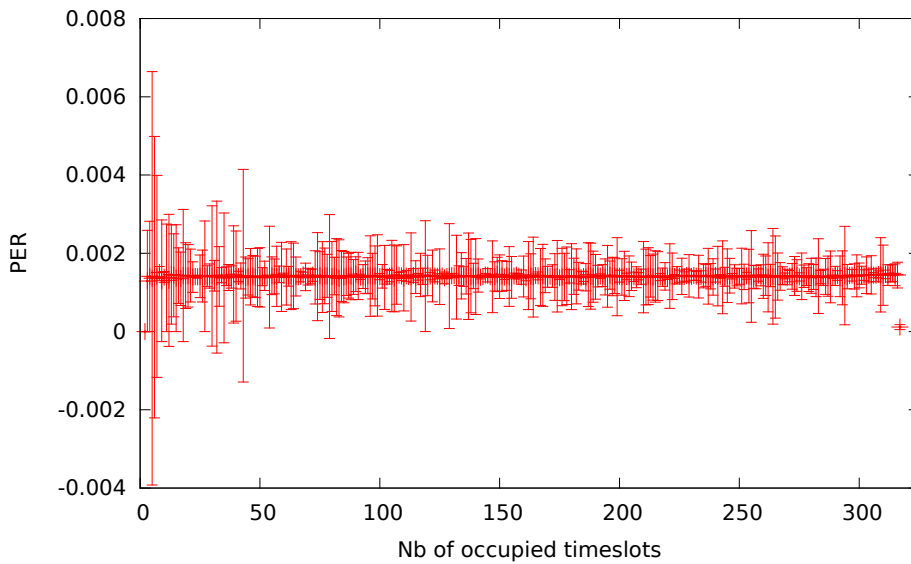


FIGURE 4.17: PER versus number of occupied timeslots

We can notice that the obtained PER is low and almost constant, which shows the efficiency of the timeslot reservation approach.

### Multihop scenario

As explained before, the multihop capabilities are required in the context of the PREDNET project. In this section, the performance of the WildMAC protocol in the multihop scenario is evaluated.

To represent a multihop scenario with the used before parameters, the nodes have to be distributed over an area larger than the one covered by a BTS. This leads to the need to simulate a large number of devices which requires an important amount of memory and increases considerably the simulation time. To avoid this problem, we decreased the communication range from 13 km to 2.6 km. The density of the nodes was adjusted to obtain 68 Rank 1 nodes in average. This enables us to activate the multihop capabilities (up to 5 hops). From Figure 4.15, we can notice, that the nodes situated far from one particular BTS become close to another one. It means that the number of higher ranked nodes decreases significantly. Thus, the traffic

load generated by the nodes is distributed over multiple BTS. To mimic this peculiarity we progressively decreased density of each rank of the nodes. An example of the adjusted in the described way topology is presented in Figure 4.18.

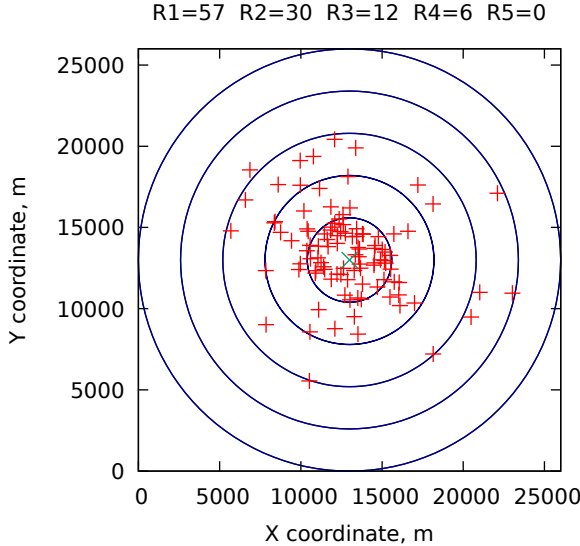


FIGURE 4.18: Example of rhinoceros distribution with reduced densities for higher ranks

In this figure, circles represent borders of the zones ensuring minimal number of hops to reach the BTS in the best case scenario (when at least one node in range is present in each zone). The total number of nodes in each zone is provided on top of the figure. We can notice also that few nodes in this example are isolated (do not have any neighbor in range). However, in real case scenario, where multiple BTS are present, this situation should not appear often.

The 100 timeslot superframe was used for the simulation, which corresponds to 300 s superframe duration. However, and even though the network load was decreased by lowering the densities of higher rank nodes, we observed network saturation if each node generates a data packet once per superframe. So, we increased the data generation period from 300 s to 900 s (1 packet each 3 superframes) to further lower the network load.

In the present scenario the nodes are considered as static.

In the proposed multihop scenario all the nodes are switched on simultaneously. Once activated, they start to discover their Rank and then act following the WildMAC protocol. For this scenario the nodes make decision regarding their rank based on 5 received beacons. The rank is discovered when within 5 received beacons at least 2 correspond to the same rank. Each node generates 100 messages. Each message generated by node or received from a higher ranked node is put in the node buffer organized as a First Input First Output (FIFO) queue. Each message from the buffer could

TABLE 4.1: PER per rank

Rank	1	2	3	4	5
Mean	0.0189555	0.0125216	0.0174567	0.0141610	0.0090788
SD	0.01910950	0.00695138	0.01197230	0.02096800	0.00430180

be transmitted up to 3 times. After that, if the sending node does not receive ACK message, the data packet is removed from the buffer. As in the one hop scenario, we performed 1000 simulations. For each simulation, the node distribution was also regenerated. The end-to-end PER, end-to-end latency and average number of physical layer transmissions per rank were chosen as performance evaluation metrics.

The end-to-end PER for each rank was calculated as defined by 4.3:

$$PER_R = 1 - \frac{RX_R}{TX_R}, \quad (4.3)$$

where  $RX_R$  is the total number of received messages from rank R nodes,  $TX_R$  is the total number of sent messages from rank R nodes and  $PER_R$  is resulting PER for rank R. The  $TX_R$  counter is incremented by each transmitting node before the first transmission of each packet. This counter, thus, is available for all the nodes. Also the transmitting nodes put the value of their discovered rank in the packet before the transmission. This initial source rank value stored in the packet is not modified by the intermediate nodes and used by the BTS at the reception in order to increment corresponding  $RX_R$  counter. The  $PER_R$  value is calculated in the end of the simulation. The obtained results from 1000 simulations are presented in the Table 4.1 as mean  $PER_R$  value for each rank along with observed Standard Deviation(SD).

We can observe low values of PER for each rank which demonstrates the reliability of the proposed solution. Relatively high values of the standard deviation represent the impact of the difference between topologies which are generated for each simulation. That also can be due to small number of generated packets by each node during the simulation.

The end-to-end latency is measured as the average time between the packet generation at the transmitter side and its reception by the BTS. As for the end-to-end PER, the latency is measured independently for each rank. To do so, each transmitter node of rank R put the current timestamp value in the packet when this latter is generated and stored in the buffer. During transmission of the packet through the network, the timestamp field is not modified by the intermediate nodes, thus, this value corresponds to the time of generation at the source node of rank R. At the reception, the BTS calculates the difference between the current time (time of the reception) and the generation timestamp stored in the packet. The initial source rank value, also stored in the packet, is used by the BTS to classify the obtained

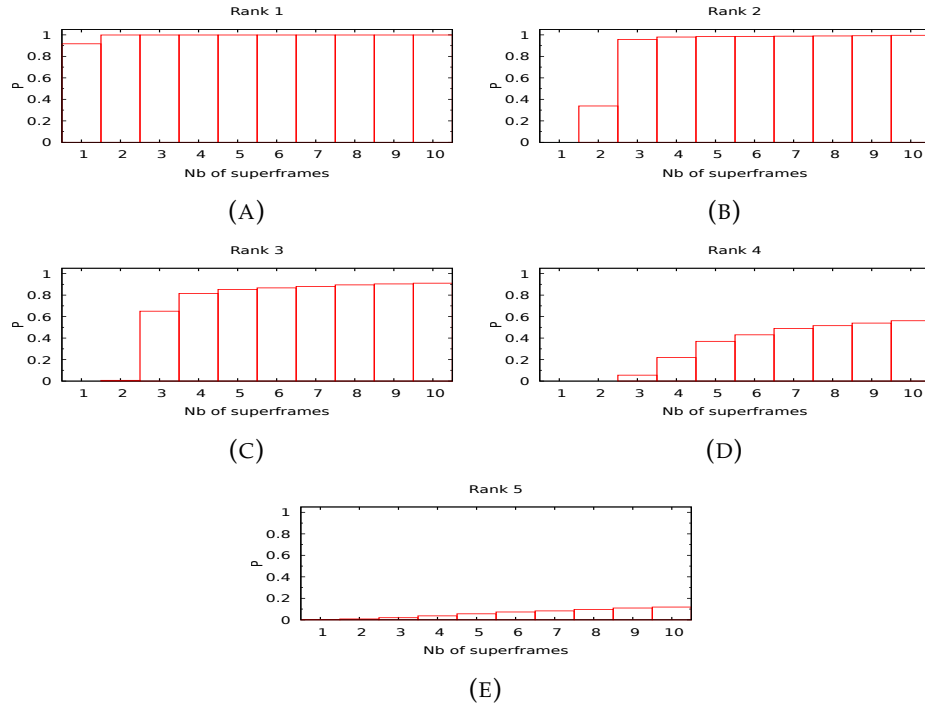


FIGURE 4.19: Probability of the reception of a message before the expiration of a given number of superframes. Initial rank: a) 1 b) 2 c) 3 d) 4 e) 5.

values of latency per rank. In the end of each simulation the average value of the latency per rank is calculated. We normalized the obtained average values of latency to the duration of the superframe. Then we calculated the probability of the reception of a message (issued from the node of rank R) before the expiration of a given number of superframes. These results are presented in Figures 4.19.

We can observe that with high probability (92%) the messages generated by the nodes of Rank 1 are delivered to the BTS within less than 1 superframe. This low latency is caused by the fact that the Rank 1 nodes have permanently reserved timeslots, which guarantees their a transmission opportunity at least once per superframe. The messages generated by the Rank 2 nodes arrive to the BTS within 2 superframes with the probability 34% and within 3 superframes with the probability 96%, thus before the generation of a new message (as mentioned, packet generation period is set to the duration of 3 superframes). The packets from Rank 3 nodes are received by the BTS within 3 superframes with the probability of 65% and within 4 with the probability of 82% which represents relatively low latency up to Rank 3 nodes. However, for the Rank 4 nodes the probability of delivery of packets within 10 superframes is only about 56%. For the Rank 5 nodes it is even worse: probability that the message is received by the BTS within 10 superframes is about 12%. The high latencies observed for the Rank 4 and Rank 5 nodes could be caused by the low node density at the edge of the simulated network in our scenario. Indeed, with low density

TABLE 4.2: Average number of physical transmissions per rank

Rank	1	2	3	4	5
Mean	1.12300	2.09670	3.15968	4.16221	5.09306
SD	0.07887	0.05244	0.10836	0.13512	0.05146

TABLE 4.3: Percentage of nodes estimated their rank as R per per zone of minimal transmissions. The used format is mean(SD); The values are given in %

Estimated rank	1	2	3	4	5
1 min TX zone	100.00(0.00)	0.00(0.00)	0.00(0.00)	0.00(0.00)	0.00(0.00)
2 min TX zone	0.00(0.00)	60.25(4.20)	33.81(1.20)	5.15(2.64)	0.79(0.35)
3 min TX zone	0.00(0.00)	0.00(0.00)	34.21(8.22)	52.80(15.46)	12.89(7.14)
4 min TX zone	0.00(0.00)	0.00(0.00)	0.00(0.00)	9.81(5.33)	71.29(24.23)
5 min TX zone	0.00(0.00)	0.00(0.00)	0.00(0.00)	0.00(0.00)	0.00(0.00)

of Rank 4 nodes, the Rank 5 nodes do not often have the opportunity to transmit their messages. Thus, the latency is high.

Table 4.2 represents the average number of physical transmissions to deliver the message from the node of rank R to the BTS. In each simulation this value is calculated as the ration between total number of transmissions by nodes of rank R to the total number of received packets at the BTS side. The table represents mean and standard deviation for this value per rank.

We observe that the number of physical transmissions is slightly greater than the rank due to the presence of retransmissions.

Finally, we evaluate the average percentage of nodes estimated their rank as R per per zone of minimal transmissions in the best case (see Figure 4.18). These results are provided in the Table 4.3.

To obtain this table, all the nodes situated in each of these 5 zones were incrementing the counters corresponding to their estimated rank at each beacon reception (there are 5 counters for each zone). At the end of the simulation, the value of each counter in a given zone was divided by the sum of all the counters in the zone. Then, the mean value of percentage as well as the standard deviation are calculated based on the results of 1000 simulations.

We can notice, that the obtained in the table values are close to triangular matrix (except the last row). Indeed, estimated rank cannot be lower than the minimal number of transmissions in the best case (when at least one node in grange is present in each zone to ensure the delivery of the packet to the BTS). However, we observe that the estimated rank is often bigger than the minimal number of transmissions in the best case for a given zone. For instance, in the zone of 2 minimal transmissions, the biggest part of the nodes (60.25% in average) estimate their rank as 2, but other nodes estimate greater values for their rank. For the zone of 3 minimal transmissions the greatest part of the nodes estimate their rank as 4 (52.8% in average) and for

the zone of 4 minimal transmissions - as 5 (71.29%). This behavior can be caused by the peculiarities of the distribution of the nodes. In some cases the node have very few (or no) neighbors from the zone of lower minimal number of transmissions. In this case, the probability to hear the beacon from the nodes in the zone closer to the BTS is small (or zero), whereas the probability to hear the beacon from a node in the same zone is high. Thus, the rank of the node will be greater than the rank of neighboring nodes from the same zone. From the Figure 4.18 we can observe that due to low node density, in the zones of high minimal number of transmissions, there are nodes which have only neighbors from the same zone. It explains the behavior observed in the table for this kind of zones (3 and 4 minimal transmissions zones): the percentage of nodes which estimated higher rank than the minimal is growing when they are further from the BTS. From the table also we observe no nodes from the zone of 5 minimal transmissions could estimate their rank. It is caused by a very low density of these nodes resulting either no nodes, or only isolated nodes present in this zone. The robustness of the rank discovery in some cases can also be increased by adjusting the number of beacons that need to be received to estimate the rank. We can note also that the nodes having the BTS in their direct neighborhood always estimate their rank as 1. Indeed, the BTS sends the beacons in the beginning of each timeslot, which increases the probability to receive it by the direct neighbors.

## 4.4 Chapter conclusion

In this chapter we proposed and evaluated WildMAC - an adaptive MAC layer protocol for the particular case of rhinoceros tracking application in the framework of the PREDNET protocol. The evaluated implementation of WildMAC is able to adapt its behavior depending their distance to the BTS. The protocol shows good performances in terms of latency and PER up to three hops, which should be enough for the implementation in the southern part of the Kruger park - considered area of deployment of the network. However, the observed increase of latency for high ranked nodes should be studied in more details.

The most important limitations of the proposed WildMAC protocol are: the number of hops are limited by the duration of the control part of the timeslot and the number of available control channels; possible network saturation in case of high density of the nodes; undefined behavior of the isolated nodes in case of very low density. These issues have to be studied and faced in the future works.

The results obtained in this chapter show the performance of the normal mode of the WildMAC protocol. However, the performance of the alarm

mode still needs to be evaluated. It is also important to carry out the evaluation in the mobility scenario. Moreover, mentioned in this chapter adaptability based on the current State of Charge of the battery should be developed and evaluated. Another possible improvement of the WildMAC protocol could be integration of support of the energy harvesting techniques (*e.g.*, harvesting of mechanical energy).

## Chapter 5

# Conclusions and perspectives

### 5.1 Conclusions

The Internet of Things not only constitutes a new step of evolution of the technology but also represents an important issue for modern telecommunications, that needs to be considered. With a constantly growing number of connected wireless devices and a lack of available radio spectrum (especially in unlicensed bands) in the near future, interference can make impossible the efficient use of connected devices and further development of the IoT. To outcome this problem, the impact of interference on radio communications in IoT and particularly in WSN context needs to be studied and efficient adaptive communication strategies must be developed, which emphasize the importance of this thesis.

The thesis was conducted in the pluridisciplinary environment of two research groups: IEMN (IRCICA) CSAM group and Inria FUN project-team. The objective was to study the problem of interference from different points of view by using the research experience on both low and high layers of WSN communication stack. Both hardware and software based approaches were used to achieve the contributions proposed in this thesis.

First, we performed hardware measurements of energy consumption of the radio module of WSN nodes combined with the interference measurements near the communicating devices. The obtained measurement results confirmed the strong impact of the interference on the energy consumption (and, thus, the lifetime for battery-powered devices) of both, transmitter and receiver WSN nodes. We emphasized the importance of developing the efficient adaptive MAC layer protocols. Indeed, one of the functions of the MAC protocol is the control of the activity of the device's RF module - the most energy hungry part of the node. We showed that when we used a MAC layer protocol with statically configured parameters, the node experienced important energy losses. For example, we observed the inefficiency of the third transmission, especially when high level of interference is observed. Indeed, we observed 0 successful transmissions after 2 consecutive failures for the highest interference level in the office environment. The possibility to adjust the number of transmissions dynamically will, thus, help improving the energy performances of WSN nodes. We carried also

out the long term hardware interference measurements during one week in IRCICA TELECOM lab and FIT IoT-LAB platform. In both cases we confirmed that the observed interference level changes depending on the position of the WSN nodes, used RF channel and time. Measurements show that the observed level of interference can be used as an indicator in order to make decisions regarding adjustment of communication parameters.

These results enabled us to achieve our second contribution - development of the adaptable Cognitive Radio based solution for WSN. This solution analyzes the observed level of interference (using RSSI measurements) by applying Thompson sampling based multi-armed bandit strategy. The evaluation via both, simulation and hardware implementation, show that this solution finds the best channel faster than other existing Cognitive Radio strategies. We also developed a multihop extension for the proposed approach and evaluated it via hardware implementation in the framework of the EWSN Dependability competition with highly interfered environment. Our solution shows up to 80% for end-to-end packet delivery rate in this setup. It confirms that the Cognitive Radio approach initially proposed for the license-based spectrum can be successfully applied to the multihop WSN operating in the ISM bands. However, the limitation of the approach described above is the inefficiency of the observed interference level as indicator for parameters adjusting in case of using the LPWAN technologies. Indeed, in LPWAN networks packets can be received even when the signal strength is below the noise floor. So, other metrics should be used to adjust communication parameters.

For our third contribution - WildMAC protocol for LoRa based animal tracking WSN - the strategy used in order to communicate with neighbors is based on the observed Rank values. Indeed, the case of wildlife animal tracking in the framework of the PREDNET project, studied in Chapter 4, supposes that the WSN is deployed in a wilderness area where low (or no) interference from other technologies is present. However, the use of the LPWAN technology covering big areas and using low data rates, makes the network itself relatively dense. Thus, the Rank based channel definition approach helps to decrease intra-network interference resulting in packet collisions. To evaluate the performance of the WildMAC protocol, the cell density was estimated theoretically, based on performed in South Africa field range measurements along with software coverage simulations. Then, the obtained values were used to configure the WSNet simulator implementation of the WildMAC protocol. The simulations were conducted for both, one hop and multihop scenarios. The simulation results show good performance of the proposed approach in terms of probability of successful timeslot reservation and packet error rate. The observed latency is acceptable in the framework of the PREDNET project (up to 3 hops), however, some lacks related to the network density are observed for 4 and 5 hops.

In both cases, the proposed adaptive MAC layer techniques (Thompson sampling based Cognitive Radio approach and WildMAC protocol) are distributed. The decision regarding the values of the parameters to be adjusted is made locally by each node. In our opinion, the capability of the node to dynamically adapt the communication parameters in a distributed way is crucial in the era of the IoT, when the centralized management of communications of billions of devices is an impractical task.

## 5.2 Impact of the thesis

The thesis led to 4 publications, both in scientific and industrial conferences. The publication in the LPWAN'16 conference revealed high interest from the industry regarding the works in the framework of the PREDNET project.

The works on the experimental study of the impact of the interference on the energy consumption were partially presented during two *Bourses aux Technologies* (Technology Days) organized by Institut Mines-Télécom and IoT WEEK by CITC. These events aim to establish connections between academia and industry. Participation in these events also showed the importance of the problems of interference and energy consumption in WSN for industrial applications.

The PIMRC'16 publication of proposed Thompson Sampling based Cognitive Radio solution was honored with the best paper award, which emphasizes the interest of the work by the scientific community.

Thanks to the co-direction and 2-month internship at the University of Stellenbosch (South Africa), the thesis also reinforced the relationship between different research labs (IEMN, IRCICA, Inria, University of Stellenbosch).

## 5.3 Perspectives

Conducted during the thesis works open multiple directions for future works and could be applied in usecases.

In short-term, the future works should be conducted to implement and evaluate some features described in this thesis, but which were not studied due to time limitations. The alarm mode proposed for the WildMAC protocol need to be implemented and evaluated. Also, the current battery State of Charge should be added as an adaptability indicator. Simulations with multiple base stations must be conducted followed by the evaluation via field hardware implementation.

In mid-term, proposed contributions could be improved. For instance, higher resolution interference measurement devices could be used in order to evaluate the impact of the very short interfering signals on the WSN

communications. Indeed, we observed inefficiency of the short-scale interference measurements based on off-the-shelf IEEE 802.15.4 transceiver. Implementation of the high resolution interference measurement device directly in the WSN node can also help improving the performances of the proposed Thompson sampling based Cognitive Radio solution due to the increased number of acquired samples. The solution should be also proposed to face the limitation of the WildMAC protocol in terms of available number of hops. Also, other solutions helping to decrease the cell density and, thus, the interference level, could be implemented and tested. For instance, the 3-sector antennas could be applied on the BTS side which will help to separate users and decrease their interfering impact on each-other.

Finally, in long-term, proposed contributions could be combined and applied to different usecases. For example, used in our first contribution energy measurement solution can be integrated directly in the WSN node. So, constantly measured values of energy consumption can be used as an additional adaptability metric. It will enable adapting the transmission power of the RF module in case of use of limited peak power energy sources (*e.g.*, microbattery, energy harvesting devices). Another possible direction is the research in the fields of the application of the Cognitive Radio techniques for the LPWANs which represent a growing interest both for industry and academia. It will improve the reliability of reception of downlink messages, which will expand possible range of LPWAN applications. In particular, it can be useful to improve the reliability of beacon reception for the proposed WildMAC protocol. The main challenge for the application of Cognitive Radio techniques to LPWANs is to develop an efficient spectrum sensing technique which is not a trivial task, since in this kind of networks messages are often transmitted below the noise floor. It is also complex when different LPWANs using different radio technologies and packet properties operate in the same band. The WildMAC protocol can be used to extend coverage of existing LPWANs by taking advantage of the multihop communications, which will increase also the reliability of transmissions. Indeed, in some cases the LPWAN nodes can become out of range of the BTS. Multihop capabilities provided by the WildMAC protocol can help to face this problem. Also, WildMAC can be applied to the Space applications of WSN, *e.g.* in exploring of other planets, where deployment of a solid BTS infrastructure is an impractical task.

Another interesting direction is the study of the coexistence between the adaptive MAC solutions sharing the same (non-licensed) band. Indeed, at the moment, when the classic, non-adaptive communication solutions are prevailing in the spectrum, adaptive techniques have an advantage. However, if all the communication techniques try to get the maximum reward from the communication, a new issue will be presented in the telecommunication.

# Bibliography

- [1] *A Technical Overview of LoRa and LoRaWAN*. LoRa-Alliance. 2015.
- [2] O. B. Akan, O. B. Karli, and O. Ergul. “Cognitive Radio Sensor Networks”. In: *Netwrk. Mag. of Global Internetwkg.* 23.4 (July 2009), pp. 34–40. ISSN: 0890-8044. DOI: [10.1109/MNET.2009.5191144](https://doi.org/10.1109/MNET.2009.5191144). URL: <http://dx.doi.org/10.1109/MNET.2009.5191144>.
- [3] I. F. Akyildiz, W.-Y. Lee, M. C. Vuran, and S. Mohanty. “A survey on spectrum management in cognitive radio networks”. In: *Communications Magazine, IEEE* 46.4 (2008), pp. 40–48.
- [4] I. F. Akyildiz, W.-Y. Lee, M. C. Vuran, and S. Mohanty. “NeXt generation/dynamic spectrum access/cognitive radio wireless networks: a survey”. In: *Computer Networks* 50.13 (2006), pp. 2127–2159.
- [5] I. F. Akyildiz, W. Su, Y. Sankarasubramaniam, and E. Cayirci. “A survey on sensor networks”. In: *IEEE Communications Magazine* 40.8 (2002), pp. 102–105.
- [6] K. H. Almotairi and X. Shen. “A Distributed Multi-Channel MAC Protocol for Ad Hoc Wireless Networks”. In: *IEEE Transactions on Mobile Computing* 14.1 (2015), pp. 1–13. ISSN: 1536-1233. DOI: [10.1109/TMC.2014.2316822](https://doi.org/10.1109/TMC.2014.2316822).
- [7] K. Amouris. “Space-time division multiple access (STDMA) and co-ordinated, power-aware MACA for mobile ad hoc networks”. In: *Global Telecommunications Conference, 2001. GLOBECOM '01. IEEE*. Vol. 5. 2001, 2890–2895 vol.5. DOI: [10.1109/GLOCOM.2001.965957](https://doi.org/10.1109/GLOCOM.2001.965957).
- [8] D. Anthony, W. P. Bennett, M. C. Vuran, M. B. Dwyer, S. Elbaum, A. Lacy, M. Engels, and W. Wehtje. “Sensing Through the Continent: Towards Monitoring Migratory Birds Using Cellular Sensor Networks”. In: *Proceedings of the 11th International Conference on Information Processing in Sensor Networks*. IPSN '12. Beijing, China: ACM, 2012, pp. 329–340. ISBN: 978-1-4503-1227-1. DOI: [10.1145/2185677.2185747](https://doi.acm.org/10.1145/2185677.2185747). URL: <http://doi.acm.org/10.1145/2185677.2185747>.
- [9] *Arduino Nano User Manual*.
- [10] K. Ashton. “That ‘Internet of Things’ Thing. In the real world, things matter more than ideas”. In: *RFID Journal* (2009). URL: <http://www.rfidjournal.com/article/print/4986>.

- [11] P. Auer, N. Cesa-Bianchi, and P. Fischer. "Finite-time analysis of the multiarmed bandit problem". In: *Machine learning* 47.2-3 (2002), pp. 235–256.
- [12] P. Bahl, A. Adya, J. Padhye, and A. Walman. "Reconsidering Wireless Systems with Multiple Radios". In: *SIGCOMM Comput. Commun. Rev.* 34.5 (Oct. 2004), pp. 39–46. ISSN: 0146-4833. DOI: [10.1145/1039111.1039122](https://doi.org/10.1145/1039111.1039122). URL: <http://doi.acm.org/10.1145/1039111.1039122>.
- [13] P. Bahl, R. Chandra, and J. Dunagan. "SSCH: Slotted Seeded Channel Hopping for Capacity Improvement in IEEE 802.11 Ad-hoc Wireless Networks". In: *Proceedings of the 10th Annual International Conference on Mobile Computing and Networking*. MobiCom '04. Philadelphia, PA, USA: ACM, 2004, pp. 216–230. ISBN: 1-58113-868-7. DOI: [10.1145/1023720.1023742](https://doi.org/10.1145/1023720.1023742). URL: <http://doi.acm.org/10.1145/1023720.1023742>.
- [14] J. Beaudaux, A. Gallais, J. Montavont, T. Noel, D. Roth, and E. Valentin. "Thorough Empirical Analysis of X-MAC Over a Large Scale Internet of Things Testbed". In: *Sensors Journal, IEEE* 14.2 (2014), pp. 383–392. ISSN: 1530-437X. DOI: [10.1109/JSEN.2013.2281910](https://doi.org/10.1109/JSEN.2013.2281910).
- [15] C. Boano, T. Voigt, C. Noda, K. Romer, and M. Zuniga. "JamLab: Augmenting sensornet testbeds with realistic and controlled interference generation". In: *Information Processing in Sensor Networks (IPSN), 2011 10th International Conference on*. 2011, pp. 175–186.
- [16] M. Bor, J. Vidler, and U. Roedig. "LoRa for the Internet of Things". In: *Proceedings of the 2016 International Conference on Embedded Wireless Systems and Networks*. EWSN '16. Graz, Austria: Junction Publishing, 2016, pp. 361–366. ISBN: 978-0-9949886-0-7. URL: <http://dl.acm.org/citation.cfm?id=2893711.2893802>.
- [17] A. Botta, A. Dainotti, and A. Pescapè. "A tool for the generation of realistic network workload for emerging networking scenarios". In: *Computer Networks* 56.15 (2012), pp. 3531–3547.
- [18] A. Brandt, J. Vasseur, J. Hui, K. Pister, P. Thubert, P. Levis, R. Struik, R. Kelsey, T. H. Clausen, and T. Winter. *RPL: IPv6 Routing Protocol for Low-Power and Lossy Networks*. RFC 6550. Mar. 2012. DOI: [10.17487/rfc6550](https://doi.org/10.17487/rfc6550). URL: <https://rfc-editor.org/rfc/rfc6550.txt>.
- [19] M. Buettner, G. V. Yee, E. Anderson, and R. Han. "X-MAC: A Short Preamble MAC Protocol for Duty-cycled Wireless Sensor Networks". In: *Proceedings of the 4th International Conference on Embedded Networked Sensor Systems*. SenSys '06. Boulder, Colorado, USA:

- ACM, 2006, pp. 307–320. ISBN: 1-59593-343-3. DOI: [10.1145/1182807.1182838](https://doi.org/10.1145/1182807.1182838).
- [20] C. Cano, D. Lopez-Perez, H. Claussen, and D. Leith. “Using LTE in Unlicensed Bands: Potential Benefits and Co-existence Issues”. In: *IEEE Communications Magazine*, Dec 2016 (2016).
- [21] E. Capo-Chichi, H. Guyennet, J.-M. Friedt, I. Johnson, and C. Duffy. “Design and implementation of a generic hybrid wireless sensor network platform”. In: *Local Computer Networks, 2008. LCN 2008. 33rd IEEE Conference on*. 2008, pp. 836–840. DOI: [10.1109/LCN.2008.4664289](https://doi.org/10.1109/LCN.2008.4664289).
- [22] J. Carle and D. Simplot-Ryl. “Energy-efficient area monitoring for sensor networks”. In: *Computer* 37.2 (2004), pp. 40–46. ISSN: 0018-9162. DOI: [10.1109/MC.2004.1266294](https://doi.org/10.1109/MC.2004.1266294).
- [23] CC2420 *datasheet*. Texas Instruments.
- [24] O. Chapelle and L. Li. “An empirical evaluation of thompson sampling”. In: *Advances in neural information processing systems*. 2011, pp. 2249–2257.
- [25] M. Chen, S. Mao, and Y. Liu. “Big Data: A Survey”. In: *Mob. Netw. Appl.* 19.2 (Apr. 2014), pp. 171–209. ISSN: 1383-469X. DOI: [10.1007/s11036-013-0489-0](https://doi.org/10.1007/s11036-013-0489-0). URL: <http://dx.doi.org/10.1007/s11036-013-0489-0>.
- [26] M. Chen and G. A. Rincon-Mora. “An Accurate Electrical Battery Model Capable of Predicting Runtime and I-V Performance”. In: *IEEE Transactions on Energy Conversion* 21.2 (2006).
- [27] A. Collins, G. Fraser, and J. Snowball. “Could a Regulated Market Approach for Rhinoceros Horns Work in South Africa? Some Practical Issues and Concerns”. In: *ESSA* (2013).
- [28] M. Coyne and B. Godley. “Satellite Tracking and Analysis Tool (STAT): an integrated system for archiving, analyzing and mapping animal tracking data”. In: *Marine Ecology Progress Series* 301 (2005), pp. 1–7.
- [29] P. Diaconis, D. Ylvisaker, et al. “Conjugate priors for exponential families”. In: *The Annals of statistics* 7.2 (1979), pp. 269–281.
- [30] F. Dressler, S. Ripperger, M. Hierold, T. Nowak, C. Eibel, B. Cassens, F. Mayer, K. Meyer-Wegener, and A. Kolpin. “From radio telemetry to ultra-low-power sensor networks: tracking bats in the wild”. In: *IEEE Communications Magazine* 54.1 (2016), pp. 129–135. ISSN: 0163-6804. DOI: [10.1109/MCOM.2016.7378438](https://doi.org/10.1109/MCOM.2016.7378438).

- [31] A. Dunkels, B. Gronvall, and T. Voigt. "Contiki - a lightweight and flexible operating system for tiny networked sensors". In: *Local Computer Networks, 2004. 29th Annual IEEE International Conference on*. 2004, pp. 455–462. DOI: [10.1109/LCN.2004.38](https://doi.org/10.1109/LCN.2004.38).
- [32] A. Dunkels. "Rime — A Lightweight Layered Communication Stack for Sensor Networks". In: *Proceedings of the European Conference on Wireless Sensor Networks (EWSN), Poster/Demo session*. Delft, The Netherlands, Jan. 2007.
- [33] A. Dunkels. *The ContikiMAC Radio Duty Cycling Protocol*. 2011.
- [34] A. Dunkels, J. Eriksson, N. Finne, and N. Tsiftes. *Powertrace: Network-level Power Profiling for Low-power Wireless Networks*. Kista, Sweden, 2011.
- [35] A. Dunkels, F. Österlind, N. Tsiftes, and Z. He. "Software-based Online Energy Estimation for Sensor Nodes". In: *Proceedings of the 4th Workshop on Embedded Networked Sensors*. EmNets '07. Cork, Ireland: ACM, 2007, pp. 28–32. ISBN: 978-1-59593-694-3. DOI: [10.1145/1278972.1278979](https://doi.org/10.1145/1278972.1278979).
- [36] A. Dunkels, F. Österlind, N. Tsiftes, and Z. He. "Software-based Sensor Node Energy Estimation". In: *Proceedings of the 5th International Conference on Embedded Networked Sensor Systems*. SenSys '07. Sydney, Australia: ACM, 2007, pp. 409–410. ISBN: 978-1-59593-763-6. DOI: [10.1145/1322263.1322319](https://doi.org/10.1145/1322263.1322319).
- [37] S. Duquennoy, O. Landsiedel, and T. Voigt. "Let the Tree Bloom: Scalable Opportunistic Routing with ORPL". In: *Proceedings of the International Conference on Embedded Networked Sensor Systems (ACM SenSys 2013)*. Rome, Italy, Nov. 2013.
- [38] S. Duquennoy, F. Österlind, and A. Dunkels. "Lossy Links, Low Power, High Throughput". In: *Proceedings of the 9th ACM Conference on Embedded Networked Sensor Systems*. SenSys '11. Seattle, Washington: ACM, 2011, pp. 12–25. ISBN: 978-1-4503-0718-5. DOI: [10.1145/2070942.2070945](https://doi.org/10.1145/2070942.2070945).
- [39] P. Dutta, M. Feldmeier, J. Paradiso, and D. Culler. "Energy Metering for Free: Augmenting Switching Regulators for Real-Time Monitoring". In: *Information Processing in Sensor Networks, 2008. IPSN '08. International Conference on*. 2008, pp. 283–294. DOI: [10.1109/IPSN.2008.58](https://doi.org/10.1109/IPSN.2008.58).
- [40] L. M. Elbroch and H. Quigley. "Social interactions in a solitary carnivore". In: *Current Zoology* (2016). ISSN: 1674-5507. DOI: [10.1093/cz/zow080](https://doi.org/10.1093/cz/zow080). eprint: <http://cz.oxfordjournals.org/content/early/2016/07/08/cz.zow080.full.pdf>. URL: <http://cz.oxfordjournals.org/content/early/2016/07/08/cz.zow080>.

- [41] H. ElSawy, E. Hossain, and M. Haenggi. "Stochastic geometry for modeling, analysis, and design of multi-tier and cognitive cellular wireless networks: A survey". In: *Communications Surveys & Tutorials, IEEE* 15.3 (2013), pp. 996–1019.
- [42] S. C. Ergen. *ZigBee/IEEE 802.15.4 Summary*. Tech. rep. University of Berkeley, 2004.
- [43] Ericsson. "More than 50 billion connected devices". In: *White Paper* (2011).
- [44] D. Evans. "The Internet of Things. How the Next Evolution of the Internet Is Changing Everything". In: *In White Paper of Cisco Internet Business Solutions Group (IBSG)* (2011).
- [45] ExtraPuTTY. URL: <http://www.extraputty.com/>.
- [46] S. Farahani. *ZigBee Wireless Networks and Transceivers*. Newton, MA, USA: Newnes, 2008. ISBN: 0750683937, 9780750683937.
- [47] F. Ferrari, M. Zimmerling, L. Thiele, and O. Saukh. "Efficient network flooding and time synchronization with Glossy". In: *Information Processing in Sensor Networks (IPSN), 2011 10th International Conference on*. 2011, pp. 73–84.
- [48] F. Ferrari, M. Zimmerling, L. Thiele, and O. Saukh. "Efficient network flooding and time synchronization with Glossy." In: *IPSN*. Ed. by X. D. Koutsoukos, K. Langendoen, G. J. Pottie, and V. Raghunathan. IEEE, 2011, pp. 73–84. ISBN: 978-1-4503-0512-9. URL: <http://dblp.uni-trier.de/db/conf/ipsn/ipsn2011.html#FerrariZTS11>.
- [49] F. S.P. T. Force. *Report of the spectrum efficiency working group*. 2002.
- [50] P. Friess and O. Vermesan. *Digitising the Industry - Internet of Things Connecting the Physical, Digital and Virtual Worlds*. River Publishers, 2016. ISBN: 9788793379817.
- [51] Y. Gai, B. Krishnamachari, and R. Jain. "Learning multiuser channel allocations in cognitive radio networks: A combinatorial multi-armed bandit formulation". In: *Symposium on New Frontiers in Dynamic Spectrum*. IEEE. 2010, pp. 1–9.
- [52] S. Geirhofer, L. Tong, and B. M. Sadler. "A measurement-based model for dynamic spectrum access in WLAN channels". In: *Military Communications Conference (MILCOM)*. IEEE. 2006, pp. 1–7.
- [53] S. Geirhofer, L. Tong, and B. M. Sadler. "Cognitive medium access: constraining interference based on experimental models". In: *Selected Areas in Communications, IEEE Journal on* 26.1 (2008), pp. 95–105.

- [54] C. Goursaud and J. M. Gorce. "Dedicated networks for IoT: PHY / MAC state of the art and challenges". In: *EAI Endorsed Transactions on Internet of Things* 15.1 (Oct. 2015). DOI: [10.4108/eai.26-10-2015.150597](https://doi.org/10.4108/eai.26-10-2015.150597).
- [55] W. Guo, W. Healy, and M. Zhou. "Impacts of 2.4-GHz ISM Band Interference on IEEE 802.15.4 Wireless Sensor Network Reliability in Buildings". In: *Instrumentation and Measurement, IEEE Transactions on* 61.9 (2012), pp. 2533–2544. ISSN: 0018-9456. DOI: [10.1109/TIM.2012.2188349](https://doi.org/10.1109/TIM.2012.2188349).
- [56] Y. Gwon, S. Dastangoo, and H. Kung. "Optimizing media access strategy for competing cognitive radio networks". In: *Global Communications Conference (GLOBECOM), 2013 IEEE*. IEEE. 2013, pp. 1215–1220.
- [57] S. Haykin. "Cognitive radio: brain-empowered wireless communications". In: *Selected Areas in Communications, IEEE Journal on* 23.2 (2005), pp. 201–220.
- [58] W. Heinzelman, A. Chandrakasan, and H. Balakrishnan. "An application-specific protocol architecture for wireless microsensor networks". In: *Wireless Communications, IEEE Transactions on* 1.4 (2002), pp. 660–670. ISSN: 1536-1276. DOI: [10.1109/TWC.2002.804190](https://doi.org/10.1109/TWC.2002.804190).
- [59] A. Hithnawi, H. Shafagh, and S. Duquennoy. "Understanding the Impact of Cross Technology Interference on IEEE 802.15.4". In: *Proceedings of the 9th ACM International Workshop on Wireless Network Testbeds, Experimental Evaluation and Characterization. WiNTECH '14*. Maui, Hawaii, USA: ACM, 2014, pp. 49–56. ISBN: 978-1-4503-3072-5. DOI: [10.1145/2643230.2643235](https://doi.org/10.1145/2643230.2643235).
- [60] G. Hufford, A. Longley, W. Kissick, U. S. N. Telecommunications, and I. Administration. *A Guide to the Use of the ITS Irregular Terrain Model in the Area Prediction Mode*. NTIA report. U.S. Department of Commerce, National Telecommunications and Information Administration, 1982.
- [61] "IEEE Standard for Information technology– Local and metropolitan area networks– Specific requirements– Part 22: Cognitive Wireless RAN Medium Access Control (MAC) and Physical Layer (PHY) specifications: Policies and procedures for operation in the TV Bands". In: *IEEE Std 802.22-2011* (2011), pp. 1–680. DOI: [10.1109/IEEESTD.2011.5951707](https://doi.org/10.1109/IEEESTD.2011.5951707).
- [62] "IEEE Standard for Information technology–Telecommunications and information exchange between systems–Local and metropolitan area networks–Specific requirements–Part 11: Wireless LAN

- Medium Access Control (MAC) and Physical Layer (PHY) Specifications Amendment 3: Enhancements for Very High Throughput in the 60 GHz Band". In: *IEEE Std 802.11ad-2012 (Amendment to IEEE Std 802.11-2012, as amended by IEEE Std 802.11ae-2012 and IEEE Std 802.11aa-2012)* (2012), pp. 1–628. DOI: [10.1109/IEEESTD.2012.6392842](https://doi.org/10.1109/IEEESTD.2012.6392842).
- [63] "IEEE Standard for Local and metropolitan area networks—Part 15.4: Low-Rate Wireless Personal Area Networks (LR-WPANs) Amendment 1: MAC sublayer". In: *IEEE Std 802.15.4e-2012 (Amendment to IEEE Std 802.15.4-2011)* (2012), pp. 1–225. DOI: [10.1109/IEEESTD.2012.6185525](https://doi.org/10.1109/IEEESTD.2012.6185525).
- [64] *IEEE Std 802.15.4-2006*. IEEE Standards Association. 2006.
- [65] R. Igual-Perez, A. Boé, N. Rolland, and L. Clavier. "Experimentation and modeling of node energy consumption in wireless sensor networks". In: *17èmes Journées Nationales du Réseau Doctoral en Micro-Nanoélectronique (JNRDM 2014)*. 2014.
- [66] *Ingenu*. Available at: <http://www.ingenu.com/>.
- [67] ITU-R. "ITU Radio Regulations". In: 1 (2012).
- [68] G. P. Joshi, S. Y. Nam, and S. W. Kim. "Cognitive Radio Wireless Sensor Networks: Applications, Challenges and Research Trends". In: *Sensors* 13.9 (2013), p. 11196. ISSN: 1424-8220. DOI: [10.3390/s130911196](https://doi.org/10.3390/s130911196). URL: <http://www.mdpi.com/1424-8220/13/9/11196>.
- [69] W. Jouini, D. Ernst, C. Moy, and J. Palicot. "Multi-armed bandit based policies for cognitive radio's decision making issues". In: *3rd international conference on Signals, Circuits and Systems (SCS)*. 2009.
- [70] P. Juang, H. Oki, Y. Wang, M. Martonosi, L. S. Peh, and D. Rubenstein. "Energy-efficient Computing for Wildlife Tracking: Design Tradeoffs and Early Experiences with ZebraNet". In: *SIGARCH Comput. Archit. News* 30.5 (Oct. 2002), pp. 96–107. ISSN: 0163-5964. DOI: [10.1145/635506.605408](https://doi.org/10.1145/635506.605408). URL: <http://doi.acm.org/10.1145/635506.605408>.
- [71] K. Karplus. "Online Library". In: (). URL: [https://compbio.soe.ucsc.edu/gen\\_sequence](https://compbio.soe.ucsc.edu/gen_sequence).
- [72] L. Lai, H. El Gamal, H. Jiang, and H. V. Poor. "Cognitive medium access: Exploration, exploitation, and competition". In: *Mobile Computing, IEEE Transactions on* 10.2 (2011), pp. 239–253.
- [73] T. L. Lai and H. Robbins. "Asymptotically efficient adaptive allocation rules". In: *Advances in applied mathematics* 6.1 (1985), pp. 4–22.

- [74] Y.-C. Liang, Y. Zeng, E. C. Peh, and A. T. Hoang. "Sensing-throughput tradeoff for cognitive radio networks". In: *Wireless Communications, IEEE Transactions on* 7.4 (2008), pp. 1326–1337.
- [75] M. López-Benítez and F. Casadevall. "Time-dimension models of spectrum usage for the analysis, design and simulation of cognitive radio networks". In: *IEEE Trans. Veh. Technol.* 62.5 (2013), pp. 2091–2104.
- [76] LoRa Alliance. Available at: <https://www.lora-alliance.org>.
- [77] J. Lunden, V. Koivunen, and H. V. Poor. "Spectrum Exploration and Exploitation for Cognitive Radio: Recent Advances". In: *Signal Processing Magazine, IEEE* 32.3 (2015), pp. 123–140.
- [78] A. Maskooki, V. Toldov, L. Clavier, V. Loscrí, and N. Mitton. "Competition: Channel Exploration/Exploitation Based on a Thompson Sampling Approach in a Radio Cognitive Environment". In: *EWSN - International Conference on Embedded Wireless Systems and Networks (dependability competition)*. Graz , Austria, Feb. 2016.
- [79] J. Mitola and G. Q. Maguire Jr. "Cognitive radio: making software radios more personal". In: *Personal Communications, IEEE* 6.4 (1999), pp. 13–18.
- [80] Y. Nam, H. Lee, H. Jung, T. Kwon, and Y. Choi. "An Adaptive MAC (A-MAC) Protocol Guaranteeing Network Lifetime for Wireless Sensor Networks". In: *Wireless Conference 2006 - Enabling Technologies for Wireless Multimedia Communications (European Wireless), 12th European*. 2006, pp. 1–7.
- [81] C. Perera, A. Zaslavsky, P. Christen, and D. Georgakopoulos. "Context Aware Computing for The Internet of Things: A Survey". In: *IEEE Communications Surveys & Tutorials* 16.1 (2014), pp. 414–454.
- [82] M. Petrova, L. Wu, P. Mahonen, and J. Riihijarvi. "Interference Measurements on Performance Degradation between Colocated IEEE 802.11g/n and IEEE 802.15.4 Networks". In: *Networking, 2007. ICN '07. Sixth International Conference on*. 2007, pp. 93–93. DOI: [10.1109/ICN.2007.53](https://doi.org/10.1109/ICN.2007.53).
- [83] J. Polastre, R. Szewczyk, and D. Culler. "Telos: Enabling Ultra-low Power Wireless Research". In: *Proceedings of the 4th International Symposium on Information Processing in Sensor Networks*. IPSN '05. Los Angeles, California: IEEE Press, 2005. ISBN: 0-7803-9202-7.
- [84] RadioMobile. Available at: <http://www.cplus.org/rmw/english1.html>.

- [85] J. Rohde and T. Toftegaard. "Mitigating the impact of high interference levels on energy consumption in wireless sensor networks". In: *Wireless Communication, Vehicular Technology, Information Theory and Aerospace Electronic Systems Technology (Wireless VITAE), 2011 2nd International Conference on*. 2011, pp. 1–5. DOI: [10 . 1109 / WIRELESSVITAE.2011.5940899](https://doi.org/10.1109/WIRELESSVITAE.2011.5940899).
- [86] K. Romer and F. Mattern. "The design space of wireless sensor networks". In: *IEEE Wireless Communications* 11.6 (2004), pp. 54–61. ISSN: 1536-1284. DOI: [10 . 1109 / MWC . 2004 . 1368897](https://doi.org/10.1109/MWC.2004.1368897).
- [87] R. Sanchez-Iborra and M.-D. Cano. "State of the Art in LP-WAN Solutions for Industrial IoT Services". In: *Sensors* 16.5 (2016), p. 708. ISSN: 1424-8220. DOI: [10 . 3390 / s16050708](https://doi.org/10.3390/s16050708). URL: [http : // www . mdpi . com / 1424 - 8220 / 16 / 5 / 708](http://www.mdpi.com/1424-8220/16/5/708).
- [88] Semtech. "AN1200.22 LoRa<sup>TM</sup> Modulation Basics". In: *Application note* (2015).
- [89] Semtech. "SX1276/77/78/79". In: *Datasheet* (2015).
- [90] S. Shakkottai, T. S. Rappaport, and P. C. Karlsson. "Cross-layer design for wireless networks". In: *IEEE Communications Magazine* 41.10 (2003), pp. 74–80. ISSN: 0163-6804. DOI: [10 . 1109 / MCOM . 2003 . 1235598](https://doi.org/10.1109/MCOM.2003.1235598).
- [91] K. Shinghal, A. Noor, N. Srivastava, and R. Singh. "Power measurements of Wireless Sensor Networks Node". In: *International Journal of Computer Engineering & Science* (2011).
- [92] SIGFOX. Available at: [http : // www . sigfox . com](http://www.sigfox.com).
- [93] A. Sikora and V. F. Groza. "Coexistence of IEEE802.15.4 with other systems in the 2.4 GHz-ISM-Band". In: 3 (May 2005), pp. 1786–1791. DOI: [10 . 1109 / imtc . 2005 . 1604479](https://doi.org/10.1109/imtc.2005.1604479).
- [94] G. H. Sim, R. Li, C. Cano, D. Malone, P. Patras, and J. Widmer. "Learning from experience: Efficient decentralized scheduling for 60GHz mesh networks". In: *2016 IEEE 17th International Symposium on A World of Wireless, Mobile and Multimedia Networks (WoWMoM)*. 2016, pp. 1–9. DOI: [10 . 1109 / WoWMoM . 2016 . 7523520](https://doi.org/10.1109/WoWMoM.2016.7523520).
- [95] R. Smith, D. Roberts, R Duffy, and F. S. John. "New rhino conservation project in South Africa to understand landowner decision-making". In: *Oryx* (2013).
- [96] P. Sommer, B. Kusy, P. Valencia, R. Dungavell, and R. Jurdak. "Delay-Tolerant Networking for Long-Term Animal Tracking". In: *CoRR abs/1506.01792* (2015). URL: [http : // arxiv . org / abs / 1506 . 01792](http://arxiv.org/abs/1506.01792).
- [97] N. Sornin, Luis, M., T. Eirich, T. Kramp, and O. Hersent. *LoRa Specification V1.0*. 2015.

- [98] I. W. Sutrisno and A. G. Wahied. "Power Enhancement for Piezoelectric Energy Harvester". In: *World Congress on Engineering (WCE)*. Vol. II. 2012.
- [99] K. Thompson, G. J. Miller, and R. Wilder. "Wide-area Internet traffic patterns and characteristics". In: *Network, iEEE* 11.6 (1997), pp. 10–23.
- [100] V. Toldov, L. Clavier, V. Loscrí, and N. Mitton. "A Thompson Sampling Approach to Channel Exploration-Exploitation Problem in Multihop Cognitive Radio Networks". In: *27th annual IEEE International Symposium on Personal, Indoor and Mobile Radio Communications (PIMRC)*. Valencia, Spain, Sept. 2016.
- [101] V. Toldov, R. Igual-Pérez, R. Vyas, A. Boé, L. Clavier, and N. Mitton. "Experimental Evaluation of Interference Impact on the Energy Consumption in Wireless Sensor Networks". In: *17th IEEE International Symposium on a World of Wireless, Mobile and Multimedia Networks (WoWMoM)*. Coimbra, Portugal, June 2016.
- [102] V. Toldov, J. Meijers, R. Igual-Pérez, R. Wolhuter, N. Mitton, and L. Clavier. "Performance evaluation of LoRa radio solution for PREDNET wildlife animal tracking project". In: *LPWAN 2016*. Paris Roissy, France, May 2016.
- [103] S. Toledo, O. Kishon, Y. Orchan, A. Shohat, and R. Nathan. "Lessons and Experiences from the Design, Implementation, and Deployment of a Wildlife Tracking System". In: *2016 IEEE International Conference on Software Science, Technology and Engineering (SWSTE)*. 2016, pp. 51–60. DOI: [10.1109/SWSTE.2016.16](https://doi.org/10.1109/SWSTE.2016.16).
- [104] A.-S. Tonneau, N. Mitton, and J. Vandaele. "A Survey on (mobile) Wireless Sensor Network Experimentation Testbeds". In: *Distributed Computing in Sensor Systems (DCOSS), 2014 IEEE International Conference on*. 2014, pp. 263–268. DOI: [10.1109/DCOSS.2014.41](https://doi.org/10.1109/DCOSS.2014.41).
- [105] K. Wang, L. Chen, Q. Liu, W. Wang, and F. Li. "One Step Beyond Myopic Probing Policy: A Heuristic Lookahead Policy for Multi-Channel Opportunistic Access". In: *Wireless Communications, IEEE Transactions on* 14.2 (2015), pp. 759–769.
- [106] W. Wang, T. O'Donnell, L. Ribetto, B. O'Flynn, M. Hayes, and C. O'Mathuna. "Energy harvesting embedded wireless sensor system for building environment applications". In: *Wireless Communication, Vehicular Technology, Information Theory and Aerospace Electronic Systems Technology, 2009. Wireless VITAE 2009. 1st International Conference on*. 2009, pp. 36–41.
- [107] XBee Series 1 datasheet.
- [108] XBee/XBee-PRO RF Modules. Digi International Inc. 2009.

- [109] B. Zeng, Y. Dong, and D. Lu. "A Point-to-Point Interference Measurement Approach for Large-Scale Wireless Sensor Networks." In: *IJDSN* 2012 (2012).
- [110] Q. Zhao and B. M. Sadler. "A survey of dynamic spectrum access". In: *Signal Processing Magazine, IEEE* 24.3 (2007), pp. 79–89.
- [111] Q. Zhao, L. Tong, A. Swami, and Y. Chen. "Decentralized cognitive MAC for opportunistic spectrum access in ad hoc networks: A POMDP framework". In: *Selected Areas in Communications, IEEE Journal on* 25.3 (2007), pp. 589–600.
- [112] G. Zhou, J. A. Stankovic, and S. H. Son. "Crowded Spectrum in Wireless Sensor Networks". In: *in Proceedings of Third Workshop on Embedded Networked Sensors (EmNets. 2006.*
- [113] R. Zhou and G. Xing. "Nemo: A high-fidelity noninvasive power meter system for wireless sensor networks". In: *Information Processing in Sensor Networks (IPSN), 2013 ACM/IEEE International Conference on.* 2013, pp. 141–152. DOI: [10.1109/IPSN.2013.6917581](https://doi.org/10.1109/IPSN.2013.6917581).
- [114] H. Zimmermann. "Innovations in Internetworking". In: ed. by C. Partridge. Norwood, MA, USA: Artech House, Inc., 1988. Chap. OSI Reference Model&Mdash;The ISO Model of Architecture for Open Systems Interconnection, pp. 2–9. ISBN: 0-89006-337-0. URL: <http://dl.acm.org/citation.cfm?id=59309.59310>.



# List of Publications

- V. Toldov, L. Clavier, V. Loscrí, and N. Mitton. "A Thompson Sampling Approach to Channel Exploration-Exploitation Problem in Multihop Cognitive Radio Networks". In: *27th annual IEEE International Symposium on Personal, Indoor and Mobile Radio Communications (PIMRC)*. Valencia, Spain, Sept. 2016
- V. Toldov, R. Igual-Pérez, R. Vyas, A. Boé, L. Clavier, and N. Mitton. "Experimental Evaluation of Interference Impact on the Energy Consumption in Wireless Sensor Networks". In: *17th IEEE International Symposium on a World of Wireless, Mobile and Multimedia Networks (WoWMoM)*. Coimbra, Portugal, June 2016
- V. Toldov, J. Meijers, R. Igual-Pérez, R. Wolhuter, N. Mitton, and L. Clavier. "Performance evaluation of LoRa radio solution for PRED-NET wildlife animal tracking project". In: *LPWAN 2016*. Paris Roissy, France, May 2016
- A. Maskooki, V. Toldov, L. Clavier, V. Loscrí, and N. Mitton. "Competition: Channel Exploration/Exploitation Based on a Thompson Sampling Approach in a Radio Cognitive Environment". In: *EWSN - International Conference on Embedded Wireless Systems and Networks (dependability competition)*. Graz , Austria, Feb. 2016